Generative design and parametric / topological optimization of cellular structures bio-inspired by additive manufacturing

Monzer Al Khalil

THÈSE DE DOCTORAT DE L'ÉTABLISSEMENT UNIVERSITÉ BOURGOGNE FRANCHE-COMTÉ

PRÉPARÉE À L'UNIVERSITÉ DE TECHNOLOGIE DE BELFORT-MONTBÉLIARD

École doctorale n°37

SPIM-Sciences Pour l'Ingénieur et Microtechniques

Doctorat en Mécanique

Generative Design and Parametric/Topology Optimization of Bio-inspired Cellular Structures for Additive Manufacturing

présentée et soutenue publiquement à Sevenans, France, le "30/11/2022"

par

M. Monzer AL KHALIL

Ingénieur en Mécanique et Conception

devant le jury composé de :

Rapporteurs:	Prof. Arnaud DELAMÉZIÈRE	Institut Mines-Télécom
	Dr. HDR Nicolas MARANZANA	École Nationale Supérieur d'Art et Métiers
Examinateurs:	Président du jury: Prof. Christian GENTIL	Université de Bourgogne
	Prof. Laurent BILLON	Université de Pau et des Pays de l'Adour
	Prof. François VILLENEUVE	Université Grenoble Alpes
Directeur de thèse:	Prof. Sébastien ROTH	Université de Technologie de Belfort-Montbéliard
Co-directeur:	Dr. HDR Nadhir LEBAAL	Université de Technologie de Belfort-Montbéliard
Encadrant:	Prof. Frédéric DEMOLY	Université de Technologie de Belfort-Montbéliard

À la mémoire de ma tatie Zouhour

فَقُل لِمَن يَدَّعي في العِلمِ فَلسَفَةً حَفِظتَ شَيئاً وَغابَت عَنكَ أَشياءُ

Translation: "Tell whoever pretends to be philosophical in their approach to science, you have learned few things, but you have missed out on a lot".

By the arabic Poet: Abu Nawwass

Remerciements

“Sois reconnaissant envers tous, tous t’enseignent.”

Bouddha

Les travaux présentés dans ce manuscrit n’auraient pas pu voir le jour sans les personnes qui y ont contribué que ce soit d’une manière directe ou indirecte. Leur support scientifique, technique ou moral a été la clé pour achever ces travaux dans les meilleures conditions.

Mes remerciements vont tout d’abord au Prof. Arnaud DELAMÉZIÈRE et Dr. HDR Nicolas MARANZANA pour avoir accepté de rapporter cette thèse et aux professeurs Christian GENTIL, Laurent BILLON et François VILLENEUVE pour avoir accepté de l'examiner.

Je ne remercierai jamais assez mes encadrants pour m’avoir accordé leur confiance afin d’effectuer cette thèse au sein de l’équipe Conception Mécanique et Modélisation Numérique (CO2M) du laboratoire Interdisciplinaire Carnot de Bourgogne (ICB) à l’Université de Technologie de Belfort-Montbéliard (UTBM). Je suis particulièrement reconnaissant à mon directeur Prof. Sebastien ROTH pour son écoute, son soutein et sa disponibilité permanente. Je remercie également mon co-directeur Nadhir LEBAAL et mon encadrant Frédéric DEMOLY pour leurs conseils indisponsables lors de la réalisation de mes travaux et la rédaction des articles puis de ce manuscrit.

Il m’est impossible de mentionner laboratoire ICB-CO2M sans remercier l’ensemble des personnes qui le compose: tous mes collègues, mes « complices » avec lesquels j’ai forgé de vrais liens d’amitiés. Merci aux docteurs Saoussen DIMASSI, Laura DELCUSE-ROBERT, Lucas DEMBINSKI aux doctorants Hadrien BELKEBIR, Kheira BENYAHIYA, Valentin MARCHAL et Lucas JIMENEZ et le technicien Hichem SERIKET, ainsi qu’aux stagiaries Louise HOHNADEL et Darshan ATHINARAYANARAO pour la belle ambiance créée. Je tiens également à remercier Dr. HDR Dominique CHAMORET pour sa confiance en mes capacités d'enseignement.

Je n’oublie pas de remercier mes amis qui ont toujours été là pour moi dans chaque étape et qui m’ont aidé à surmonter toutes les difficultés : Sylvain, Pauline, Christian, Anna-Karen, Xianlong, Jean-Jacques, Shuangshuang et surtout mes meilleurs amis d’enfance le Dr. Alaeddine, les ingénieurs Ahmad, Abdelsalam et Mohamad.

Finalement, je tiens à remercier toute ma famille pour leur soutien et amour inconditionnels y compris mes neveux et nièces, mes sources de joie. Mes plus sincères remerciements vont aux merveilleuses femmes qui m’ont élevé et qui ont fait de moi la personne que je suis aujourd’hui : maman, mes sœurs, mamie et mes quatres taties. Mes pensées vont particulièrement à ma tatie Zouhour qui nous a quittés et à qui je dédicace cette thèse de doctorat.

Abstract

Biomimicry is the practice of learning from nature and imitating its different functionalities. Nature proposes complex forms and objects which inspired designers and engineers to conceive and find solutions for their engineering problems. The fabrication of these complex objects is particularly ensured by the different Additive Manufacturing (AM) techniques. Generally, biomimicry can be addressed at different levels, forms, textures, and behaviors, but in AM, it is presented under two main types. The first is the customization of parts (medical prosthesis, implants or custom sport equipments). And the second consists in the optimization for specific properties such as stiffness and lightness (light parts in aerospace or automotive applications). Other types and forms of biomimicry for AM include the incorporation of real biological data, distribution of materials as in cellular and lattice structures, and integrating multifunctionality in design. Particularly, cellular and lattice structures are considered as biomimetic due to their resemblance to biological structures. The utility of their integration in optimization and AM techniques has been proven by several studies mainly in terms of weight reduction, stiffness, and energy absorption rate increase. Taken the fact that a link exists between biomimicry, cellular structures, optimization, and AM, the following question arises: “What is the utility of biomimicry in optimizating and manufacturing cellular parts that respond to mechanical properties and constraints (lightweight and high stiffness) imposed by AM?”. To be able to answer this question, this research work will focus on highlighting the importance of employing biomimetic algorithms and forms in designing and optimizing lightweight cellular structures with high stiffness. The first contribution focuses on studying the importance of combining topology and parametric optimizations in designing and modeling cellular structures having a good stiffness-to-weight ratio. The study is divided into two cases and special interest is paid to the comparison between the two cases. In both cases, a Design Of Experiments (DOE) and a sensitivity study are conducted. The first case consists of a uniform lattice distribution while the second is a variable-density lattice distribution study. It is shown that the second case provids a better weight and a better strength thus reaching the goal of having a better strength-to-weight ratio. However, the biomimetic aspect is not covered in the first contribution . Thus, in a second part, the Lindenmayer systems (L-systems) – tree growth grammars – are used and a specific distribution is used along the Principal Stress Lines (PSLs) directions imitating the material growth aspect in bone structures. Numerical simulations and parametric optimization schemes based on an L9 DOE sensibility study were conducted. Results show the effectiveness of this method in adapting mechanical structures to various loading cases as well as guaranteeing a good stiffness-to-weight ratio. In the third contribution, a more advanced parametric optimization approach is applied in order to find better results for optimal L-systems beams’ sections: meta-modeling optimization algorithm based on metaheuristics and knowledge.

Keywords: biomimetic design; parametric optimization; simulation; additive manufacturing.

Résumé

Le biomimétisme est la pratique d'apprentissage de la nature et de l'imitation de ses différentes fonctionnalités. La nature présente des formes complexes qui ont inspirées les concepteurs et les ingénieurs à concevoir et à adresser des solutions à leurs problèmes d'ingénierie. La fabrication de ces objets complexes est particulièrement assurée par les différentes techniques de la Fabrication Additive (FA). En général, le biomimétisme peut être abordé à différents niveaux, dont les formes et les comportements. Mais en FA, il est présent sous deux facettes. La première est la personnalisation des pièces (prothèses médicales, implants ou équipements sportifs). La deuxième consiste à optimiser des propriétés spécifiques telles que la rigidité et la légèreté (plus particulièrement dans les domaines de l'aérospatial et de l'automobile). D'autres types et formes de biomimétisme pour la FA comprennent l'intégration de données biologiques réelles, la distribution de la matière comme dans les structures cellulaires et en treillis (lattices), et l'intégration de la multifonctionnalité dans la conception. En particulier, les structures cellulaires ou en lattices sont considérées comme biomimétiques en raison de leur ressemblance aux structures biologiques. L'utilité de leur incorporation dans les techniques d'optimisation et de FA a été prouvée par de nombreuses études principalement en termes de réduction de la masse et d'augmentation de la rigidité et le taux d'absorption d'énergie . Considérant qu'il existe un lien entre le biomimétisme, les structures en lattices, l'optimisation, et la FA, la question scientifique peut se poser de la manière suivante : "Quelle est l'utilité du biomimétisme dans la fabrication et l'optimisation des structures cellulaires bioimétiques répondant aux propriétés et contraintes mécaniques (légèreté et rigidité) imposées par la FA ?". Pour répondre à cette problématique, les travaux de recherche présentés dans cette thèse mettent l'accent sur l'importance de l'utilisation d'algorithmes et de formes biomimétiques dans la conception et l'optimisation de structures en lattices. La première contribution se focalise sur le couplage des optimisations topologique et paramétrique et leur rôle dans la conception et la modélisation de structures lattices présentant un bon rapport masse/rigidité. Une étude comparative entre deux cas de figures a été menée : une distribution uniforme de lattices et une distribution à densité variable. Il a été démontré que le deuxième cas offre une masse plus légère et une meilleure rigidité, atteignant ainsi l'objectif d'avoir un meilleur rapport rigidité/masse. Cependant, l'aspect biomimétique n'a pas été abordé dans la première partie. La deuxième partie porte sur l'utilisation des systèmes de Lindenmayer (L-systèmes) – grammaires de croissance des arbres/plantes – suivant les directions des lignes isostatiques imitant ainsi la propriété de croissance de la matière dans les structures osseuses. Basé sur ce concept, des simulations numériques et une méthode d'optimisation paramétrique basée sur une étude de sensibilité L9 DOE ont été menées dans le but de trouver les structures présentant une masse et une rigidité optimales. Les résultats ont montré l'efficacité de cette méthode pour adapter les structures mécaniques aux différents cas de chargement et garantir un bon rapport masse/rigidité. Dans une troisième partie, une méthode d'optimisation paramétrique a été

utilisée pour optimiser les sections des poutres constituants les L-systèmes en utilisant un algorithme d'optimisation basé sur une approche méta-heuristique.

Mots-clés : conception biomimétique; optimisation paramétrique, simulation, fabrication additive.

Table of Contents

List of Figures

List of Tables

List of Acronyms

Term	Definition
AM	Additive Manufacturing
CAD	Computer-Aided Design
CAE	Computer-Aided Engineering
CCD	Central Composite Design
DACE	Design And Analysis of Computer Experiments
DfAM	Design for Additive Manufacturing
DOE	Design Of Experiments
FA	Fabrication Additive
FEA	Finite Element Analysis
KLE	Kerhunen-Loeve Expansion
KSO	Kriging Swarm Optimization
L-systems	Lindenmayer systems
MARS	Multivariable Adaptive Regression Splines
MLS	Moving Least Square
PSL	Principal Stress Line
PSO	Particle Swarm Optimization
RBF	Radial Basis Functions
RSM	Response Surface Models
SDB	Swarm DataBases
TO	Topology Optimization

Chapter 1: Introduction and Research Context

"Although nature commences with reason and ends in experience, it is necessary for us to do the opposite, that is to commence with experience and from this to proceed to investigate the reason."

Leonardo Da Vinci

"Imagination is more important than knowledge. Knowledge is limited. Imagination encircles the world"

Albert Einstein

1.1. Background

The evolution of biological organisms and structures over the 3.8 billion years has permitted them to develop their functionalities and mechanisms and optimized them in a way to adapt to the constraints imposed by the organism itself or by the external environment [1,2]. Learning from the functions of these complex biological structures helps to provide new sustainable solutions for engineering and design problems. The act of inspiration by nature is often known as "bio-inspiration". A more sophisticated and notorious appellation is "biomimicry" defined by Janine Benyus in 1997 [3] as "the conscious emulation of nature's genius". Biomimicry has found its way into several applications and domains, such as commercial and industrial energy generation [4], pharmaceuticals and chemical manufacturing applications [5], automobile and aviation [6], robotic [7,8], and additive manufacturing (AM) [9,10]. The list of bio-inspired designs and products is non-exhaustive, but they all represent a proof of nature in inspiring designers, scientists, and engineers in elaborating structures with good multifunctional properties such as increased efficiency, reduced light reflection, flexibility, lightweight, increased strength, and resiliency, cost-effectiveness, and waste reduction (see Figure 1).

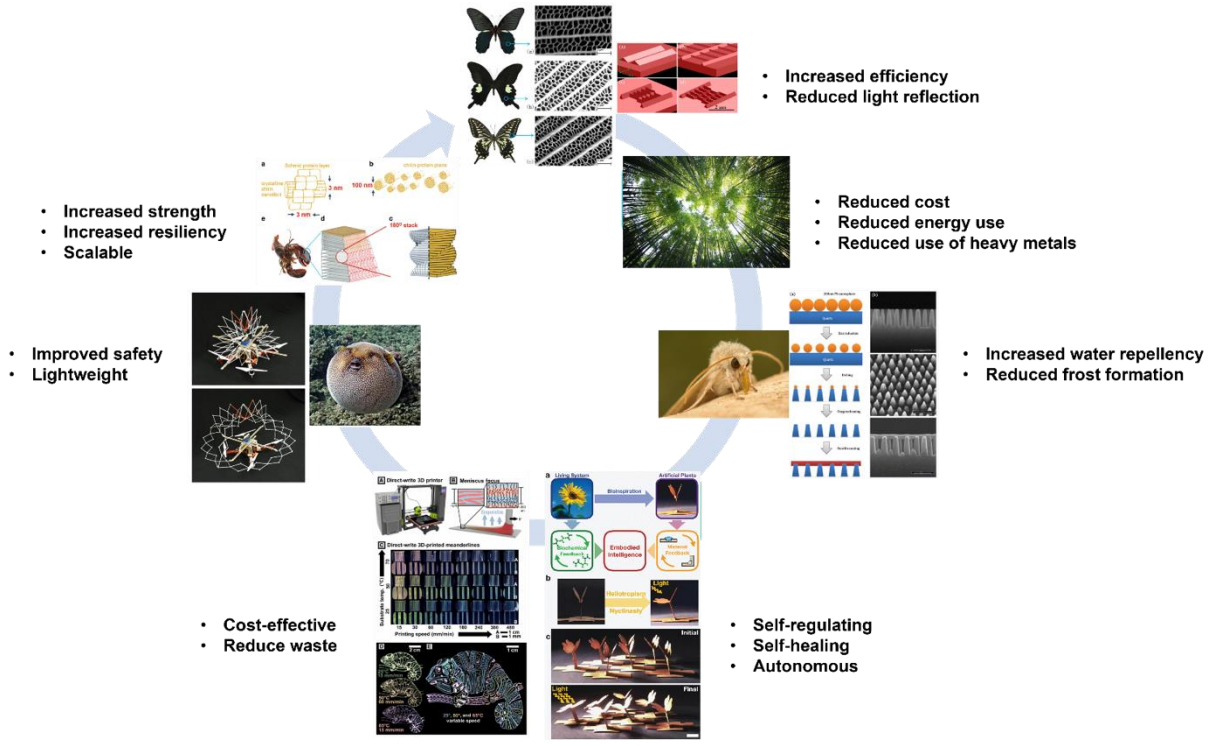

Figure 1. Benefits of each bio-inspired design in the clockwise direction: anti-reflective solar panels inspired by butterfly wings [4], low-energy chemical reactions inspired by photosynthesis[1] [5], anti-icing surface inspired by moth eyes [6], self-repairing robot inspired by plants [7], colorful 3D printing inspired by chameleons [9], safer aerial robot inspired by pufferfish [8], 3D printed concrete inspired by lobster shell [10].

[1] *asknature.org*

In the engineering field, biomimicry consists in studying biological systems, using the information extracted from nature, and applying it to solve problems for different engineering applications. In nature, biological organisms possess hierarchical architectures and structural features with dimensions ranging from the nano to macro-scale [11,12]. The ability to translate these structural features and properties of organisms into physical objects is assured by different AM techniques. Indeed, as shown in the examples in Figure 1, natural living species continue to be a huge source of inspiration for engineers and designers [13]. The freedom of design and to produce complex structures offered by AM , constitute the main aims of biomimetic design for AM. In order to generate complex biomimetic geometries and designs to be printed by different AM techniques, many design principles can be used. Generally, two principal different and opposite broad approaches exist: the solution-driven, and the problem-driven design approaches [3,14,15]. The first approach is when the designer/engineer innovates a new design idea by inspiration from biological models in nature. The second approach consists in finding an anological solution existing in nature for a specific engineering or design problem. In addition to these approaches, three transversal approaches are described: customized and freeform design, simulation-driven design, and lattice design. In contrast to the first two approaches, the transversal ones can be used together, with or without input from nature. Customized and freeform design is the process of manipulating curved surfaces to generate personalized and unique designs that are suitable for a specific purpose while keeping functionality. For example, tree-like support structures, nervous-system-inspired shadow, or hierarchical networks with nodes that continually branch and merge [16,17]. This is the most basic of the biomimetic design methodologies, and it is very beneficial for customization in prostheses and implants, as well as in creative design. The design need for prostheses and implants is based on a biological form, thus the biomimetic description. Simulation-driven design is a potential new method that has evolved in recent years and is particularly effective for lightweight engineering design. This involves structural optimization (more specifically topology optimization (TO) or generative design), which comprises an iterative simulation and material removal procedure to improve the needed material distribution or stiffness for a set of predicted load situations [18-20]. This stepwise optimization method is comparable to most evolutionary processes in nature and removing material from low-stress locations is a similar optimization approach utilized in natural systems. Therefore, this process was classified as biomimetic. The incorporation of lattice or cellular designs into topology optimized designs is a highly relevant approach that is frequently combined with the former methods: the use of additively manufactured lattice or cellular structures in topology optimized models [21]. Cellular or lattice structures are often utilized in natural systems due to their desired and tailorable features, including low lightweight, high specific stiffness, fracture toughness, and crack growth stopping. In the area of cellular structure designs, lattice structures are often considered biomimetic due to their resemblance to porous materials in nature such as honeycombs and trabecular bone. Biomimetic lattice structures may follow stochastic design strategies that permit obtaining structures with optimized strut thicknesses and lengths [22]. The latter statement and described methods and approaches highlight the utility of TO and lattice

incorporation to produce structures with optimal properties using different AM techniques. AM is known for fabricating cellular and lattice structures due to the excellent properties that they possess such as lightweight, important energy absorption characteristics, high strength-to-weight ratio, and high specific rigidity [23-25]. For these reasons, lattice structures have been increasingly used in multiple domains such as in biological sciences, automotive, and aerospace industries [26,27]. The advances in AM techniques and their capability of producing lattice structures generally and bio-inspired cellular structures particularly leads to the establishment of the optimization domain. This domain, especially TO is, as beforementioned, linked to AM domain in terms of weight and material use, and cost reduction [28]. TO is a way of "removing material" where it is not needed. In lattice structure fields, parametric optimization becomes of importance especially when it comes to optimizing lattice struts' thickness and cross-section in order to obtain a lightweight and resistant structure [21]. The latter statement can be perceived as a cross-objective of multiple domains: nature is a viable example for optimized structures and biological designs; one of the AM goals is to produce lightweight and resistant parts; TO permits reducing weight, and parametric optimization allows obtaining structures with a good strength-to-weight ratio. Therefore, the challenge remains in coupling the bio-inspired design domain, AM domain, and optimization domains: An optimized bio-inspired design for AM.

1.2. Research Context and Objectives

Biomimicry is a field that investigates nature's greatest ideas (for example, biological structures and systems) and then imitates them to address engineering issues. The term "biomimicry" is employed specifically in the context of AM, when the design is realized utilizing TO and lattice structures, even if the resultant cellular structure does not have a biomimetic shape, behavior, or functionality. It is considered biomimetic due to its resemblance to several lightweight structures found in nature [29]. TO and the use of lattices in AM has become an emerging topic of design and a viable route for new uses of the technology. Design complexity with AM may be completely exploited, allowing the production of lightweight and customized stiffness [18]. In the light of what is evoked so far, an important question arises: *"What is the cross-domain coupling the biomimicry, design, AM, and optimization domains? How can it be emphasized?"*. The answer starts with the analysis of the sub-domains in Figure 2.

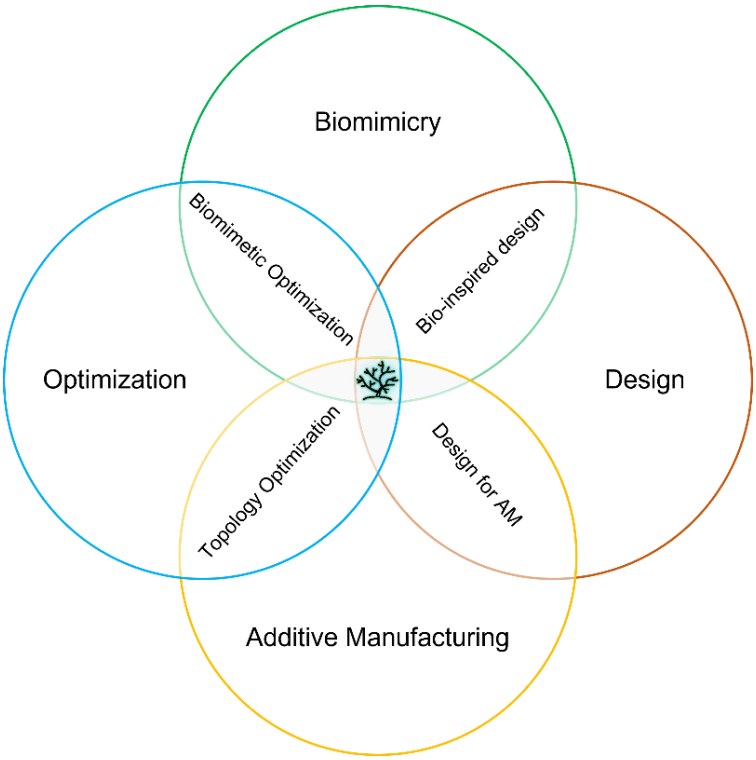

Figure 2. The cross-domains of the different domains discussed in the dissertation.

Bio-inspired design

The bio-inspired or biomimetic design domain is broad, and it cannot limit itself to one specific application sector. As stated before, biomimicry means emulating nature, and in engineering field, it means using nature's biological structures to find a solution for engineering problems. There exist several approaches to elaborate a biomimetic design and all of them require finding "analogies" [30,31]. The challenge consists in the choice of the level and approach of biomimicry while designing a bio-inspired model for a specific application [32,33], and the understanding of the design phase in which biomimicry is to be applied.

Design for AM

Design for AM or simply DfAM is the process of designing and optimizing a product in conjunction with its manufacturing system in order to reduce development time and costs while also improving performance, quality, and profitability [34,35]. In the literature, researchers have evoked DfAM and the related geometric limitations [36], its use in assembly-oriented designs [37], and most importantly its role in designing cellular structures [38]. Set apart from the fact that some cellular and lattice structures are considered biomimetic, few are the studies that talk about biomimetic designs for AM. The challenge then is in the application of biomimicry in a way to meet AM requirements by reducing costs but improving performances at the same time.

TO for AM

For the past two decades, manufacturing-oriented TO or TO for AM has been increasingly employed to produce optimal lightweight structures [18,39,40]. Indeed, for topology optimized structures, AM frees engineers from the constraints of traditional production processes, allowing them to focus on designing lightweight, high-performance structures. TO, on the other hand, is a useful strategy for additively made items with lightweight and novel configurations. Integration of TO with AM is a critical step towards structural design and production alignment [41]. However, when designing a topology-optimized model, few problems and imprecisions can be encountered due to mesh resolution and manufacturing errors and constraints [42]. While biomimicking a biological structure, the question about reducing these constraints is then accentuated.

Biomimetic Optimization

Generally, the term Biomimetic Optimization is not often used in the literature. When it is used, it is specifically for the field of optimization algorithms inspired by nature such as optimization algorithms inspired by ants and swarms behavior [43], firefly, and bacterial foraging algorithms [44]. Indeed, the optimization process often uses an iterative simulation process analogous to biological evolution [29]. Taking the hypothesis of "nature already offers optimized structures and solutions", one can say that biomimetic optimization has been existing for 3.8 billion years. However, optimization does not only limit itself to the topology, but it also covers the variation of material distribution and parametrization inside a structure. Hence, the question of coupling different optimization schemes in order to obtain an optimal design has to be emphasized.

To summarize, design methods for AM and biomimicry have been the topic of design approaches but work that seamlessly integrates these two features is unusual. Optimization techniques based on series of numerical simulations of a previously established geometry provide the designer greater control over the geometry in contrary to optimization techniques that arise from constraints and business rules. This method necessitates a set of numerical simulations to establish a generation algorithm, which will be followed by a set of simulations to optimize the distribution of material described by highly exact grammars.

In fact, AM and optimization domains have been a center of interest of several research inside the ICB UMR 6303 CNRS lab more specifically the Design, Optimization, and Mechanical Modeling (CO2M) department. The lab possesses several research axes and one transversal axis (Figure 3). The main axes are the following:

- Advanced mechanical systems design ;
- Modeling and numerical optimization in mechanics;
- Heat transfers and thermo-physical couplings;
- Quantum information for nanoscale integration of quantum communication protocols ;

- Optimization of manufacturing processes.

The transversal axis “Design, modeling and optimization for AM and 4D printing” studies the methods and tools for a AM-oriented design, 4D printing based on smart materials, vibro-acoustics for the characterization of parts obtained by AM. This PhD thesis titled “Generative Design and Parametric/Topology Optimization of Bio-inspired Cellular Structures for Additive Manufacturing” is part of the transversal axis work and is financed by the Ministry of Higher Education, Research and Innovation.

Based on the previous sections and the lab’s work axes, this PhD focuses on studying bio-inspired designs following different optimization and numerical simulations schemes while respecting the AM constraints and limitations. The following related objectives can be addressed:

- Propose an optimization scheme or framework that optimizes the material distribution and parametrization in a cellular structure.
- Propose a bio-inspired method based on a generative grammar in the goal of optimizing the stiffness-to-weight ratio, hence ensuring a biomimetic design for AM.
- Investigate optimization algorithms to allow for better parametric results to reduce weight and increase stiffness.

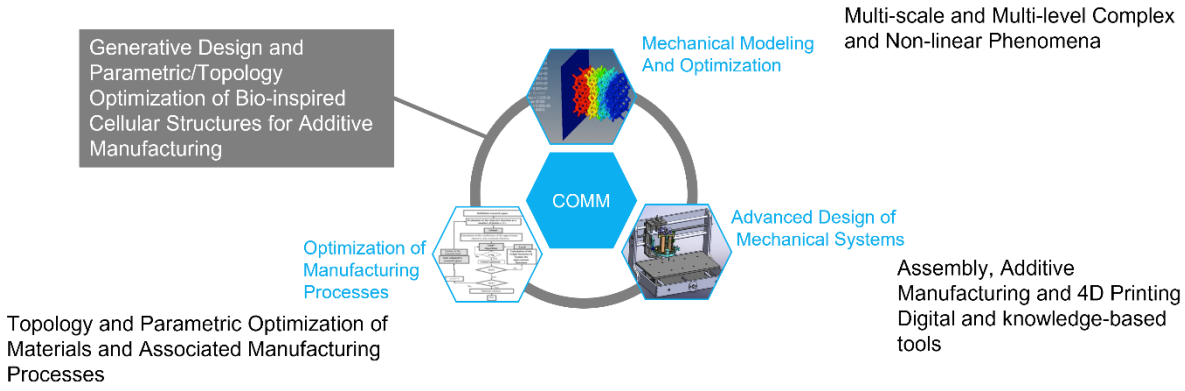

Figure 3. Research fields inside the ICB-CO2M lab.

1.3. Thesis Structure

Figure 4 describes the structure of the PhD dissertation and how the state of the art, research questions, and contributions are presented. After this introductory chapter of research context and related objectives, the posterior chapters are divided as follows:

Chapter 2 conducts a literature review of the domains of biomimetic design levels, aspects, and approaches for AM and optimization as well as lattice and cellular structures.

Chapter 3 addresses the intersection of both "Design for AM" and "Topology Optimization" cross-domains. It presents a coupled topology/parametric optimization framework of lattice structures for AM. This contribution focuses on a comparison between a uniform lattice distribution and a variable-density lattice structure. It emphasizes the role of the optimization framework in reducing weight and ensuring a high rigidity. However, it should be noted that while the use of lattice structures is biomimetic (as stated in the section 1.1), the bio-inspired strategy in this chapter is not fully covered. A more comprehensive examination of bio-inspired methods will be discussed in the fourth chapter.

Chapter 4 delves into the cross-domains of "Bio-inspired Design", "Design for AM", and "Topology Optimization". It presents a biomimetic method based on L-systems distribution along the principal stress lines (PSL) directions in a design space and using three different load cases. The aim of this contribution is to support one of the objectives of AM which is optimizing the strength-to-weight ratio. Nevertheless, the method outlined in this chapter involves a series of numerical simulations that are based on a design of experiments approach. However, this method is not entirely accurate as it relies on having prior knowledge of the optimal range for the variables being optimized. Therefore, the next chapter presents a new method that utilizes a combination of biomimetic parametric optimization techniques to improve precision.

Chapter 5 covers the integrality of the cross-domains presented. Thus, it allows reaching the final objective of this PhD thesis. It consists in conducting a parametric optimization algorithm on beam elements used in the L-systems distribution along the PSL directions using a low-cost meta-modeling algorithm based on metaheuristics and knowledge.

Chapter 6 discusses and concludes the presented research works and discusses the proposed contributions as well as the perspectives and future research works.

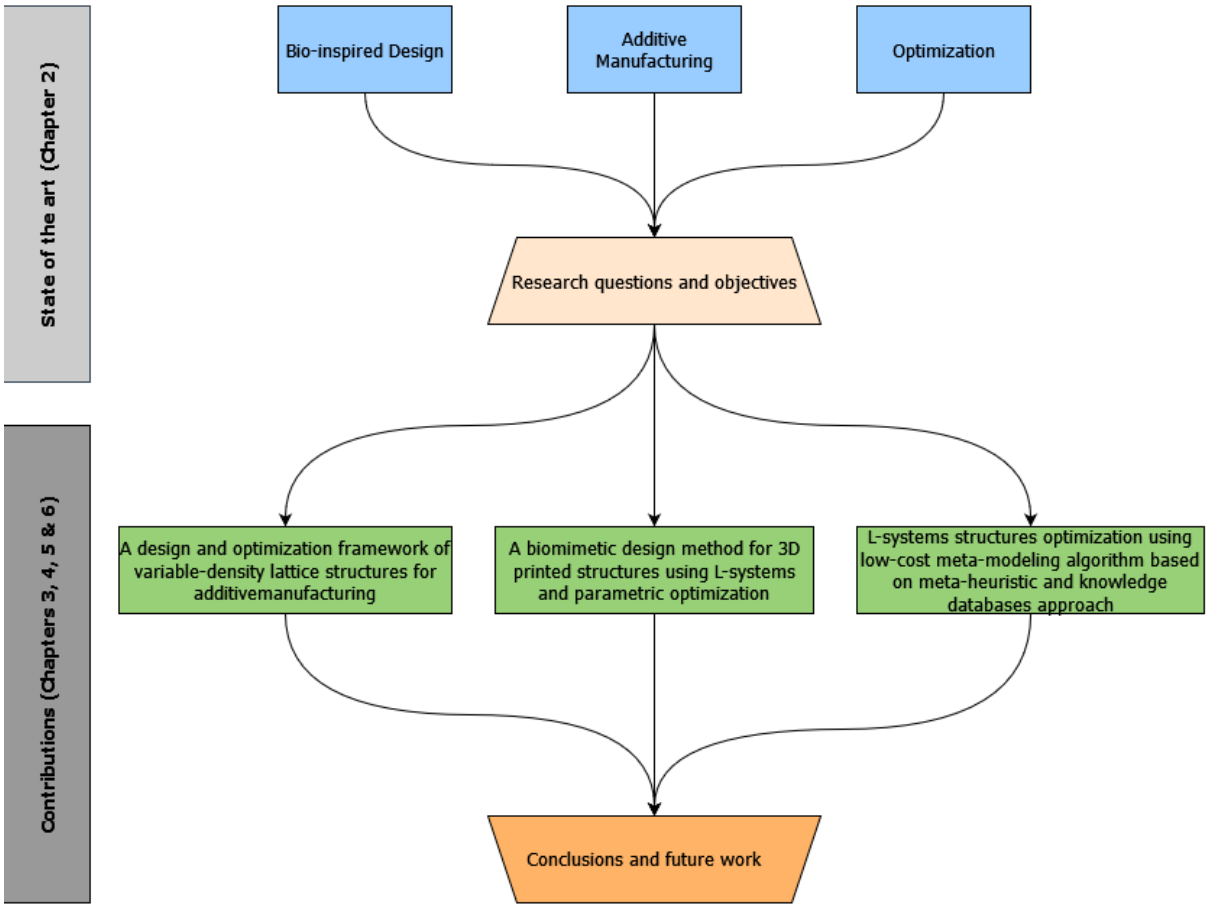

Figure 4. Structure of the PhD dissertation.

Chapter 2: State of the art and Research questions

"I have been impressed with the urgency of doing. Knowing is not enough; we must apply. Being willing is not enough; we must do."

Leonardo Da Vinci

"Look deep into nature, and then you will understand everything better."

Albert Einstein

2.1. Introduction

This thesis dissertation addresses the topic of bio-inspiration. In this context, the scope of methodological support to facilitate the integration of life sciences knowledge into technological development is of particular interest. As highlighted in the first chapter, relevant research originates in design engineering, life sciences, as well as in the field at the crossroads of these two scientific fields. This chapter highlights the constraints imposed by AM techniques to be considered while modeling biomimetic designs and the role of optimization in meeting the requirements inflicted by these techniques in terms of material distribution and mechanical properties. In the first two sections, the evolution of biomimicry will be discussed and the levels of imitating nature using different approaches will be detailed, thus linking biomimetic design to the three fields of AM, optimization, simulation, and lattices. In the third section, the research questions will be addressed, and to which later chapters will respond.

It is important to mention that the state of the art related to each cross-domain introduced in the first chapter will be detailed separately in the introductions of chapters 3, 4, and 5 as follows:

- the issues and research problems linked to design and optimization for AM and the use of lattice structures;
- the natural properties and aspects that inspired the development of the tool in the fourth chapter and how biomimetic design can solve the issues addressed in the previous chapter;
- the use of biomimetic parametric optimization in latter research works and their application in a biomimetic design problem.

2.2. Bio-inspiration: an overview

Boundaries of bio-inspiration, despite the simplicity of its definition, should be delineated: Its interdisciplinary nature and scope make it necessary to take a certain step back to understand the concept and its application in different domains.Thus, several sub-concepts should be addressed and explained (Figure 5).

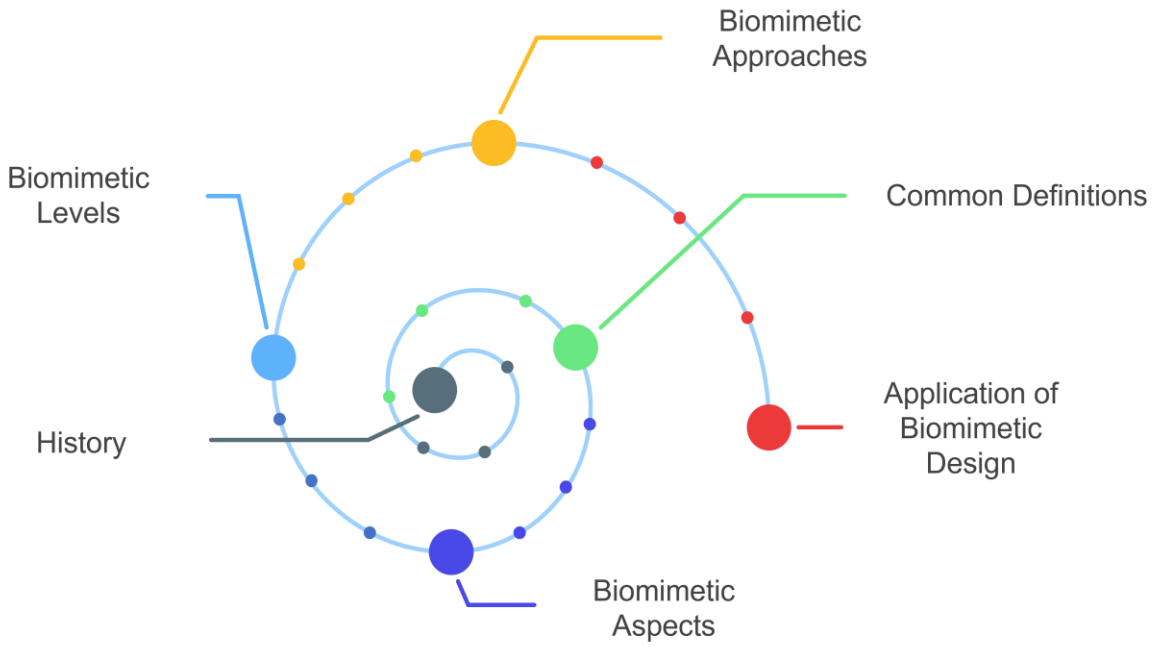

Figure 5: Overview and sub-concepts of bio-inspiration.

2.2.1. History

The exact date of emergence of bio-inspiration is hard to define and formulate. If any, one of the first traces to be considered dates back to the Renaissance through Leonardo da Vinci and his studies of bird's flight and his design of his Ornitoptera and automatons [45].

Abbas Ben Fernas (810-887), who instigated the human sedition of air fly, never stopped trying to decipher the mechanism carried out by birds [46]. Nearly a thousand years later, at the end of the 19th century, Otto Lillenthal (1911) designed his sailing aircraft after studying the lift capacity of the upper surface of the bird's wings. Another century will pass before Clement Ader, fascinated by bats, realizes his third aircraft with unprecedented features of air dynamics [47]. All this work, among many others, led the Wrights brothers to success in 1903 [48], with Flyer inspired by the Eagle, which ended up leaving a bioimmune footprint in flight. Many of the innovations in aviation to date (such as the Great American Bird Wings, and insect-inspired microdrones) are still inspired by nature (Figure 6).

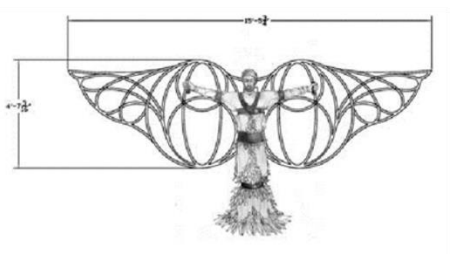

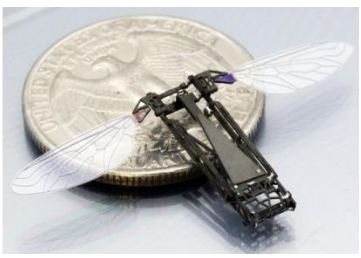

Figure 6. Left to right: Bio-inspired aviation and flight from Abbas Ibn Firnas flight to Clement Ader airplane to insect-inspired microdrones.

In other domains, bio-inspired architecture emerged at the end of the 19th century. The Eiffel Tower (1889) is an often-unexpected example of bio-inspiration. Forty years after its construction, Hermann von Meyer laid the foundation for the tower during a study in Zurich that looked at trabeculae, a latticework of bony protrusions that can withstand tons of pressure. The transfer of knowledge between Zurich and Paris was handled by Karl Cullman, who translated Meyers' discovery into the mathematical model that Gustave Eiffel used to build his famous tower [49]. However, the Eiffel Tower is not the only example that highlights the bio-inspiration in art and architecture. Ripley & Bhushan (2016) [50] have enumerated several examples in these domains (Figure 7):

- Support columns in Durham Cathedral in Durham, UK, under the direction of William of St Carilef (completed c. 1100) inspired by individual trees.
- Support columns in La Sagrada Familia in Barcelona, Spain, by Antoni Gaudí (1882), inspired by groups of trees.
- Rib vaulting in Exeter Cathedral in Exeter, UK, by an unknown architect (completed c. 1400), inspired by ribs with intercostal muscles.
- Composition in Gray and Light Brown by Piet Mondrian (1918), organized by the golden ratio.
- Bone Chair and Bone Armchair by Joris Laarman (2006, 2008), inspired by bone structure.

Special attention can be paid to the Bone Chair and Bone Armchair example as the process used can be utilized in other domains of applications. In fact, Joris Laarman studied how the internal structure of the bone grows and used software to create the structure of the chair in much the same way. This process required removing material where the structure could be lightened and adding material where the structure needed to be strengthened. This created a chair that is structurally very sturdy, yet lightweight in both weight and appearance. Joris Laarman has used this process in different fields going from furniture to 3D printed bridges [51].

Figure 7. Examples of bioinspiration in architecture and art derived from nature: support columns in Durham Cathedral in Durham, UK, under the direction of William of St Carilef (completed c. 1100), inspired by individual trees; support columns in La Sagrada Familia in Barcelona, Spain, by Antoni

Gaudí (1882), inspired by groups of trees; rib vaulting in Exeter Cathedral in Exeter, UK, by an unknown architect (completed c. 1400), inspired by ribs with intercostal muscles; Composition in Gray and Light Brown by Piet Mondrian (1918), organized by the golden ratio; Bone Chair and Bone Armchair by Joris Laarman (2006, 2008), inspired by bone structure.

Architecture is not the exclusive domain of expression over the ages of bio-inspiration. Similarly, science has benefited greatly from the dissemination of knowledge from life. It was in 1637 that René Descartes based on the work of William Harvey first articulated the idea that animals can be assimilated into "machines", operating according to mechanical principles. This approach influenced the work of Giovanni Borelli (2012) as a starting point for the field of scientific research that constitutes biomechanics. Similarly, science has greatly benefited from the dissemination of living knowledge.

- Eli Metchnikoff (Nobel Prize 1908) laid the foundations of the non-organ-specific autoimmune defense, phagocytosis, in 1882, by observing the universality of the defense mechanism of the larvae of starfish. He later referred to his discovery as "immunity."
- Paul Portier and Charles Richet (Nobel Prize 1913) discover anaphylactic shock (heightened immune response) by studying the venom secreted by the fishing filaments of oceanic physeal jellyfish.
- Hodgkin and Huxley (Nobel Prize 1963) explained the mechanism of transmission of nervous impulses through experiments on squid.
- Kandel (Nobel Prize 2000) discovered the key elements of Aplysia's long-term memory.

2.2.2. Common definitions of bio-inspiration

Bio-inspiration has been existing since ancient times, but its approach and fromalization have evolved throughout the centuries. In the course of this evolution, concepts relating to bio-inspired design have been defined in different ways within the literature and within the ISO/TC266 norm [52]. The definitions serve both to specify, but also to delineate what is included, and therefore reciprocally what is excluded, from each of the terms. Common global definitions according to two previous PhD theses stated that bio-inspiration is:

"... a methodological approach to understand, model and transfer problem-solving strategies from the living world to lead to technological innovations." [53]

"a range from simple inspiration promoting creativity in general to the design of new solutions." [54]

Bionics

The term bionic is a construction based on the Greek root βίος (bíos) ("life") to which is added, in French, the suffix –ic from electronics, in English, the suffix –ics from electronics, and in German, the suffix –ik from mechanik.

As the oldest term related to biological inspiration, it would still be an oversimplification to stay on strict etymology in order to understand the meaning and origin of the term. According to the Academy's Dictionary, the term "bionic", "consisting of the radicals of biology and the final of electronics", is "a science that studies biological processes from a technical point of view, to discover principles that can be applied in the military or industrial field." So, bionics invest especially in the mechanical properties of life, and strive to transfer them to the field of engineering; thus, incorporating robotics, and developing bio-inspired or biomechanical sensors [55].

Biomimicry

The first mention of the term is attributed to Merril (1982) [56] and their formalization of the thesis work in the field of chemistry entitled “Biomimicry of the Dioxygen Active Site in the Copper Proteins Hemocyanin and Cytochrome Oxidase”. The growth of this term took place during the 1990s, through the emergence of green bio-inspiration [57]. Nachtigall (1997) [58] was one of the first to introduce sustainability criteria as an integral part of bionics. It is under the influence of Benyus (1997) [3] through her book "Biomimicry: Innovation Inspired by Nature", that the term acquires the importance that is today, as well as its meaning:

“… a new science that studies nature's models and then imitates or takes inspiration from these designs and processes to solve human problems.”

Biomimetics

The word biomimetics is built on the same Greek root βίος bíos coupled with the ancient Greek μιμητικός, mīmētikós ("imitative"). The foundations of the term are, as for the bionic, deeper than its simple semantic analysis.

The first use of the adjective biomimetic was anonymously attributed, by the Oxford English Dictionary, to the index of volume 132 of the magazine Science, published in 1960. The index refers to two articles, each proposing a new name for a convention on devices simulating biological functions [59]. According to Pohl & Nachtigall (2015) [30] in their book “Biomimetics for Architecture & Design”, biomimetics is the most recent terminology and is the most professionally accepted. While the “biomimicry” term’s literal meaning is “imitation of life”, the term “biomimetics” means understanding biological structures and processes and their comparable applications or procedures. Pohl & Nachtigall (2015) [30] extended the meaning of the term “biomimetics” as follows:

“Biomimetics is not the mere imitation of nature, neither in material and functional nor in creative regard, rather the grasping of natural principles to aid in the comprehension of analogous, technological questions, which could then be solved by the applications of optimized technologies.”

According to the definitions presented, the terms bio-inspiration, bionic, biomimicry, and biomimetic can be distinguished according to a specificity of analogy and a relative domain of application. According to these lines of analysis, bio-inspiration ranges from the simple inspiration promoting creativity in a general way (relative to the divergent phase of creativity), to the design of new solutions (relative to the convergent phase of creativity). This concretization of ideas can be based on a vague analogy by adapting generic principles extracted from biology (bio-inspired design) or by abstraction, transfer, and application of knowledge from specific biological systems (Biomimetics). The definition of biomimetics implies a fine understanding of the underlying phenomena discovered in nature, which is not indispensable for bioinspired design.

The terms “bioinsp*” and “biomim*” have been increasingly used in the literature over the last two decades. A quick research of these keywords on the Collection Web of Science shows that the number of publications using these terms has been multiplied by ten in 2021 in comparison to 1998 (Figure 8). The importance of bio-inspiration in different application fields is then underlined and the biomimetic design has been revolutionary.

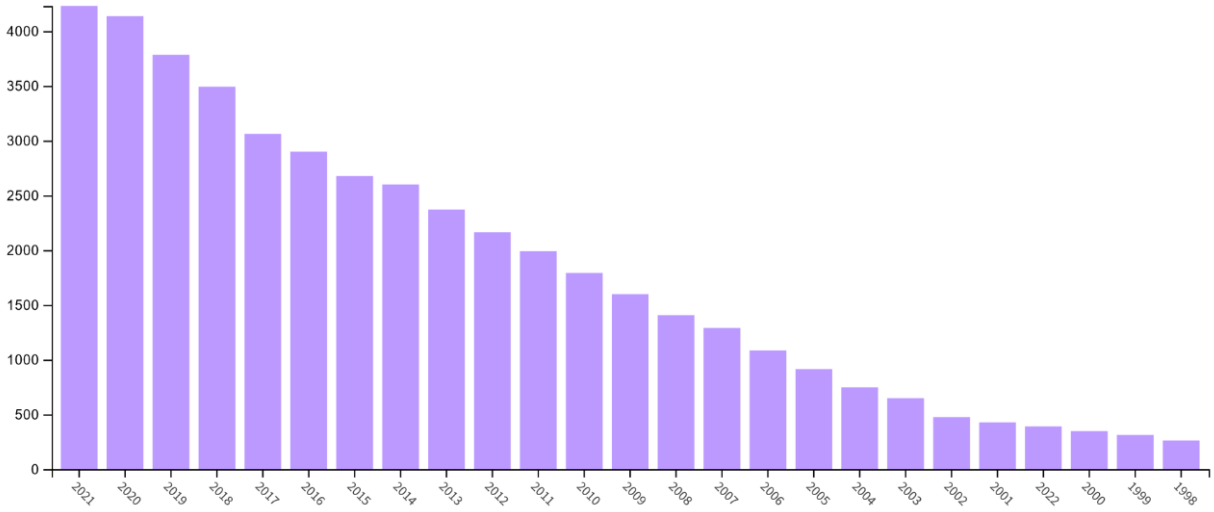

Figure 8. Data illustration of the research of "bioinsp" OR "biomim*" in the Web of Science database (introduit la date de la requete).*

2.3. Biomimetic Design

Biomimetic design is an interdisciplinary approach; it links biology and technology to generate knowledge that transcends disciplinary boundaries. Helms et al. (2009) [60] defined bio-inspired design as the use of “biological systems to develop solutions to engineering problems”. Understanding a biomimetic design’s aspects, levels, and approaches is required for its elaboration. This section will focus on the first cross-domain the “bio-inspired design” as shown in Figure 2 in the first chapter.

2.3.1. Biomimetic Design Aspects

In their book “A practical Guide to Bio-inspired Design”, Hashemi Farzaneh & Lindemann (2019) [61] enumerated “Ten Amazing of Bio-inspired Design”. They can be summarized as follows:

- ***Abundance of Biological Solutions***

Biology offers a large pool of possible solutions to technical problems. In the digital age, access to biological inspirations is also becoming easier. Digital databases such as ***asknature.org*** provide access to thousands of biological inspirations.

- ***Optimization***

It can be assumed that, if a biological system is optimized, the bio-inspired design is optimized as well. “Biological systems have been optimized by evolution” [62]. Biological systems must fulfill multiple goals but most of these goals remain unknown. In addition, many species have developed similar solutions to similar problems, despite having different ancestry. For example, African and American cactuses are very similar in the form of water-retaining properties. They both adapt to hot and dry climates similarly. This convergence of adaptation can be seen as a powerful indicator of an optimized solution [63].

- ***Synergy Effects and Transdisciplinarity***

Technical product development can not only benefit from biologically inspired designs, but also from biological research. Nachtigall [58] has defined technical biology as the study of nature using the tools of science. He argues that one must have a good understanding of technical biology before attempting to design with bio-inspired principles.

- ***Multifunctionality of Biological Systems***

Multiple requirements must be met by biological systems while limited resources are used. Particularly, the functionality of a technical application can be inspired by a biological system. This results in multifunctional biological products [60]. For example, several biological materials, such as bones or shells, are resistant, lightweight, and self-healing. This combination of functions and properties is certainly of interest for technical materials.

- ***Integration of Material, Shape, and Function***

The design principle of “form follows function” is frequently used in both architecture and industrial design. Technical systems are often made of monolithic materials (such as steel) and perform functions on only a few or one scale level: Biological systems frequently use both the composite material qualities and form to fulfill functions on various scales. One example cited by Hashemi Farzaneh & Lindemann

(2019) [61] is the tree or torrent frog's toe pad structure. Its form on the microscale and nanoscale (hecamers) appears to be responsible for its adhesive qualities which are observable at the macroscale level (pillars).

- ***Discovery Beyond that Which is Human-like***

The biomimetic design does not only focus on the inspiration from only humankind. It is an extended domain that counts on the understanding of the plants and animals' forms, growth, properties, and ecosystems.

- ***Flexibility of Bio-inspired Design***

Bio-inspired design is very adaptable and flexible. One can rapidly look for inspirations by using the internet. It is also possible to explore for current technological knowledge to better understand the "how to adapt the bio-inspired design". In fact, flexibility here means that the designer can apply natural and biological data in multiple domains. And that is what is called "interdisciplinary collaborative research projects": Bio-inspiration is not restricted to a particular domain application.

- ***Sustainability***

Biology can provide a fundamentally different approach to sustainable design. The traditional approach to achieve sustainability is to reduce the effect of technology on the environment, for example by reducing the systems' weight to minimize the materials' waste. The bio-inspired approach can be founded on an understanding of a full ecosystem, its elements, and balancing interactions.

- ***Biodiversity***

Bio-inspired design has a potential to benefit society in addition to being useful for science and technology. It draws attention to the benefits of biodiversity and the creative solutions found in nature. Innovative bio-inspirations that assist technology advancement cannot be achieved unless biodiversity is maintained. This insight is essential in a time where the development of industry and preservation of environment are still seen as diametrically opposed.

- ***Bioligization***

Designing biological systems requires an understanding of biology at the molecular level. Additionally, it requires a multidisciplinary approach: the differences between the traditional natural sciences of biology, chemistry, and physics on the one hand, and the technical, and engineering disciplines on the other hand, becomes blurry. Technology may progressively incorporate biological systems into technological systems rather than just mimicking them. This expands the scope of biomimetic design

and may aid in the resolution of some of the century's most pressing issues, such as energy consumption and sustainable economies [64].

2.3.2. Biomimetic Design Levels

Although numerous biomimetic approaches were briefly enumerated in the last section, only three levels of biomimicry are required to deepen the understanding of bio-inspiration. Janine M. Benyus [65] suggested that mimicking nature can be classified into the following three levels:

- ***Natural form level:*** Nature gives a complete image of a wide range of shapes and forms. These forms allow the organisms to adapt to the changing conditions in their habitat.
- ***Natural process level:*** Many species encounter similar environmental issues as humans, but they strive to address their problems within the constraints of energy and material availability, and they continue to create solutions even when environmental obstacles alter. The behavior of the organism is replicated and imitated in this level of biomimicry, not the organism itself.
- ***Natural ecosystems level:*** This level of biomimicry has the design advantage of being able to be combined with two other levels of biomimicry as well as sustainability principles. This level is further subdivided into the "circular economy," which means that no byproducts should exist.

To better understand these levels, Figure 9 illustrates the examples enumerated by Janine M. Benyus [65] in “A Biomimicry Primer”. At the form level, one can mimic the hooks and barbules of an owl’s feather to create a fabric that opens anywhere along its surface for example. At the process level, the self-assembly at body temperature property that the owl feather possesses can inspire the field of green chemistry. At the ecosystem level, the owl’s surrounding ecosystem that made the owl have these features should be a source of inspiration for sustainability. As Janine M. Benyus [65] stated:

“Our owl-inspired textiles must be part of a bigger economy focused on repairing rather than depleting the world and its inhabitants. We are missing the point if we employ green chemistry to manufacture bio-inspired textiles but have people weave them in sweatshops, load them into polluting vehicles, and distribute them far distances.”

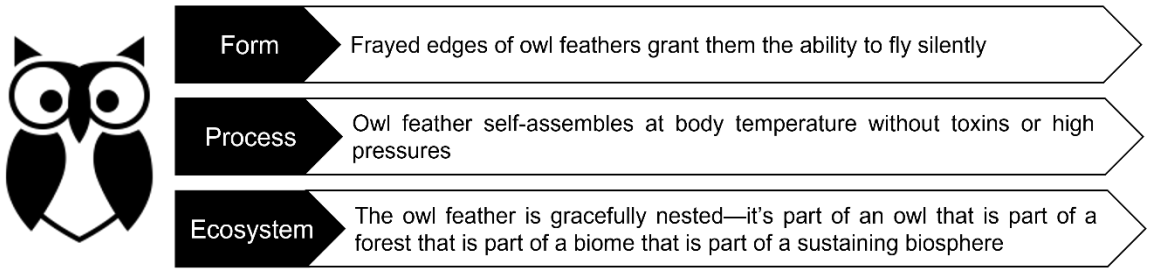

Figure 9. Understanding the biomimicry levels through owls.

2.3.3. Biomimetic Design Approaches

Considering that biomimicry is a design process, elaborating the biomimetic product can follow two different approaches: the ***Top-Down*** approach and the ***Bottom-Up*** approach. According to a research held at the Georgia Institute of Technology by Helms et al. [60], the first consists of six steps while the second of seven steps (Figure 10).

Top-Down Approach

This approach has different names as ‘‘Design looking to biology”, ‘‘Top-down Approach”, ‘‘Problem-Driven Biologically” Inspired Design”, and ‘‘challenge to biology” (Biomimicry Institute).

In this approach, designers look for answers in the living world, which necessitates the identification of problems by designers, who are then compared to organisms that have addressed comparable difficulties by biologists. The problem-based approach model follows a set of processes that are non-linear and dynamic in nature, in the sense that the outcomes of later stages frequently impact earlier stages through iterative feedback and refinement cycles [60]. This technique might be a means to start the shift of the artificial environment from an unstainable to a more effective paradigm.

Bottom-Up Approach

Just like the previous approach, this approach has different names and expressions such as “Biology Influencing Design”, “Bottom-Up Approach”, “Solution-Driven Biologically Inspired Design”, and ‘‘Biology to design”.

In this approach, the design process depends on having knowledge of relevant biological or ecological research rather than determined design problems. The way designers think about and prepare solutions to problems has the potential to change as a result of this strategy. The fact that biological research must be undertaken and then judged to be pertinent or not, is a drawback of this approach from the perspective of design.

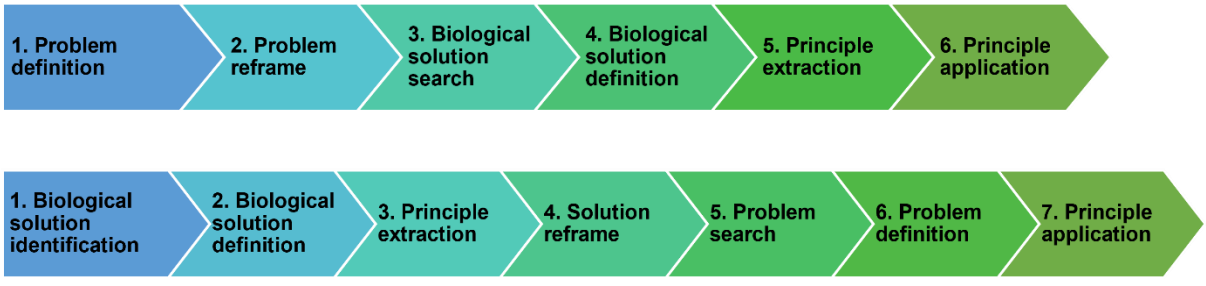

Figure 10. Top-down approach (up) versus Bottom-up approach (down) as defined by Helms et al. [60].

However, du Plessis et al. (2019) [29] identified three more different ways of obtaining a designed biomimetic model: customized and freeform design, simulation-driven design, and cellular and lattice design (Figure 11). These approaches will be detailed in the next sections.

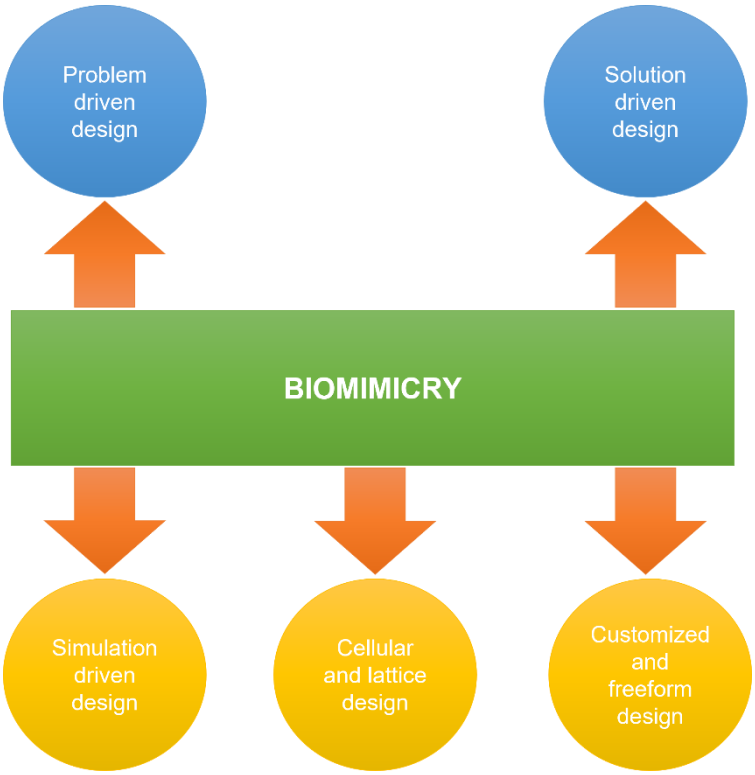

Figure 11. Biomimetic design approaches for AM as described by du Plessis et al. (2019) [29].

Customized and freeform design

The ease of subtractive manufacturing results in classic designs with straight angles and flat surfaces. Sophisticated manufacturing processes (such as AM, many-axes machining, advanced casting techniques, and so on) have grown more accessible and viable in recent years, giving design engineers greater latitude to develop components with more complicated designs. These new design skills enable organic shapes and freeform designs, which are sometimes referred to as biomimetic because their organic shapes resemble natural structures and, in the case of medical devices, the forms are sometimes designed to fit natural materials like bone implants. Curves and organic forms predominate in natural structures because they strike a compromise between minimal energy and material usage on the one hand, and maximum work return on the other hand. This should be assured while remaining within the constraints or the organism's growth potential. Freeform and customized design may be referred to as biomimetic as they share similar characteristics with natural structures but lack the limitations imposed by the organism itself [66]. Traditional engineering thought is generally confined to expertise with right angles and flat surfaces, despite the design freedom. Additional tools are required to make the most of this increased creative flexibility. One of these is the use of rational B-spline (PolyNURBS) to shape curved and organic surfaces. Biomimetic designs with curved surfaces that imitate natural formations

are possible using these techniques. These are particularly important tools in the latter stages of topology optimization, as well as in real biomimetic reverse engineering structures, allowing for models with curved geometries. These tools not only enable creative curved forms in a relevant workspace, but they also successfully transform them into geometries suited for simulation and AM. The main advantage of the freeform design tools is the ability to create artistic curved and organic features resembling biological structures. They are especially used in arts, fashion, and jewelry artistic creations [67].

Simulation-driven design

One of the first pioneers in the simulation-driven design must be Julius Wolff, an orthopedic surgeon of the 19th Century, who stated that:

"As a consequence of primary shape variations and continuous loading, or even due to loading alone, the bone changes its inner architecture according to mathematical rules and, as a secondary effect and governed by the same mathematical rules, also changes its shape." [68].

From this arose the notion of topology optimization, which is based on the idea that a structure may be optimized by tracking load routes and then adjusted to match a certain mechanical need.

In the early 1990s, the first industrial-class software solutions including design principles, the capacity to collect 'loading,' and the limitations to automatically construct 'biomimetic' design were launched. This was largely the start of CAE simulation as a source of design inspiration. Many manufacturing restrictions have been incorporated throughout time to shape these designs so that they are aware of downstream production and apply to various manufacturing processes. If the part is made via extrusion, the extrusion constraints will result in a form that can be extruded over the corresponding design space. Overhang limitations in AM provide geometries with minimal support requirements during construction in a particular print direction, such as fewer horizontal sections. In AM, there are a variety of manufacturing constraints, as stated in previous sections, that may be introduced into the design optimization process, and it is through incorporating them into the topology optimization process that designs that are suitable for production can be created. In the context of AM, simulation-driven design refers to the use of simulation to numerically create and optimize a given space to match some desired performance requirements under a set of loading and/or manufacturing constraints. In the context of AM, this can refer to either topology optimization or generative design, which are typically used interchangeably because they both entail simulation. The term "topology optimization" refers to the process of improving a "starting" form or design space. Exploring several different designs inside a particular space to identify an ideal solution from several probable solutions that match the same performance requirements is referred to as generative design. In DfAM, both techniques are targeted at developing lightweight components that predominantly include material where the load is encountered, and material is eliminated where it is not required. This simulation and material removal or addition

procedure is continued iteratively until an optimization objective is met, and this iterative approach can be compared to the evolutionary process [18].

Cellular and Lattice design

Cellular and lattice structures are abundant in nature under several forms, shapes, and arrangements. The most known examples of these structures are bee's honeycomb, trabecular bone, and wood cells [69]. The fundamental advantage of cellular or lattice structures is their ability to achieve performance goals while allowing for substantial weight reduction, which is a natural concept [70]. Effective stiffness and strength of lattice materials are generally customized to the application and can be locally altered. Lattices may be used for more than just light weighting: they have remarkable thermal, acoustic, and energy absorption rates when compressed and they play an important protective role in nature [71,72].

From an engineering point of view, cellular materials are created in commercial software programs using various ways. Traditional CAD software use mesh-based representations, but recent software developments are investigating the use of volumetric object representation to generate surfaces and implicit modeling via the definition of fields and equations to create cellular structures (like Ntoplogy for example [73]). Mesh-based techniques permit integrating lattices in complex parts and components. The disadvantages here lie in the limitation of the design options: the structure is constituted of struts only, there is no control over the build angles. The user can choose a unit cell from a larger range of cellular designs using the volumetric representation technique (struts, sheets, carrying unit cell size and angles, number of struts and nodes, etc). The repeated unit cell technique makes the design process easier by allowing for comparatively straightforward prediction of the structure's mechanical characteristics.

Figure 12 depicts a succession of unit cells and their matching repetitive lattice structures. Although they all have the same overall density, the designs result in varying minimum feature thicknesses and pore diameters. The first four are strut-based designs, followed by four minimal surface designs. The latter may be found in nature [74] and has been proven to have favorable qualities for use in bone implants [75]. These minimum surfaces are sheet-based designs that are frequently self-supporting and have zero average curvature at every point on the surface, resulting in a more evenly distributed stress distribution inside these structures.

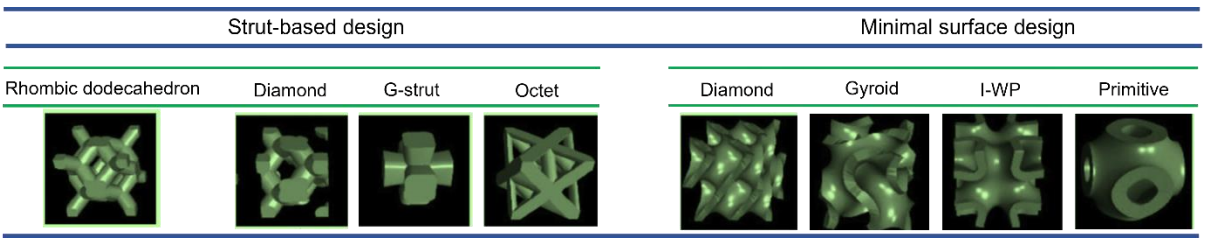

Figure 12: Unit cell designs of different types of lattices [76].

The most common application of lattice architectures, which has prompted a lot of studies, is in medical implants. Pore diameters are often modest in this application, necessitating small feature sizes in general. Thicker lattices may be preferred in non-medical applications, such as lightweight constructions for aircraft or automotive parts, to emphasize mechanical reliability and strength [77-78].

Despite the expanding availability of design tools that can generate cellular structure designs, determining the optimal unit cell for a certain application is not always obvious – and this becomes much more difficult in the case of multi-functional design. The biomimetic design may play a vital role in this setting, by assisting in the development of structure-function correlations based on observations of cellular materials in nature and using them to drive cellular material choices. Natural cellular materials include the whole parameter space employed in design, from beam or strut-based materials to surface-based materials, as illustrated in Figure 13, as well as structures that incorporate both types. These cellular components can be found both inside a form (such as bone) and on its surface in nature [79].

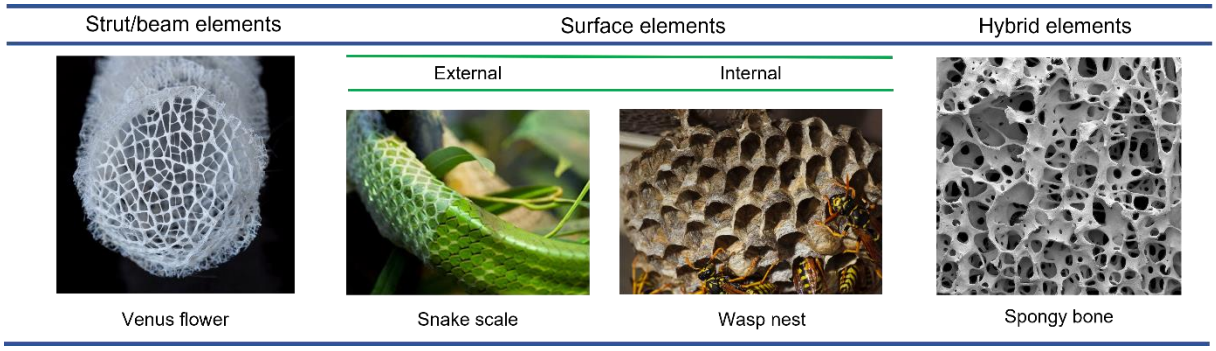

Figure 13: Examples of cellular structures in nature classified by their type and form [80].

2.4. Research context and questions

In previous sections, biomimetic design was introduced, and its different definitions, aspects, levels, and approaches were detailed. However, each of the approaches presents several limitations. Both Bottom-Up and Top-Down approaches necessitate knowledge of problems and solutions presented in nature that can be applied to the design and parts. Freeform design does not have limitations, it does not depend on a design space, which can be a drawback while elaborating concepts that use genertative design methods. The simulation-driven design depends on a series of numerical simulations which can be expensive. Although knowing this information ahead of time is essential for a qualified and high-productive design process. As for lattice and cellular design, the distribution of unit cells must be well thought out in order to meet the requirement of the designer. In this dissertation, these requirements are imposed by AM techniques: lightweight and high stiffness. Thus, the following research questions (RQ) arise:

- RQ1: Which strategy should be used to achieve a lattice structure with a good stiffness-to-weight ratio? Which is more suitable: a uniform or a variable-density lattice distribution?

- RQ2: How can one improve the stiffness of bio-inspired mechanical parts and structures while assisting the designer in defining a preliminary design space using biological algorithms and aspects?
- RQ3: Which optimization technique is more suitable to obtain a better parametrized cellular biomimetic structure?

In order to answer these questions, three research objectives were studied (Figure 14):

- A design and optimization framework of variable-density lattice structures for additive manufacturing.
- A Biomimetic Design Method for 3D-Printed Lightweight Structures Using L-Systems and Parametric Optimization.
- L-systems structures optimization using a low-cost meta-modeling algorithm based on meta-heuristic and knowledge databases approach.

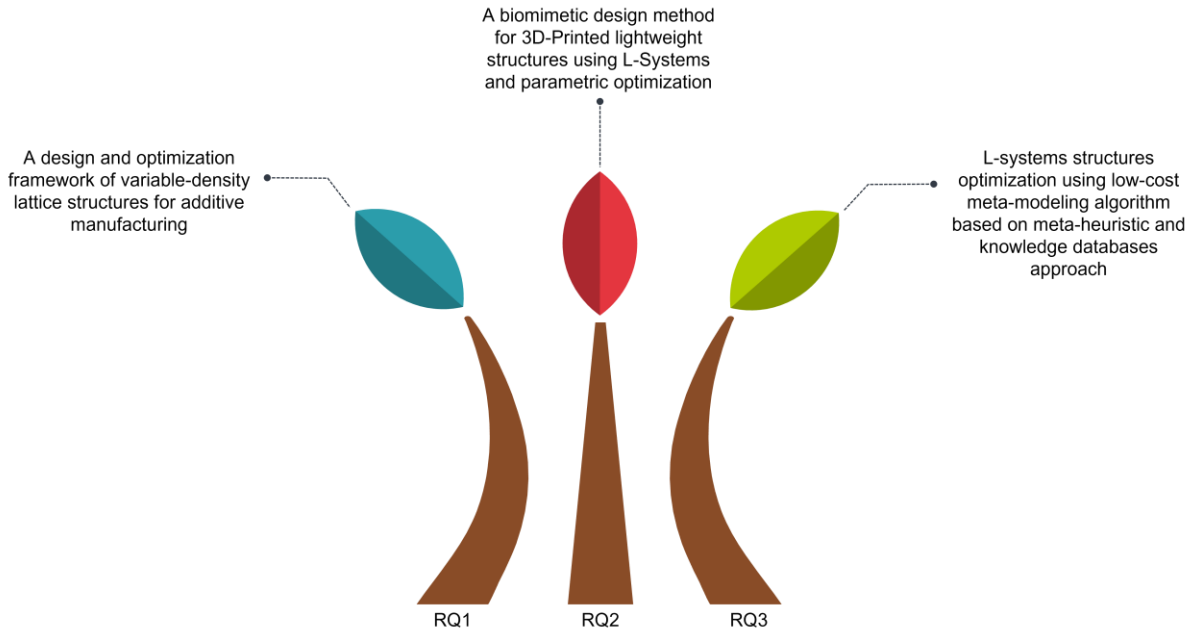

Figure 14: Research objectives related to each research question.

Chapter 3: A design and optimization framework of variable-density lattice structures for additive manufacturing

"The noblest pleasure is the joy of understanding."

Leonardo Da Vinci

"We cannot solve our problems with the same thinking we used when we created them."

Albert Einstein

3.1. Abstract

With the development of additive manufacturing (AM), research interest is currently focused on lattice structures development due to their interesting mechanical properties. It implies the opportunity at the engineering level to be able to specify – beyond the shapes – mechanical properties distributed in the space to be manufactured. This study aims at introducing a design and optimization framework for AM, which highlights variable-density lattice structures. By processing both a topology optimization within a rough design space and a design of experiments driven parametric optimization, the development process of suitable and specific strength structures for AM becomes seamless and efficient.

3.2. Introduction

The exponential development of additive manufacturing (AM) technology and associated materials provide design freedom in developing complex parts or/and even assemblies [81], whether in terms of their shape, structure or even their behavior in response to a stimulus in the broader context of 4D printing [82–84]. In such a context, numerous scientific efforts have been made to develop lattice structures (i) optimized in terms of their configuration or even their density at fixed shape, and (ii) topologically optimized, thus influencing their shapes [85]. Due to its printing capabilities and its layer-by-layer deposition mode, AM processes and techniques are suitable to fabricate lightweight and lattice structures [86]. According to Pan et al. [87], the combination of lattice structures and AM technology provides an opportunity to develop complex structures whether for industrial design or a wide spectrum of application domains like aerospace, automotive and medical fields [88]. Fabricating lattice structures with AM technology has several advantages, it indeed provides design flexibility including a wide range of sizes, materials (rubber, metal, alloy, ceramic, fiber, etc.) [89], automated processing, energy saving and cost reduction [16,90]. These advantages are directly related to the mechanical properties of lattices, whether lightweight, high specific strength, high stiffness, and high energy absorption rate [38]. A physical object incorporating lattice structures can also exhibit interesting functional properties like shock/sound absorption and heat dissipation [26,27].

To ensure an efficient distribution of materials at the right place in the part to be manufactured, researchers have developed many methods and approaches. Lattice structures can then be defined according to multiple distribution patterns, such as periodic [91], functionally graded [92] and variable-density [93]. By considering such distributions, research work has been addressed on the optimization of thickness and cross section of periodic lattice structures. Rosen [21] have used the lattice strut diameter as an optimization variable and have reduced their number by structuring the lattice struts in thickness groups. Numerical simulations were necessary for each iteration, which leads to time-consuming tasks and the size and number of struts were not considered. In a more advanced study, the

bidirectional evolutionary structural optimization method has been proposed by Tang et al. [94], where the design space is divided into different volumes to fill in the lattices where it is needed. Similarity to Rosen's work [21], an evolutionary topology optimization (TO) is used to determine the optimal struts cross section. Another method based on heuristic optimization using a reduced number of variables was introduced by Nguyen et al. [95]. In their method, a minimal and a maximal diameter were defined so that the lattice strut diameter is interpolated according to the local stress value. The second method is to change the space or the frame of the structure. A lattice structure comprises several unit cells distributed periodically in the 3D design space. The goal here is to resize or reform the unit cells. Chen [96] has proposed a redistribution of matter based on the stress distribution and has used the "warping" spatial deformation technique. In a similar way, Brackett et al. [42] have introduced a dithering-based method to generate variable volume lattice cells for AM, where the size and shape of lattices depend on the distribution of stresses in the design space.

In addition to design methods that aim to redistribute material within a design domain for better performances, few are dedicated to adapt the shape and orientation of the unit cell of lattices to the given design conditions. The design methods for a conformal lattice structure are first proposed by Wang and Rosen [97,98]. The shape and the orientation of the unit lattice cells are altered to suit the macro shape of the design domain. Wang [99] provided a case study to compare the performance between a compliant network and an ordinary periodic network. The result shows that a conformal network can have better resistance than a periodic network as the unit cells of lattices is reoriented according to the external loads. Instead of conforming to the initial 3D design space, an adaptive load lattice design method is proposed by Teufelhart and Reignhart [100-102]. In this design method, the network frame is constructed based on the force flow within the design domain, which allows the orientation of each network of unit cells to be aligned with the principal stress direction of the structure.

Despite all these studies present in the literature, a major drawback can be outlined: they are costly in terms of computational performances, and the computational performances were not called although knowing this information beforehand is primordial to have a qualified and high productive design process. In addition, some of these studies use periodic lattices without considering the removal of material in the unnecessary places and its densification in the places where the stress is important. To face the drawbacks existing in previous studies in terms of reduction of optimization variables, computational time, lack of parametrization strategies, the proposed method aims at gathering both TO for specifying the needed material at the right place through the design space and a parametric optimization of lattice struts ensuring optimized strength-to-weight ratio. The strategy is conducted using two variables which are the cross section and the lattice distribution density, therefore only two variables for the first case of study and six variables for the second. It relies on an optimization through several numerical simulations following the design of experiments combinations. The optimal structure, presenting the best compromise between a light weight and a high strength, is identified after series of

effective simulations and sensibility study. This study does not limit itself to the use of uniform periodic lattices, but it is extended in a way to investigate the effect of variable-density lattices on the weight and the strength of the structure. It also answers the issue of integrating lattices in complex geometries.

3.3. Materials and Methods

The research objective is to introduce a design and optimization framework for AM, which highlights variable-density lattice structures within a design space. By processing both TO on a 3D rough design geometry and design of experiments (DOE) driven parametric optimization, the development process of suitable and specific strength structures for AM becomes seamless and efficient. As such, Figure 15 presents an overview of the proposed framework to compute and generate variable-density lattice structures in a straightforward manner. The resultant optimal structure is printed by a material jetting process (PolyJet®) using a VeroWhite material on a Stratasys® 3D printing machine.

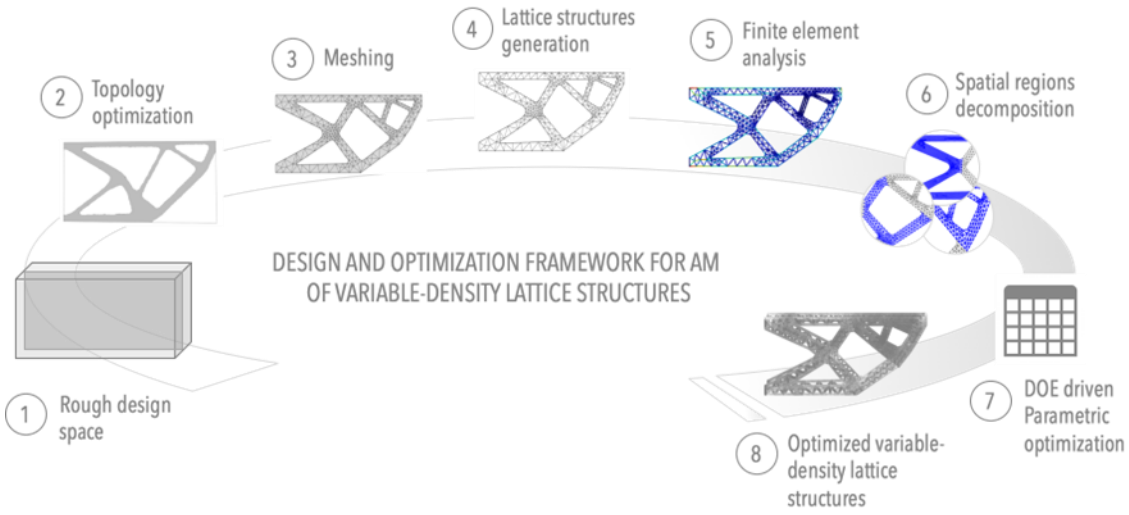

Figure 15: Proposed framework for design and optimization of variable-density lattice structures.

3.3.1. Steps 1 and 2: Rough design space definition and topology optimization

The initial geometry or 3D design space introduced here is a parallelepipedal solid, which has been deliberately kept simple for the sake of clarity. This cantilever part, fixed on the left side, has to support a load of 200 N on its extreme right side. This rough design space associated with its boundary conditions exhibits a plane of symmetry and can then be studied as a 2D (400 x 900mm) classical rectangular surface, as presented in several studies in the literature [103]. From this 2D design input, the geometry presents two points pin at the left side and subjected to a 200 N point load at the right side (see Figure 16). By considering such boundary conditions, a preliminary numerical simulation is conducted to collect the displacement and elasticity limits results. Built on this, two types of TO approaches - respecting different objectives - are then applied: (i) weight minimization (as illustrated in Figure 17.a)

and (ii) stiffness maximization (as presented in Figure 17.b). The resultant geometries, which are generally similar in shape but have different internal material distribution, are then smoothed. Due to its strengthened feature, the selected geometry is the one related to the optimization according to the stiffness maximization.

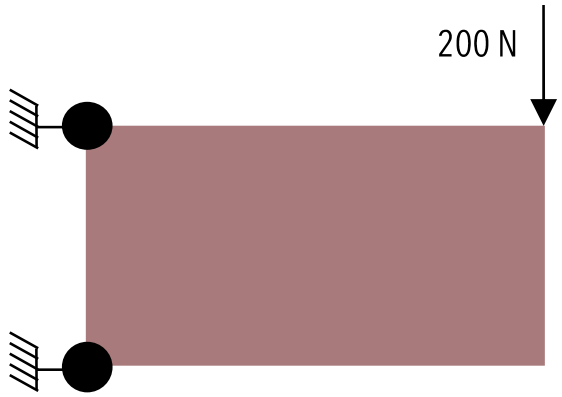

Figure 16: Rough 2D design space with boundary conditions for TO.

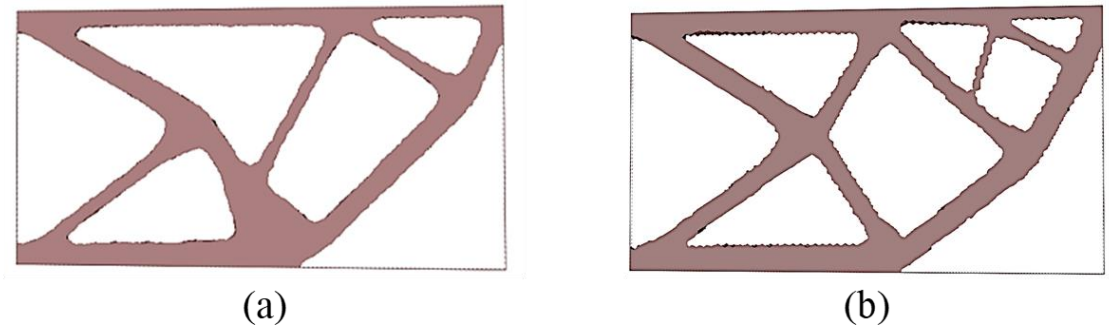

Figure 17: Topology optimized geometries related to (a) weight minimization and (b) stiffness maximization.

3.3.2. Steps 3 and 4: 2D model meshing and lattice structures generation

To work on a topologically optimized geometry, it is a question to define a strategy for lattice structures generation. The present steps aim at defining lattices structures based on a 2D mesh model. This means the resulting topology optimized geometry is beforehand meshed with a computational software like COMSOL Multiphysics®. The proposed meshing follows a triangulation process of the geometry. Figure 18.a shows the 2D mesh model of the topologically optimized geometry, in which minimum and maximum number of elements have been set up and the distribution pattern in the fillets and the corners of elements. For example, setting a large gap between the minimum and maximum number will lead to a coarse geometry with different size of elements while reducing this gap will give a more uniform and finer mesh. An original way of creating lattice consists in reusing the 2D mesh to build the struts forming the lattices (see Figure 18.b). To do so, a MATLAB® program has been specifically developed to extract data from 2D mesh model such as number of mesh points, mesh points coordinates, number of nodes per element and element type (line, triangular, quadrilateral, etc.). By capturing the data in matrix form,

elements connectivity is processed and converted into beam elements. The connection of the elements will be a part of the geometry and will form its entity while the mesh is the subdivision of the geometric space into discrete elements.

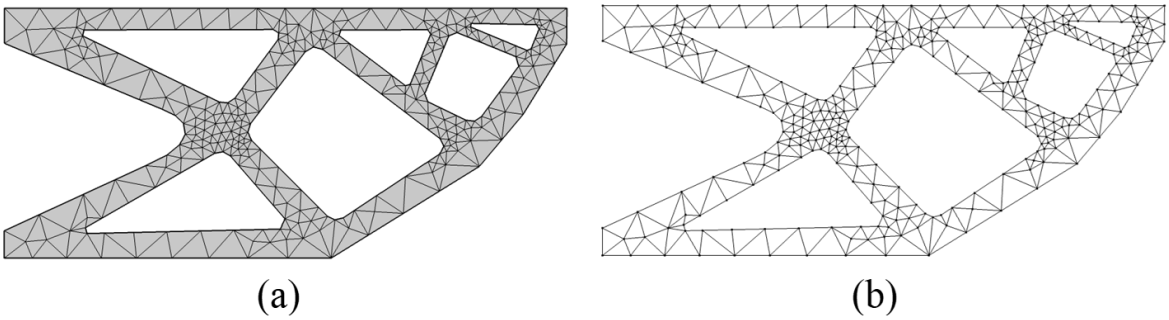

Figure 18: The transformation of a (a) 2D mesh model into (b) a latticed model via a developed MATLAB® application.

3.3.3. Steps 5 and 6: Finite element analysis and spatial regions decomposition

A numerical simulation is then carried out on the initial lattice structures – initially inspired by the 2D mesh model – via the commercial software COMSOL Multiphysics®, in order to determine the most deformed regions and that undergo the highest stress. The structure now presents two linear pins at the left side and a bending point load of 200 N on the right side. The material chosen is VeroWhite and has a Young Modulus of 2495 MPa, a Poisson ration of 0.38 and a density of 1174 kg/m^3. The aim of this study is to find an optimal lattice distribution and a correct parametrization. In order to reach this objective, it was necessary to study a uniform lattice distribution at first to determine the regions where it is necessary to add more material and then proceed to decompose the structure accordingly. The lattice distribution in the lattice structure is this study driven by the density. The latter is defined as the ratio of the volume of the lattice structure (V_l) to the solid structure (V_s) (Figure 17.b) with identical thickness $\rho^* = V_l/V_s$. The volume of the lattice structure changes according to the values of the cross sections thus causing a variation in the relative density. Logically, by increasing the cross section and increasing the number of elements in the structure, the relative density increases, and it approaches a value equal to 1 ($0 < \rho^* < 1$). Two main configurations are then distinguished as follows:

(1) **First configuration.** This configuration consists in three types of uniform lattice distribution (Figure 19). The terms coarse, normal and fine correspond to a pre-set minimal and maximal mesh element size as shown in Table 1.

(2) **Second configuration.** This configuration derives from the first one by using the numerical simulation results for von Mises stress (see the results section). It was noticed that the regions where the load is applied and where the structure is pinned, present higher von Mises stress values than those in the rest of the structure. The structure is then decomposed into three zones as shown in Figure 20.

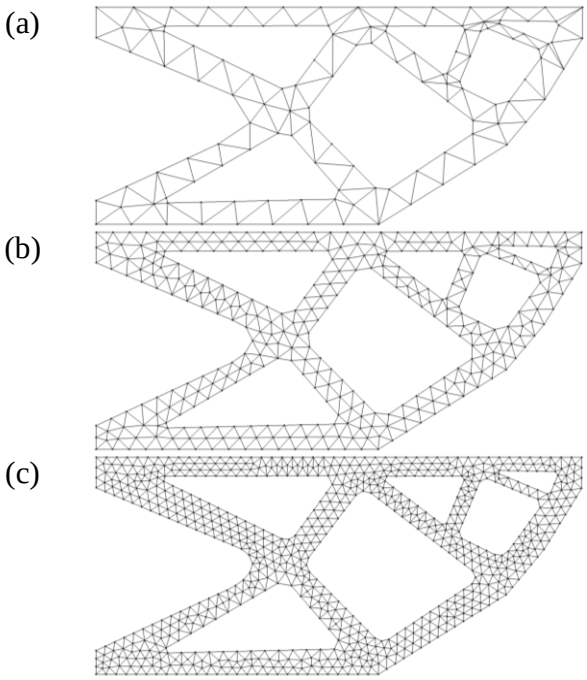

Figure 19: Illustration of the three different lattice distributions for the first case study (a) coarse, (b) normal and (c) fine.

Table 1: Element size definition for the three mesh types.

Mesh Type	Coarse	Normal	Fine
Minimal size [mm]	8	6	4
Maximal size [mm]	7.9	5.9	3.9

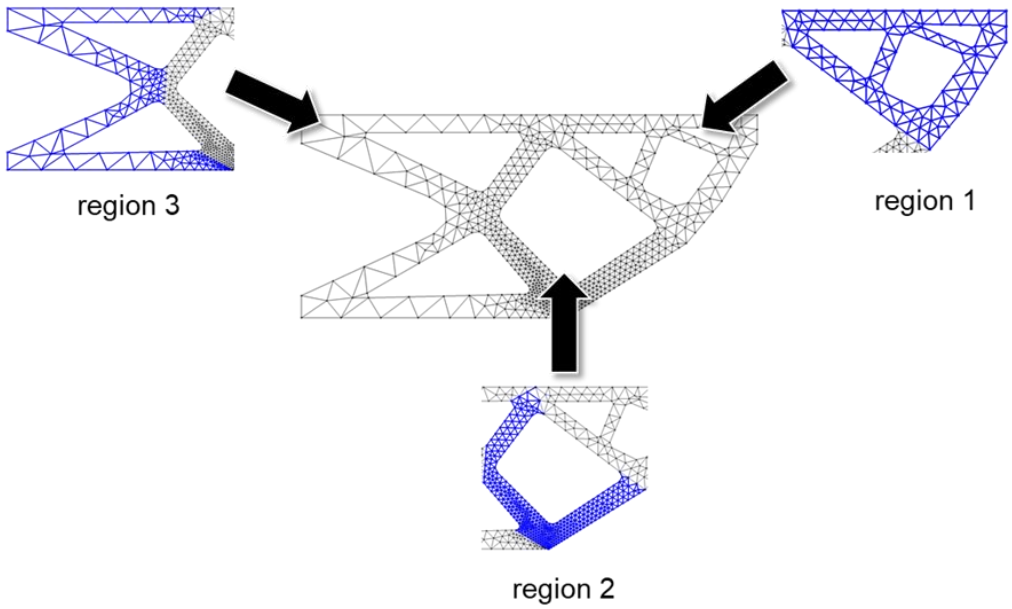

Figure 20: Definition of three regions for the second case of study.

3.3.4. Steps 7 and 8: DOE driven parametric optimization and selection of the optimized variable-density lattice structures

In this part, studying the influence of lattice distribution or density and that of the cross section of the unit cell is of interest. This is done via a study of a Design of Experiment (DOE). In fact, DOE is a system for designing experiments and evaluating the collected knowledge. The procedure makes it possible to use a small number of experiments in which many experimental conditions are routinely and simultaneously varied in order to obtain optimal performances of a given problem. The model can be used to understand the influence of the experimental parameters on the outcome. The DOE studied in this chapter presents two factors: the lattice distribution and the beam cross section. The role of these parameters in structural design helps obtaining a structure with an optimal specific strength. The effect of these two factors (lattice distributions and cross section widths) are analysed in function of von Mises stress and structure weight (represented by the volume of the structure). It is important to indicate that this study takes a rectangular cross section into account whose thickness (t) on the axis z is fixed at 10 mm and whose width (w) will be variating according to the three levels in the DOE. As mentioned in steps 5 and 6 of Figure 15, two configurations are studied and are explained in the next sub-sections:

(1) First configuration. A one-region study where nine possible combinations of three different types of lattice distributions (coarse, normal, and fine) and three different rectangular cross section widths (1, 1.5 and 2 mm) are investigated (Figure 19). The effect of these two factors (struts width and lattice distribution) is then studied in a L9 Taguchi Orthogonal Array Design (Table 3);

(2) Second configuration. Dividing the structures into three regions and where three different types of lattice distributions and widths are applied on each region (Figure 20). The effect of these two factors (width and lattice distribution) for each zone forms a total of six factors. This corresponds to a DOE equivalent to a L27 Taguchi Orthogonal Array Design (Table 4).

The same configuration was studied by using three types of weighted functions depending on the von Mises stress and the volume and that via a second L27 Taguchi Orthogonal Array Design (Table 5).

Table 2: DOE levels.

Level	Width [mm]	Lattice distribution
1	1	Coarse
2	1.5	Normal
3	2	Fine

Table 3: DOE L9 showing the von Mises stress and the volume of the one-region study.

Exp.	Width [mm]	Lattice distribution	von Mises [MPa]	Volume [10^{-4} m^3]	Lattice Density
1	1	1	25.30	1.39	0.10
2	1	2	20.26	2.29	0.16
3	1	3	16.34	3.34	0.23
4	2	1	17.06	2.09	0.14
5	2	2	13.70	3.43	0.24
6	2	3	11.13	5.02	0.35
7	3	1	12.95	2.79	0.19
8	3	2	10.42	4.58	0.32
9	3	3	8.52	6.69	0.46

Table 4: L27 DOE of von Mises and volume. A, B, and C refer respectively to the strut's width of the first, second and third regions, while D, E, and F refer to the three lattice distribution types of the first, second and third regions, respectively.

Exp.	A	B	C	D	E	F	von Mises [MPa]	Volume [10^{-4} m^3]
1	1	1	1	1	1	1	24.40	1.50
2	1	1	1	1	2	2	23.93	1.80
3	1	1	1	1	3	3	15.50	3.87
4	1	2	2	2	1	1	16.60	2.32
5	1	2	2	2	2	2	16.62	2.79
6	1	2	2	2	3	3	16.60	5.76
7	1	3	3	3	1	1	16.26	3.50
8	1	3	3	3	2	2	16.27	4.38
9	1	3	3	3	3	3	16.27	6.60
10	2	1	2	3	1	2	15.79	3.70
11	2	1	2	3	2	3	12.90	4.43
12	2	1	2	3	3	1	15.48	3.64
13	2	2	3	1	1	2	12.68	3.06
14	2	2	3	1	2	3	10.73	4.02
15	2	2	3	1	3	1	14.66	4.36
16	2	3	1	2	1	2	19.98	2.93
17	2	3	1	2	2	3	15.97	3.65

18	2	3	1	2	3	1	23.06	4.08
19	3	1	3	2	1	3	12.44	4.60
20	3	1	3	2	2	1	12.91	3.32
21	3	1	3	2	3	2	12.16	4.78
22	3	2	1	3	1	3	16.50	4.45
23	3	2	1	3	2	1	24.63	3.70
24	3	2	1	3	3	2	22.90	4.41
25	3	3	2	1	1	3	13.68	4.08
26	3	3	2	1	2	1	18.40	3.42
27	3	3	2	1	3	2	16.03	5.27

Table 5: DOE of three different weighting approaches. A, B and C refer respectively to the strut's width of the first, second and third regions, while D, E and F refer respectively to the first, second and third lattice distributions. s1,s2, and s3 represent the three weight sum functions.

Exp.	**A**	**B**	**C**	**D**	**E**	**F**	**s_1**	**s_2**	**s_3**
1	1	1	1	1	1	1	0.30	0.39	0.49
2	1	1	1	1	2	2	0.33	0.41	0.50
3	1	1	1	1	3	3	0.43	0.42	0.40
4	1	2	2	2	1	1	0.24	0.27	0.29
5	1	2	2	2	2	2	0.30	0.32	0.34
6	1	2	2	2	3	3	0.71	0.67	0.63
7	1	3	3	3	1	1	0.39	0.39	0.39
8	1	3	3	3	2	2	0.52	0.50	0.48
9	1	3	3	3	3	3	0.82	0.76	0.70
10	2	1	2	3	1	2	0.41	0.40	0.40
11	2	1	2	3	2	3	0.45	0.41	0.37
12	2	1	2	3	3	1	0.40	0.39	0.38
13	2	2	3	1	1	2	0.26	0.24	0.22
14	2	2	3	1	2	3	0.35	0.30	0.25
15	2	2	3	1	3	1	0.48	0.45	0.42
16	2	3	1	2	1	2	0.40	0.43	0.47
17	2	3	1	2	2	3	0.41	0.40	0.40
18	2	3	1	2	3	1	0.62	0.66	0.70

19	3	1	3	2	1	3	0.46	0.41	0.37
20	3	1	3	2	2	1	0.30	0.28	0.26
21	3	1	3	2	3	2	0.48	0.43	0.37
22	3	2	1	3	1	3	0.53	0.51	0.50
23	3	2	1	3	2	1	0.60	0.66	0.72
24	3	2	1	3	3	2	0.26	0.35	0.44
25	3	3	2	1	1	3	0.42	0.39	0.36
26	3	3	2	1	2	1	0.43	0.45	0.46
27	3	3	2	1	3	2	0.63	0.60	0.56

3.4. Results

3.4.1. First Configuration

Table 1Table 3 represents the L9 Taguchi Orthogonal Array Design consisting of two factors and three levels as well as the lattice structure relative density. The numbers 1, 2 and 3 correspond to the level of each factor as explained in Table 2. A response parameter is needed for finding out the influence of the selected and the response function is taken as the maximal value of the von Mises stress and the volume which are reported as the two conflictual response.

Figure 21 and Figure 22 represent the von Mises stress results for the experiments (1–3). 4 and 7. They permit visualizing the von Mises stress change for the same width but different lattice distributions (Figure 21) and for the same lattice distribution but different widths (Figure 22). It is important to indicate that, for better results visualization, the width scale in these figures is set to 2.

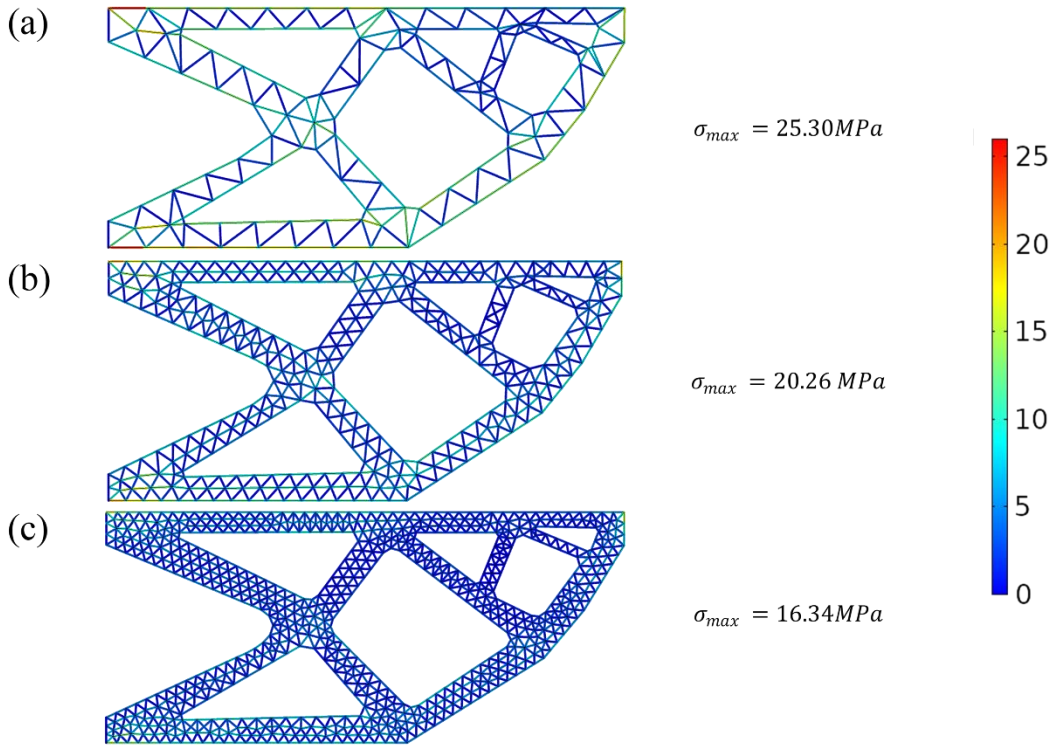

Figure 21: von Mises stress for the same width of 1mm (level 1) and different lattice distributions.

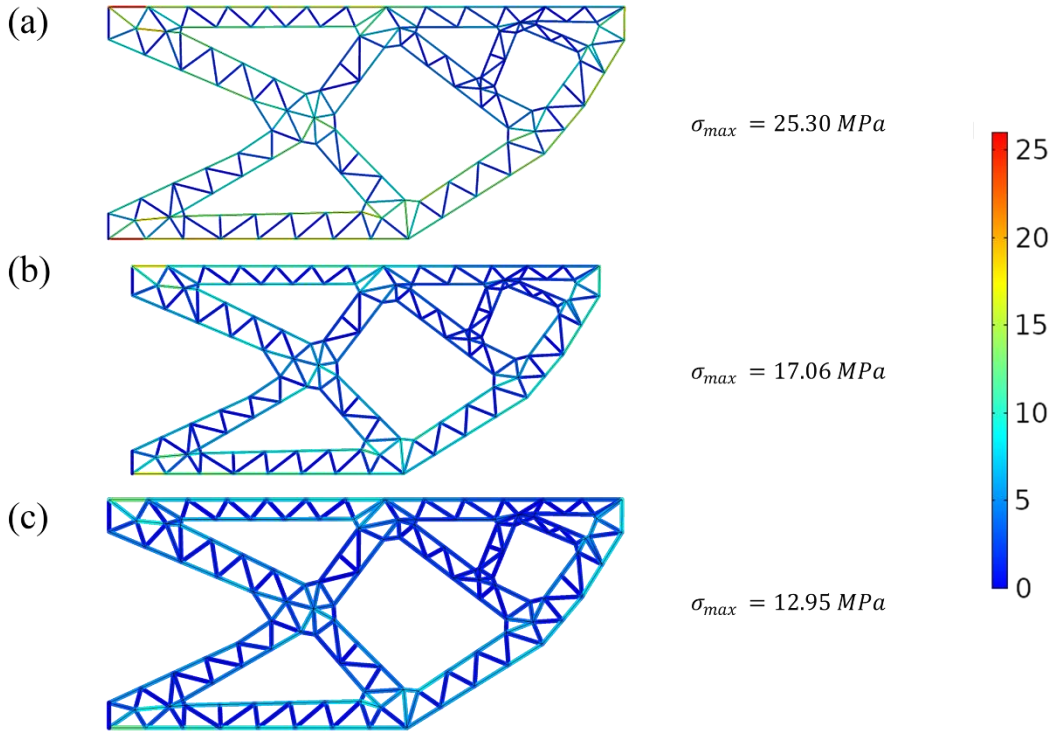

Figure 22: von Mises stress for the same coarse lattice distribution (level 1) and different widths (a) 1 mm. (b) 1.5mm and (c) 2 mm.

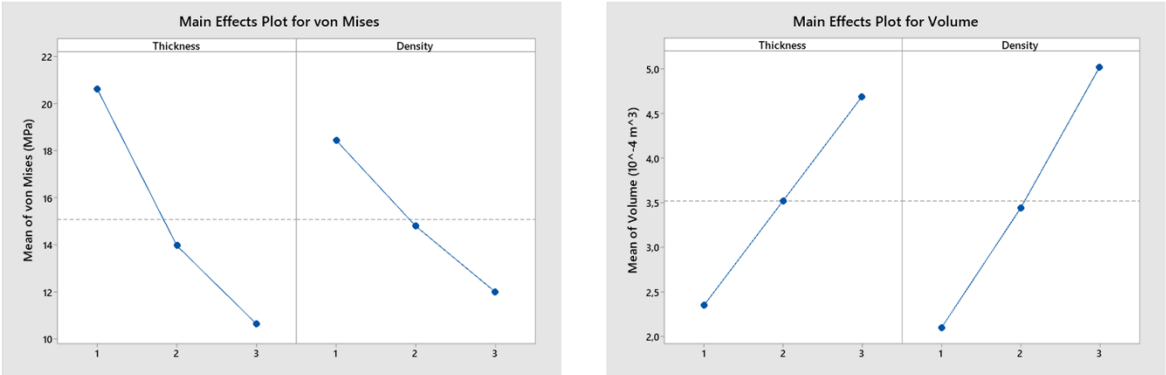

(a) (b)

Figure 23: One-region study of width and lattice distribution effect on the von Mises (a) stress and (b) the volume.

3.4.2. Second Configuration

In the objective of putting the right material quantity at the right place using lattices – at the same time as keeping a sufficient mechanical strength – a three regions study was conducted. Based on the von Mises stress results in the oneregion study, the structure is divided as follows: the regions 1 and 3 correspond to the areas where the load and the boundary conditions are applied, and the region 2 corresponds to the area where the stress is relatively low (see Figure 21). Numerical simulations have been conducted and the von Mises stress and the volume results have been collected and represented in the DOE in Table 4. For 27 different lattice distributions, nine widths combinations are used respecting the Taguchi's L27 orthogonal array (consisting of six factors and three levels). The numbers 1,2 and 3 refer to the levels of both the width and the lattice distribution. A, B, and C refer respectively to the strut's width of the first, second and third regions while D, E, and F refer respectively to the lattice distribution of the first, second and third regions. Figure 24 shows the results of the von Mises stress for the combinations highlighted in Table 4. It is important to indicate that, for better results visualization, the width scale in these FiguresFigure 24, Figure 26 and Figure 28 is set to 2.

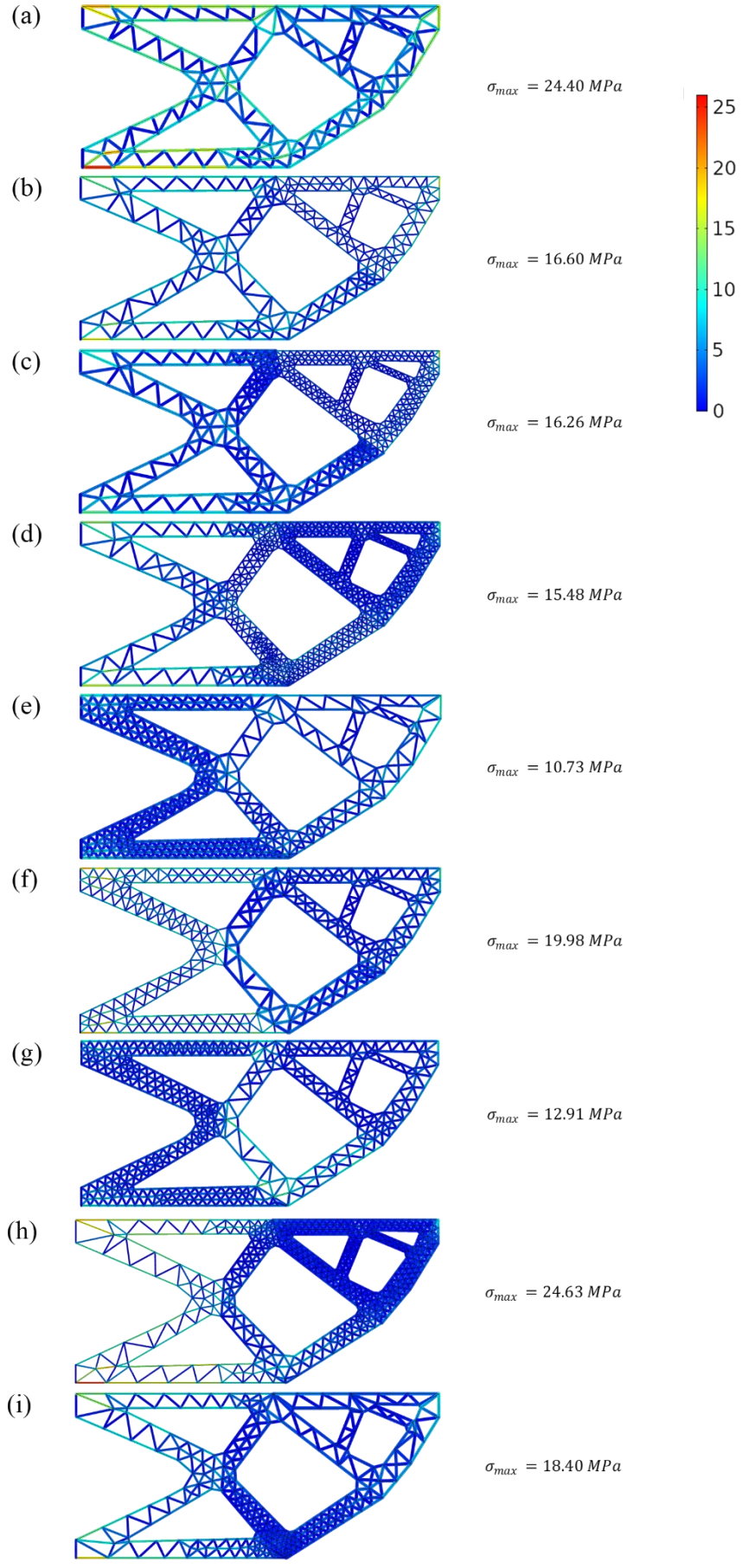
(a)
$\sigma_{max} = 24.40\ MPa$
(b)
$\sigma_{max} = 16.60\ MPa$
(c)
$\sigma_{max} = 16.26\ MPa$
(d)
$\sigma_{max} = 15.48\ MPa$
(e)
$\sigma_{max} = 10.73\ MPa$
(f)
$\sigma_{max} = 19.98\ MPa$
(g)
$\sigma_{max} = 12.91\ MPa$
(h)
$\sigma_{max} = 24.63\ MPa$
(i)
$\sigma_{max} = 18.40\ MPa$
25
20
15
10
5
0

Figure 24: von Mises stress for nine combinations of the three regions study (highlighted in blue in the DOE).

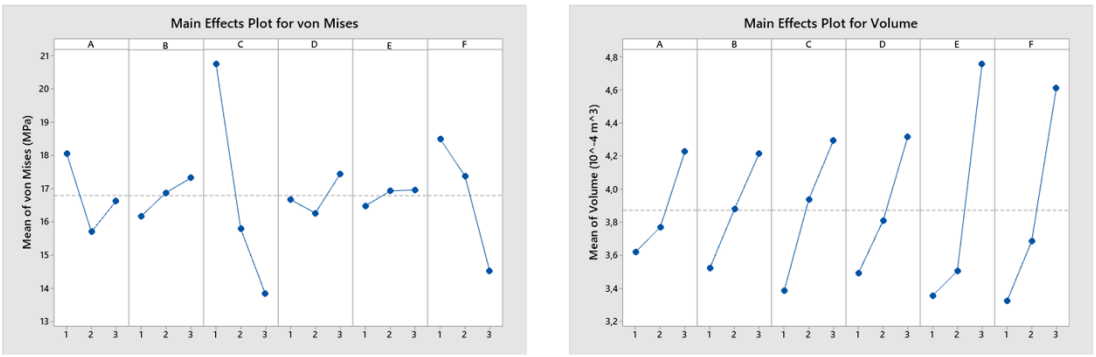

Figure 25: Three regions study of struts width and lattice distribution density effect on the von Mises (a) stress and (b) the volume, A, B and C refer respectively to the strut's width of the first, second and third regions. while D, E and F refer to the three lattice distribution types of the first, second and third regions, respectively.

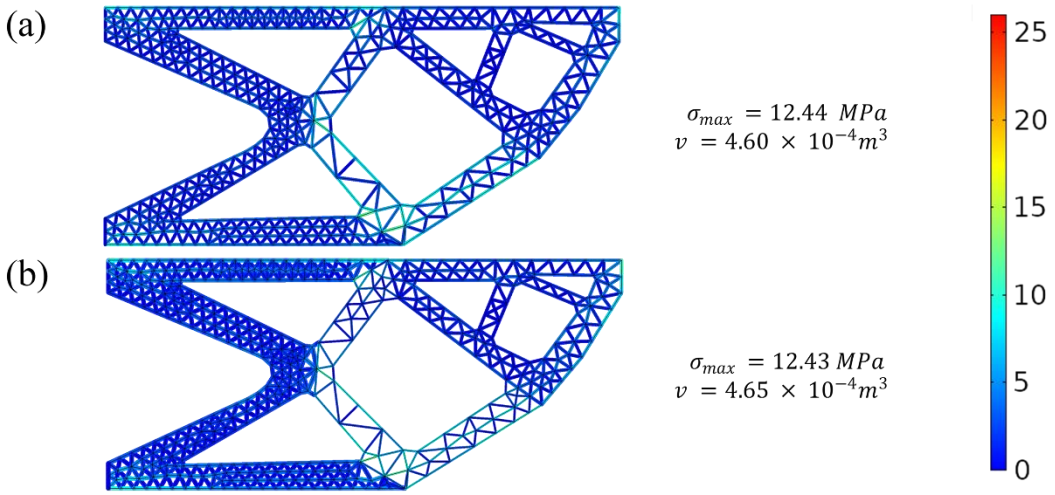

Figure 26: The von Mises stress results comparison between the combination of the first experiment in Table 3 (a) and the minimal combination obtained in the study of the effect of width and lattice distribution on the von Mises stress (b).

To find a better compromise between the width and the lattice distribution to obtain optimal results considering the von Mises stress and the volume, a weight function is applied and the result of the application of this function will be called the weight sum. The first step is to calculate the the normalized von Mises stress f_s (1) and the normalized volume f_v (2). The values will then vary between 0 and 1.

$$f_s = \frac{(\sigma - \sigma_{min})}{(\sigma_{max} - \sigma_{min})} \quad (1)$$

$$f_v = \frac{(v - v_{min})}{(v_{max} - v_{min})} \quad (2)$$

The second step consists in calculating the sum function using the weighting influence parameters. In this study, three configurations have been investigated:

- 50% for the von Mises stress and 50% for the volume;
- 40% for the von Mises stress and 60% for the volume;
- 30% for the von Mises stress and 70% for the volume.

The sum functions can be written in the following forms:

$$\begin{cases} s_1 = 0.5f_s + 0.5f_v \\ s_2 = 0.4f_s + 0.6f_v \\ s_3 = 0.3f_s + 0.7f_v \end{cases} \quad (3)$$

The results of the 27 combinations for the von Mises stress and the volume are collected in the DOE in Table 5 and thus for the three weighting sums.

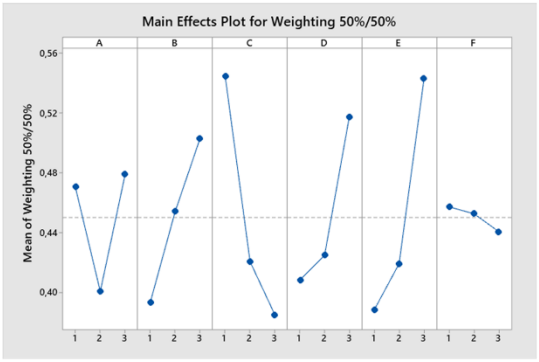

(a)

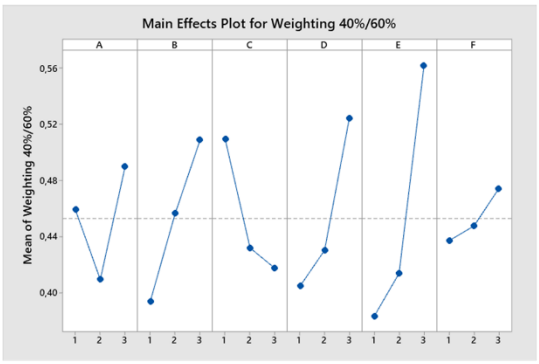

(b)

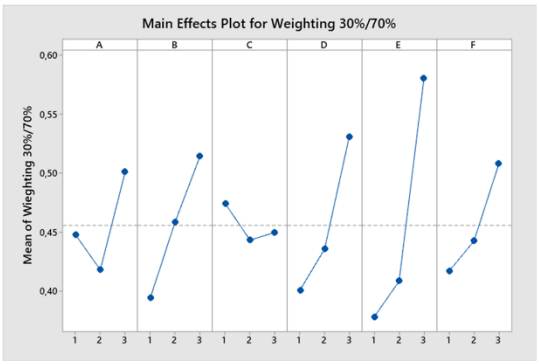

(c)

Figure 27: Study of the weighting effect on the von Mises stress and the volume (a) 50%/50%, (b) 40%/60% and (c) 30%/70%. A, B and C refer respectively to the strut's width of the first, second and third regions, while D, E and F refer respectively to the first, second and third lattice distributions.

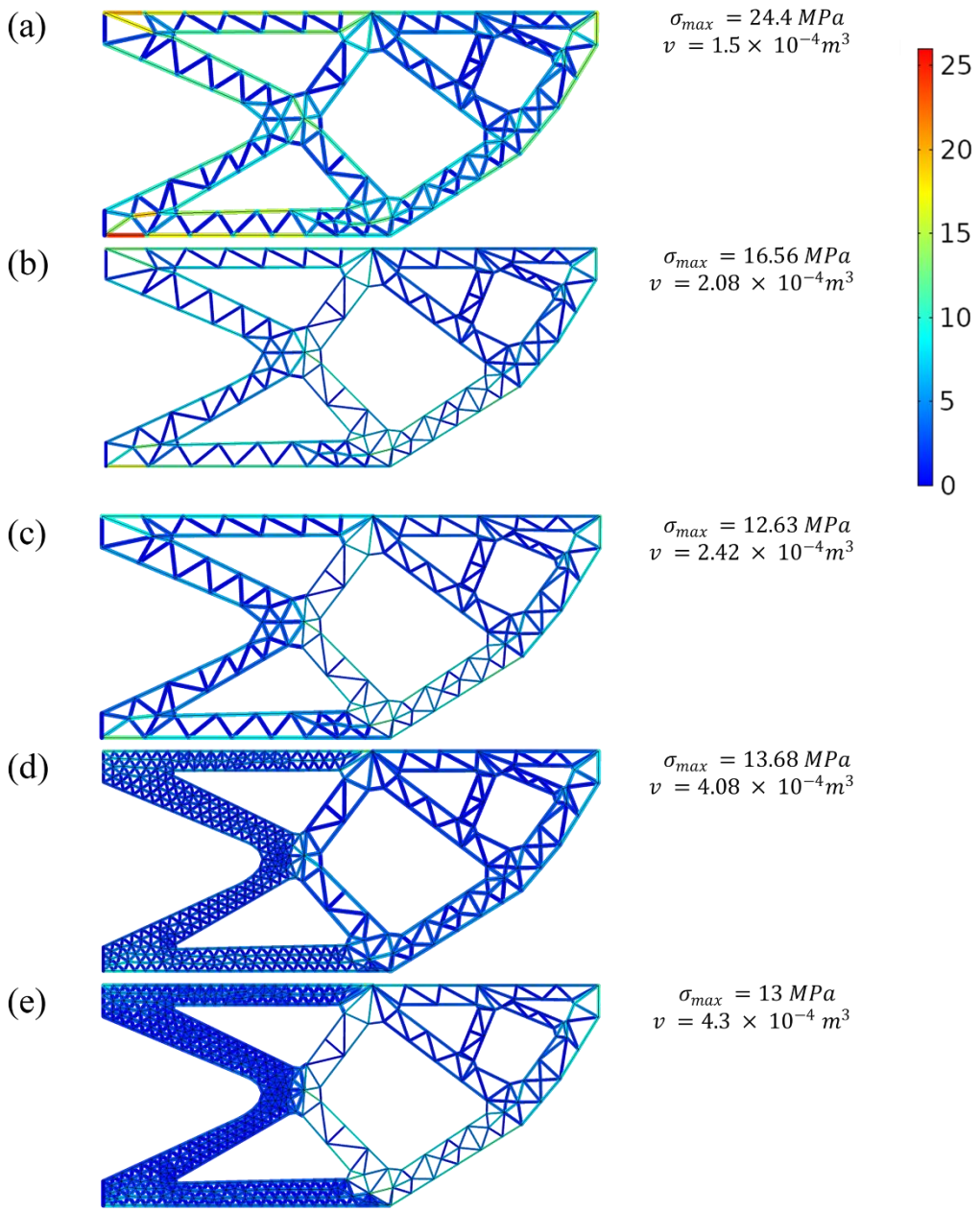

Figure 28: The von Mises results comparison between (a), (d) the combination in the first and 25th experiments in Table 3 and (b), (c), (e) the minimal combinations obtained in the study of the weighting effect on the von Mises stress and the volume.

3.5. Discussion

3.5.1. First Configuration

As stated in the section 3.3, the tool developed in this study aims to transform the mesh generated via COMSOL Multiphysics software into beam elements. This tool is applicable for 2D as well as for 3D geometries and it follows an automated process in several steps. The first steps consists in defining the

mesh strategy on COMSOL Multiphysics whether for the first or the second configuration (mesh size, type, and density). The data is then exported into a .txt format to be used by the code developed on MATLAB. Then the second step consists in using these data to generate the beam elements that will form the lattice structures. The mesh connectivity matrix is consequently transformed into Bézier Polygones taking into account the mesh type and coordinates. The final step involves the transfer of the new lattice structures to COMSOL Multiphysics tool in which the cross-section thicknesses are assigned according to the parameters defined in the DOE. These structures are then simulated numerically. The results of these numerical simulations are presented in the section 3.4. and are discussed in this section.

Table 3 shows that the relative density of the lattice structure changes with the change of the cross-section width and the distribution. Its value is comprised between 0.096 and 0.19 for a coarse distribution, between 0.16 and 0.32 for a normal distribution and between 0.23 and 0.46 and thus for different widths. Based on Table 3, it is noticed that the change of the lattice distribution level for the same width w_1 = 1 mm (level 1) leads to a decrease of the von Mises stress from 25.30 MPa (Exp. 1) to 16.34 MPa (Exp. 3), which corresponds to a decrease percentage of 35.41%. As for the volume. it increases from 1.40×10^{-4} m^3 to 3.35×10^{-4} m^3 . The same variation is noticed for w_2 = 1.5 mm (level 2): the decrease percentage of the von Mises stress is equal to 35.76% and the volume increases from 2.10×10^{-4} m^3 to 5.02×10^{-4} m^3 (Exps. 4-6). For w_3= 2 mm (level 3). the decrease percentage of the von Mises stress is of 34.20% and the volume increases from 2.79×10^{-4} m^3 to 6.70×10^{-4} m^3 (Exps. 7-9). However, for a fixed lattice distribution and variable widths, one can identify the following variation: for the coarse lattice distribution (level 1), the von Mises stress decreases from 25.30 MPa (Exp. 1) to 12.95 MPa (Exp. 7) corresponding to a percentage of 48.80% and the volume increases from 1.40×10^{-4} m^3 to 2.79×10^{-4} m^3 . For a normal lattice distribution (level 2), the decrease percentage of the Von-Mises stress is of 48.57% and the volume increases from 2.29×10^{-4} m^3 to 4.58×10^{-4} m^3 (Exps. 2 and 8). For a fine lattice distribution, the decrease percentage of the von Mises stress is of 47.85% and the volume increases from 3.35×10^{-4} m^3 to 6.70×10^{-4} m^3 (Exp. 3 and 9). It is important to outline that all the von Mises stress values are lower than the yield strength of VeroWhite material which is equal to 49.9 MPa.

Figure 21 shows the results of the von Miss stress distribution for the same width w_1= 1 mm and different lattice distributions (Exps. 1, 2 and 3 in Table 3) while Figure 22 shows the von Mises stress results for the same coarse lattice distribution and different widths (Exps. 1, 4 and 7 in Table 3). The same scale is adapted to distinguish the stress change. It is noticed that the maximal stress is in the regions where the loads and the boundary conditions are applied.

The results presented in Table 3, Figure 21, and Figure 22 show that increasing both the cross-section width of the lattice structures and their distribution decreases the von Mises stress and increases the volume. However, one cannot predict the effect of the DOE variables on the results. For this reason, a

study of the cross-section width and the lattice distribution effect on the von Mises stress and the volume is conducted in Figure 23a, b.

Main effect plot for the first configuration is shown in Figure 23. The influence of each factor on response function is analysed by main effect plot respectively for the maximum value of Von-Mises stress (Figure 23a) and the structure volume (Figure 23b). For the main effect plot. the slope justifies the effect of each parameter. Parameters having highest inclination have a greater effect while parameters having a horizontal plot have minimal effect on the response function.

Figure 23a shows that the slope of the width has the highest inclination while that of the lattice distribution has a moderate slope i.e., the width effect decreases from 20.63 MPa to 10.63 MPa (variation of 10 MPa) and the lattice distribution effect decreases from 18.44 MPa to 12 MPa (variation of 6.44 MPa). That means that the width effect on the von Mises stress is greater than that of that of the lattice distribution. Moreover, the width and the lattice distribution effect on the volume is ascending i.e., the width effect decreases from 2.35×10^{-4} m^3 to 4.69×10^{-4} m^3 (variation of 2.34×10^{-4} m^3) and the lattice distribution effect decreases from 2.10×10^{-4} m^3 to 5.02×10^{-4} m^3 (variation of 2.92×10^{-4} m^3). This means that the lattice distribution effect on the volume is slightly more important than that of the width. The latter conclusion shows that the two design variables present a high interaction. A further calculation of effects is conducted in Table 6. It shows the effect percentage of the width and the lattice distribution on the von Mises stress and the volume. Table 6 proves that the width effect on the von Mises is indeed more important than that of the lattice distribution. On the other hand, it shows that the effect percentage of the interaction, between both the design variables, is of 68.10%. That means that the volume depends on both the width of the cross section of the lattices and their distribution inside the structure.

Table 6: Effect percentage of the width, the lattice distribution and their interaction on the von Mises stress and the volume.

	Width	**Lattice distribution**	**Interaction**
von Mises	69.62%	28%	2.38%
Volume	12.50%	19.40%	68.10%

By a further analysis of the minimal calculated values in Figure 23a, b. the following is concluded:

- A strut width of 2 mm (level 3) and a fine lattice distribution (level 3) give a minimal von Mises stress value (Figure 23a). This combination is denoted (3-3);
- A strut width of 1 mm (level 1) and a coarse lattice distribution (level 1) provide a minimal volume value (Figure 23b). This combination is denoted (1-1).

The previously deduced combinations (1-1) and (3-3) are studied in the DOE in Table 3 (Exps. 1 and 9). for which the von Mises stress and volume are calculated. They give a minimal volume and von Mises stress, respectively. However, if one must choose a combination that provides good compromise

between reducing weight reduction and increasing strength, a uniform width of 2 mm and a coarse lattice distribution would be of interest (Exp. 7 in Table 3).

3.5.2. Second Configuration

According to Table 4, for 27 different lattice distributions, nine width combinations are used respecting the norms of a L27 Taguchi design of experiment. In some combinations – more particularly in experiments 4 to 9 – it is noticed that the lattice distribution does not influence the von Mises stress results.

In similarity to the one-region study, Figure 24 (a to i) shows the von Mises stress results for multiple widths and lattice distributions. It is shown that the minimal von Mises stress calculated is equal to 10.73 MPa (Figure 24e) and it corresponds to experiment 14 in Table 4 while the maximal von Mises stress calculated is of 24.63 MPa (Figure 24h) and it corresponds to Exp. 23 in Table 4. The rest of the figures demonstrates that the von Mises stress depends on the variation of the width and the lattice distribution. Figure 25 shows the effect of the widths (A-B-C) and the lattice distributions (D-E-F) of the three regions on the von Mises stress and the volume, respectively. In Figure 25a. the width effect of the third region is the most important and has a negative slope while that of the second region has a slightly positive slope. The lattice distribution effect of the third region is also the most important. Figure 25b shows that the effects of the lattice distribution of the second and the third regions on the volume are the most important. That means that fact that the structure is and pinned in the third region means that the structure should be reinforced in the less resistant areas by increasing both the lattices width and their distribution.
By further analysis of Figure 25a.b, as previously explained, the combinations that allow to have the minimal volume and the minimal von Mises stress respectively are the following:

- A combination consisting of a width of 1 mm (level 1) and a coarse lattice distribution (level 1) in the three regions (Figure 11b) gives the minimal volume. This combination is denoted (1-1-1,1-1-1) and it corresponds to the first experiment in Table 3;
- A new combination gives the minimal von Mises stress, and it consists of both (i) a width of 1 mm (level 1) in the first and the second regions and a width of 2 mm (level 3) in the third region, and (ii) a normal lattice distribution in the first region (level 1), a coarse lattice distribution in the second region (level 2) and a fine lattice distribution (level 3) in the third region.

The second combination denoted (1-1-3,2-1-3) is studied numerically and the von Mises and volume results (Figure 26b) are compared to those of the combination in Exp. 14 in Table 3 (Figure 26a). These combinations are compared for the reason of having the same lattice distribution but different widths. The obtained results are relatively the same with a difference of 1% and 2% for the volume. The results

of the effect of the width (A-B-C) and the lattice distribution (D-E-F) for the three regions on the three cases of the weighting sum, are illustrated in Figure 28 (a.b. c). It is noticed that the effects of the width and the lattice distribution of the first and second regions become now more important. That means that the weighting functions allows a better compromise between the two DOE responses. Three optimal combinations are deduced from Figure 27 as follows:

- A combination consisting of width of 1.5 mm (level 2) and a coarse lattice distribution (level 1) in the first region, a width of 1 mm (level 1) in and a coarse lattice distribution (level 1) in the second region and a width of 2 mm (level 3) and a fine lattice distribution (level 3) in the third region. This combination is denoted (2-1-3,1-1-3) (Figure 27a);
- A combination consisting of a coarse lattice distribution (level 1) in the three regions with a width of 1.5 mm (level 2) in the first region, a width of 1 mm in the second region (level 1) and a width of 2 mm (level 3) in the third region. This combination is denoted (2-1-3.1-1-1) (Figure 27b);
- A combination consisting of a coarse lattice distribution (level 1) in the three regions with a width of 1.5 mm (level 2) in the first and the third regions. and a width of 1 mm in the second region (level 1). This combination is denoted (2-1-2,1-1-1) (Figure 27c).

The combinations are then studied numerically, and their results were compared to similar combinations having the same lattice distributions: The results of the von Mises stress and the volume of the combination (2-1-3,1-1-3) (Figure 28e) are compared to those of the combination of the experiment 25 in Table 4 (Figure 28d). It is noticed that the von Mises stress decreases from 13.68 MPa to 13 MPa but the volume slightly increases from 4.08×10^{-4} m^3 to 4.3×10^{-4} m^3. The results of the von Mises stress and the volume of the combinations (2-1-2,1-1-1) and (2-1-3,1-1-1) (Figure 28b and c) are compared to those of the combination of the first experiment in Table 4 (Figure 28a). Compared to Figures Figure 28aFigure 28b shows a von Mises stress decrease of 32% for a volume increase of 38.35% while Figure 28c shows a von Mises stress decrease of 48.24% versus a volume increase of 61%. However, to find the best combination that assures the best material distribution and its best cross section width, a weighting study is conducted in Table 7. The same weighting sums are calculated as described in Equation 3. By comparing the values in Table 7, the sum with the minimal value corresponds to the optimal combination. Thus, the combination (2-1-3,1-1-1) is considered as the combination that can ensure the best material distribution and cross section.

Table 7: Weighting sums results for the three optimal combinations.

A	**B**	**C**	**D**	**E**	**F**	s_1	s_2	s_3
2	1	2	1	1	1	0.43	0.39	0.36
2	1	3	1	1	1	0.17	0.16	0.16
2	1	3	1	1	3	0.20	0.24	0.27

The optimized lattice structure is then additively manufactured by material jetting process and more particularly with PolyJet® technique using VeroWhite material on a Stratasys® machine (Figure 29).

Table 8 represents a comparison between the related work in the state of the art and the present study. Such a comparative study permits not only to investigate the advantages and results of each group of research papers but also to show their lacks that the current work aims to fill. As already stated in the introduction, the advantage of the method employed in this chapter based on design of experiments is to reduce computational costs by reducing the number of the design variables. The parametrization and material distribution strategy are motivated by the results of the numerical simulation results of the full solid structure in a way to obtain lattice distribution densities lower than 1 and thus meeting the goals of this study in decreasing weight and keeping the strength as close as possible to that of the solid structure. Moreover, the design of experiments followed by a sensitivity study permits visualizing several material distributions thus identifying the optimal structure. In addition, this study serves as a comparison between a uniform lattice distribution and a variable-density one. The optimal uniform lattice structure obtained in the one zone study gives a von Mises stress equal to 12.95 MPa and a volume of 2.79×10^{-4} m^3 while the optimal variable-density lattice structure obtained in the three zones study gives a von Mises stress equal to 12.63 MPa and a volume of 2.42×10^{-4} m^3 . Although the values are quite close, it is concluded that a variable-density structure possesses a better weight reduction and exhibits less material than the uniform density structure.

This structure consisted of lattices, as aforementioned, possess a lightweight and a relatively important strength. These properties, conformally to most of lattice-integrated structures, allow their production by different AM techniques without dramatically increasing the manufacturing costs [85]. These arguments related to lattices advantages for AM are confirmed by several researchers [103-106]. At any rate, this framework can be generalized to cover different types of geometry whether in 2D or 3D and to consider the anisotropic behaviour imposed by different additive manufacturing techniques. In fact, the results of this study can be modified with the change of the topology optimization objective function and the additive manufacturing technique chosen to print the lattice structure. Future work will be dedicated to the improvement of this framework especially by integrating AM constraints like angles and overhangs in the detailed design phase. The angle a cell is printed at can affect the success of a print because it influences the amount and placement of supports required. For example, if a large cubic truss is printed directly on the build platform horizontal members will be unsupported. In general, a well-chosen and oriented lattice is self-supporting, which does not require support structures. Oftentimes, a structure can be oriented to reduce support structures. If the structure is simply rotated 45 degrees, the members are now self-supporting [109]. This means that the positions and the nodes and elements connectivity should be modified in the initial steps in a way to transform them into lattices that respect the manufacturing constraints.

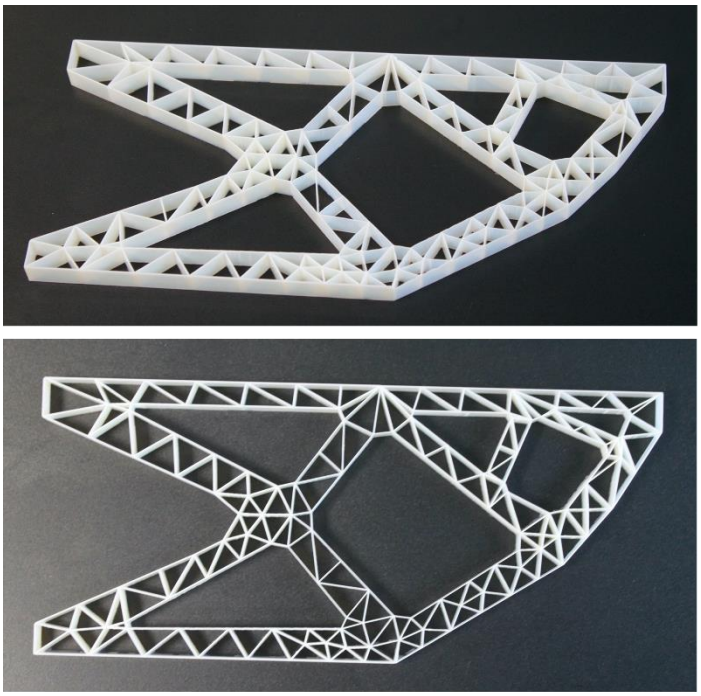

Figure 29: 3D printed lattice structures using PolyJet® technique and VeroWhite material.

Table 8: Comparison of related works with the current study.

References	Objective	Methods	Results and Advantages	Disadvantages	To improve
Lim et al. [91] Cheng et al. [93] Tang et al. [94] Nguyen et al. [95]	Enhance the performance of the products, minimize weight and material use, and maximize effective flexural and torsional rigidities	Algorithm-based (genetic, bi-directional evolutionary and heuristic) and homogenization-based topology optimization	A noticeable weight reduction	The algorithms and the computation are time costly	Reduce the number of the optimization variables
Chen [96] Brackett et al. [42] Song [107]	Have an efficient design and control the density of internal structures	Design methods based on mapping microstructure into design space	Solution time reduced to 50% and material saving	Cross-section and strut diameter (thickness) not considered	Define a parametrization strategy
Wang and Rosen [98] Wang [99]	Replace thick part sections with thinner ones and develop a unit truss approach to facilitate the design	Parametric modelling method to create truss structures to enhance a part's mechanical and/or dynamic properties	Obtention of truss structures with thinner part sections	Numerical simulation was not conducted to validate the efficiency of the proposed methods in weight reduction	Conduct numerical simulations to validate the proposed design strategy

Teufelhart and Reignhart [101]	Production of lightweight components	Optimization approach using periodically arranged lattice structures	Enhancement of the force-to-weight and the stiffness-to-weight ratios	Severe notch stresses appearing at the nodes where the beams are merging and very manual process	Improve numerical models by paying attention to the element's connectivity
Teufelhart and Reignhart [102,103]	Production of lightweight components	Optimization approach which adapts the course of the structure to the flux of force in a part	Improvement of the stiffness-to-weight ratio	The dependencies between the parameters' number of struts', their diameter and their angles are not examined in detail	Define a parametrization strategy
Wang et al. [108]	Increase the force-to-weight and the stiffness-to-weight ratios	Design optimization of heterogeneous conformal lattice structures based on principal stress lines and that ensures an optimal cross-section distribution in the structure	The maximum force-to-weight ratio and the stiffness-to-weight ratio of the optimized heterogeneous conformal lattice structure are increased by 11.8% and 41.8% respectively compared with homogeneous conformal lattice structure	The number of the principal stress lines is taken randomly	Argument the choice of the number of the principal stress lines to better understand the material distribution in obtained structures
Lebaal et al. [105]	Optimize the parameters and the topological distribution of lattice cells in a constrained design space to gain both mass and computation efficiency for structure design	Optimization method using design of experiment and surrogate model	A remarkable weight reduction	Work limited to uniform lattice configuration	Investigate a variable-density case of study
The present work	Gather both topology optimization for specifying the needed material at the right place through the design space and a parametric optimization of lattice struts therefore	Design and optimization framework for AM, which highlights variable-density lattice structures: processing both a topology optimization on a rough design space and a design of experiments driven	Several but fast numerical simulations and effect studies emerging from a defined topology optimization and parametrization strategies lead to obtaining an optimal configuration that provides a good	The study is limited to 2D extruded structure and doesn't consider all the constraints and anisotropy of additive manufacturing	Augmenting the study in terms of optimization on 3D models and integrating additive manufacturing constraints

ensuring optimized strength-to-weight ratio	parametric optimization	compromise between weight reduction and stiffness increase

3.6. Conclusion

In this study, a variable-density lattice structures design and optimization framework has been proposed. It combines TO and parametric optimization to obtain a lightweight structure that is suitable to AM. More specifically the novelty of the proposal is the comprehensive and efficient digital chain generating AM-friendly lattice structures in a topologically optimized design space. Different DOE configurations have showed that reinforcing the structure with a lattice distribution density where it is needed and assigning a rectangular cross section accordingly can help obtaining a high specific strength. The development process of suitable and specific strength structures for AM becomes now seamless, efficient and can be applied to any design solutions. To demonstrate the added value of the proposal, a case study has been introduced and developed with the support of computational programs and tools.

To validate the efficiency of the proposed method in meeting the goals of weight reduction and strength increase, the study was divided into two cases and special interest was paid to the comparison between the two cases. In both cases, a design of experiments and a sensitivity study are conducted. The first case consisted in a uniform lattice distribution while the second is a variable-density lattice distribution study. Despite the closeness of the results of both cases, it can be concluded that the second case provided a better weight and a better strength thus reaching the goal of having a better strength-to-weight ratio. The overall procedures are exhibited in a reasonable computational time which is an answer to the one of the issues of design optimization: computational time and cost.

Future work will be dedicated toward (i) augmenting the study in terms of optimization on 3D models and (ii) integrating AM constraints as an additional means to identify appropriate lattice structures in consistency with the selection of both the material and the AM technique. Depositing the right material at the right place in a layer-by-layer fashion implies the opportunity at the engineering level to be able to specify – beyond the shapes – mechanical properties distributed in the space to be manufactured. Next research effort will also be focused on the computation and generation of bio-inspired lattice structures exploiting principal stress lines and variable-density unit cells especially.

Chapter 4: A biomimetic inspired design method for 3D printed structures using L-system and parametric optimization

"All our knowledge has its origins in our perceptions."

Leonardo Da Vinci

"I have no special talent. I am only passionately curious."

Albert Einstein

4.1. Abstract

Biological structures and organisms are determined and optimized to adapt to changes and constraints imposed by the environment. The multiple functionalities and properties exhibited by such structures are currently a source of inspiration for designers and engineers. Thus, biomimetic design has been increasingly used in recent years with the intensive development of additive manufacturing to deliver innovative solutions. Due to their multifunctional properties combining softness, high stiffness, and light weight, many potential applications can be seen in the medical, aerospace, and automotive sectors. This chapter introduces a biomimetic design and geometric modeling method of 3D-printed lightweight structures based on L-systems generated and distributed along their principal stress lines. Numerical simulations and parametric optimization were conducted with three case studies to demonstrate the relevance and applicability of this method in adapting mechanical structures to various load cases as well as ensuring a proper stiffness-to-weight ratio.

4.2. Introduction

Nature exhibits many optimized structures in terms of properties and functions (i.e., light weight, flexibility, high stiffness, etc.) as survivors of natural stimuli and constraints over time. Learning from these biological structures allows their effective use in applications and provides new solutions for engineering problems in a sustainable manner. The latter statement falls under the broader paradigm biomimicry. According to Benyus [65], biomimicry is an “innovation inspired by nature” or “the conscious emulation of nature’s genius”. To mimic complex structures and properties of biological materials, biomimetic design has been investigated in multiple application sectors such as aerospace [110], automotive [111,112], and medicine [113], to name a few. This research field and the inherent complexities of these structures have been deeply addressed over the last decade with the intensive development of additive manufacturing (AM) technologies. Since its invention in 1984 [114], multiple AM processes and techniques have been proposed to increase both design and fabrication freedoms in terms of shape complexity, hierarchical complexity, material complexity, and functional complexity [115], leading, for instance, to physical objects with the desired properties and functionality [116-124]. AM is also suitable for lattice structure design, exhibiting light weight and strength behavior, similarly to porous materials in nature like honeycombs and trabecular bone [29]. These structures are categorized as homogeneous periodic, homogeneous conformal, heterogeneous periodic, and heterogeneous conformal depending on the distribution of the unit cells [86,125-131]. Their mechanical behavior is determined by cell topology, geometry, orientation, and size design elements. There, to achieve performance objectives such as part stiffness or strength, these structures may be spatially tuned by altering the aforementioned variables. Although the homogeneous and periodic lattice structures allowed gains in reducing part weight, good mechanical performance can only be achieved via the consideration

of coordinated load [132,133]. These kinds of material distribution for parts under realistic loads are inconsistent with the heterogeneous stress distribution. In contrast, natural organisms exhibiting lightweight structures, such as bones and wood, are non-uniform heterogeneous cellular, with cellular topology, geometry, orientation, and size tailored to the magnitude and orientation of the applied loads [99,134]. Stava et al. [135] used cyclic internal hollowing, local thickening, and support to optimize the structure for given loads and restrictions. Alzahrani et al. [136] developed a heuristic technique that totalizes the relative density information collected to automatically predict the diameter of the strut in the structure, under a variety of stress scenarios. As a result, replacing the solid structure with a non-uniform load-adapted heterogeneous lattice structure and fulfilling the design requirements of the part's mechanical performance is a scientific challenge [19,137].

Developing biomimetic lattice structures becomes, therefore, promising to achieve lightweight stiffness performance. The varying spongy trabecular structures of bone and local tissue variation in seashells (pearl oyster) are illustrative examples of this aim [138]. In hierarchical structures, there is a gradient of increasing density in the radial direction from the interior spongy (trabecular) bone to the exterior compact (cortical) bone. This property results from a natural remodeling process and adaptation to mechanical loads described byWolff's law [69]. Several studies were based on the architecture of the bone, and some bone mimicking mechanical structures were implemented. Robles-Linares et al. [139] focused on the modeling of the cortical bone microstructure for AM and its characteristics in the body depending on several mechanical loads and constraints [140]. Banijamali et al. [141] described the effects of different loadings on the morphology of the trabecular bone. Design, simulation, characterization, and manufacturing of bone implants and prostheses, and femoral stems were also a large center of interest [141–144]. Daynes et al. [145] and Audibert et al. [146] also worked on the bone's inner pores' distribution that follows the principal stress lines' (PSLs) trajectories and demonstrated the effectiveness of their biomimetic method in enhancing the properties and the weight of the structure. Tam et al. [147] investigated the fused filament fabrication (FFF) technique along PSLs to overcome the inherent anisotropy (direction-dependent properties) of AM. Teufelhart [148] evaluated the performance of a periodic structure with the flux of force-adapted structure with straightened struts, demonstrating that it can only handle axial force and has greater stiffness and strength.

Indeed, PSLs are orthogonal curves in which the tangent, at any point of any curve, has the direction of one of the principal stresses at that point [149]. They represent an appropriate description of the behavior of the structure, as they provide a wider visualization of the applied load effect on the object/structure. It particularly shows the lines of the material continuity within a design space, and they may derive from the classical Michell structural optimization of truss structures [150,151]. One of the main issues which can be faced is the appropriateness and the fabricability of PSLs in AM. Prior research works have successfully addressed the topology design method based on PSLs for AM of two-dimensional structures [146,152]. According to Li and Chen [153], PSLs do not depend on the scaling of the material stiffness

and the applied load but rather on the design boundaries, the location and the degree of the force, and the boundary conditions. Moreover, PSLs represent a continuous field in which they can either cross multiple design boundaries or be fully periodic. These mechanical and geometric properties prove the usefulness of PSLs as AM printing paths [108]. Based on the aforementioned statements and the literature, PSLs can serve as guidelines or paths for material growth and distribution inside a structure. A similar strategy was developed by Kirk et al. [154] and Ulu et al. [155] to enhance structural performance of additively manufactured objects through build orientation and gradient paths.

Plant growth algorithms and theories developed by Lindenmayer and Prusinkiewicz are widely known as L-systems [156]. From a geometric point of view, L-systems are a formalism to model the development of growing linear and branching structures, from basal filamentous organisms to trees to entire plant ecosystems [157,158]. Efforts in this research area are mainly focused on their graphical representation and computation [159,160]. However, interesting studies showed root system models using L-systems and proved their effectiveness in estimating the shear strength of root–soil composites [161,162]. Such systems have provided promising results when coupled with topology optimization algorithms. For instance, Bielefeldt et al. [163] proposed a genetic algorithm that encodes design variables and governs the development of the structure. An interpreter is required to translate genomic information into structural topologies, therefore leading to adaptive structures capable of achieving multiple design objectives in light weight and increasing stiffness. L-systems have also been combined with cellular automaton to generate mechanical structures for multiple mechanical conditions [164]. Tree-like systems or fractals have also inspired engineers to develop heat exchangers and cooling systems. A review of fractal heat exchangers has demonstrated their big advantages in lowering the pressure drop and in maintaining a uniform temperature [165]. Then, the generalization of L-systems within a structure for objectives of light weight is a challenge. The utility of integrating L-systems inside mechanical structures can be validated via numerical simulations using different FEA software such as ANSYSWorkbench and COMSOL Multiphysics. Indeed, numerical simulations of bioinspired mechanical structures and composites have proven the effectiveness of emulating nature in its aspects and shapes [166-168].

Despite all the research works based on L-systems in the aforementioned domains, there is still a lack in the application for biomimetic lightweight structures with high stiffness in AM. To address this challenge, this chapter proposes a novel computational design method based on L-systems generated and distributed along the PSLs' directions. By considering a rough design space, multiple load cases and boundary conditions are investigated. The resulting tree-like structures are studied through numerical simulations followed by a design of experiments (DOE). The latter scheme of parametric optimization utilized the branches' thicknesses as two design variables for the models using the first and second PSLs directions separately. This method aims to find the optimal structure after conducting a series of

simulations and sensitivity studies. Thus, the effectiveness of using L-systems and PSLs in finding the best compromise between light weight and high strength can be confirmed.

4.3. Materials and Methods

The research objective is to obtain optimized lightweight and stiff structures by a novel biomimetic method. Figure 30 describes an overview of the computational design method for AM of lightweight structures, which leverages a full control of the geometric definition. The latter is built upon the L-systems generated and distributed along PSL's directions in a way to emulate the material growth and remodeling inside biological structures [108,169,170]. Although this method can be applied to all types of loading conditions such as flexion, torsion, and impact, this chapter, studies only the compression and shear cases. Three load cases were investigated in order to study different material growth behavior. The final steps of this method consist of parametric optimization to determine the best material distribution. The resultant optimal 2D structure is then thickened for AM, leading to a 2.5D structure. To fabricate the structure, the material jetting process is utilized, especially the PolyJet technique using VeroWhite material on a Stratasys Objet260 Connex3 machine. VeroWhite is fabricated by Stratasys [171] and located at 7665 Commerce Way, Eden Prairie, MN 55344 and 1 Holtzman St., Science Park, PO Box 2496 Rehovot 76124, Israel. The photosensitive VeroWhite resin has a Young's Modulus of 2495 MPa, a yield strength equal to 49.9 MPa, a Poisson ratio of 0.38, and a density of 1174 kg/m^3. The simulations conducted in this chapter follow Hooke's elastic law. Each step of the proposed method is further detailed in the next subsections.

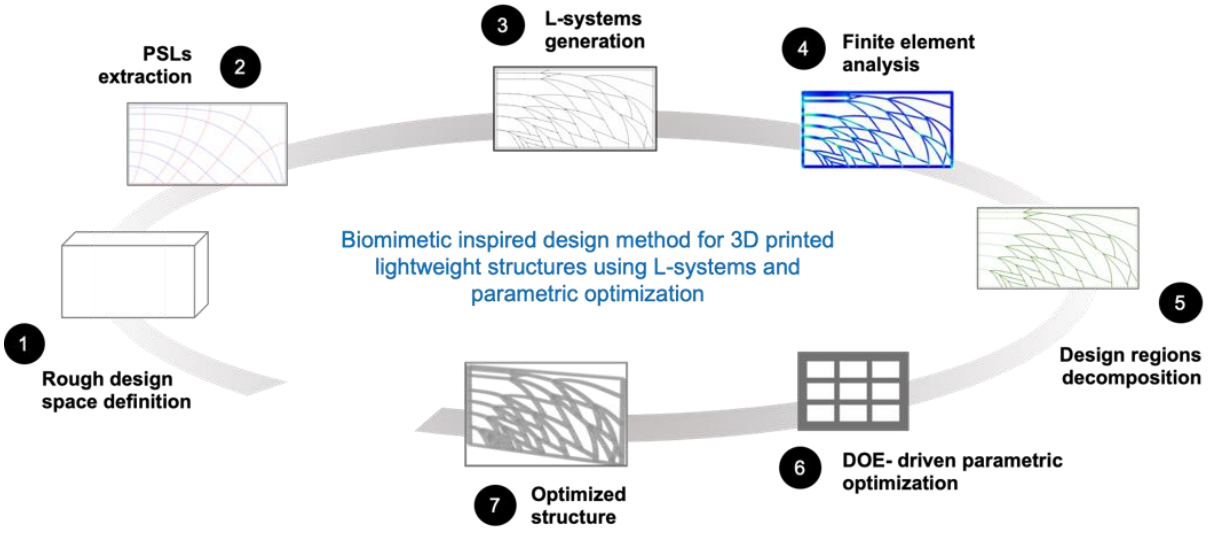

Figure 30: Overview of the proposed computational design method for AM of lightweight structures using L-systems and parametric optimization.

4.3.1. Rough design space definition

The initial rough design space – illustrated in Step 1 of Figure 30 – consists of a 2D rectangular cantilever geometry (100 x 200 mm) as already chosen as classical examples in the literature [103,172]. This design space is clamped at its lower boundary and is subjected to three load cases as illustrated in Figure 31 to investigate three different behaviors of material growth: a compressive load (CL) of 60 N (Figure 31a), a shear load (SL) of 60 N (Figure 31b), and a mixed compressive/shear loads (CSL) of 60 N respectively (Figure 31c).

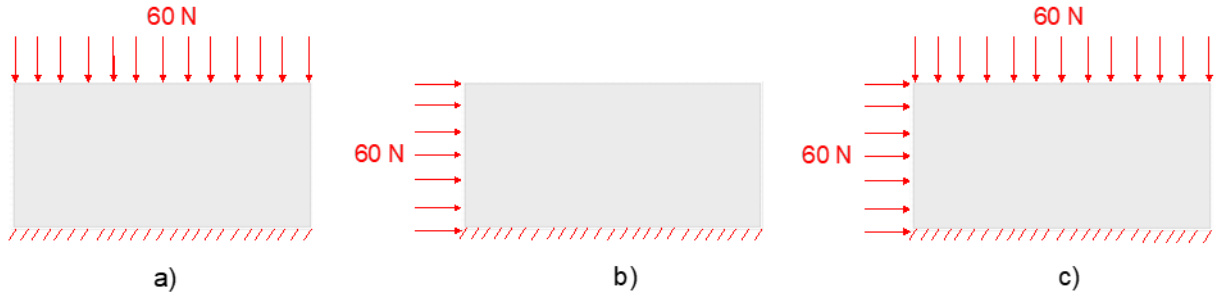

Figure 31: The three studied load cases applied to a 2D design space: (a) compression (CL), (b) shear (SL), and (c) compression-shear (CSL).

4.3.2. PSLs extraction

The next step of the bio-inspired design method (Step 2 of Figure 30) aims to determine and extract PSLs exhibiting load case-dependent trajectories [173,174]. In the 2D design space, only two PSL directions (denoted as first and second PSL directions) are significant. According to Daynes et al. [145], PSLs are free of shear stress since they are aligned with the principal stress trajectories. The numerical construction of the PSLs can be performed via the use of mathematical models [103,133,144]. In this research work, numerical simulations, using solid mechanics formulation, are conducted on the 2D design space via the commercial software COMSOL Multiphysics® 4.3a. Using the load case and the boundary conditions expressed in Figure 31, PSL's trajectories are computed in streamline forms (see Figure 32). The extraction of PSLs includes their points and vectors coordinates for further guiding L-systems computation.

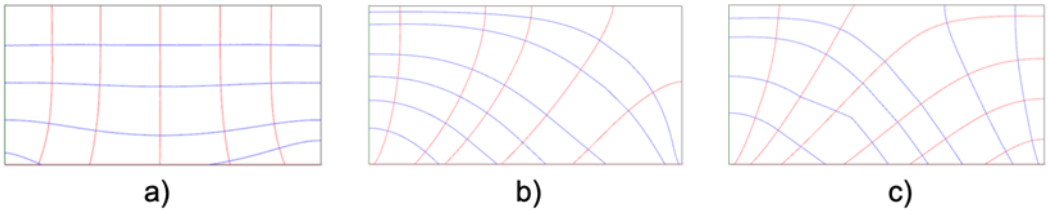

Figure 32: First (in blue color) and second (in red color) directions of PSLs for the three load cases: (a) CL, (b) SL, and (c) CSL.

4.3.3. L-systems generation along PSLs

L-systems are rewriting systems that use several strings with different designations [157]. Specific characters are used for the graphical interpretation using turtle graphics, i.e. each character or string commands the turtle to achieve an action. As a matter of example, the string F commands the turtle to draw a line of a length *l* and an angle *α* while string X commands the turtle to skip a line of a length *l* and an angle *α*. Among the numerous shapes and possibilities that L-systems offer, Table 9 shows the list of strings constituting the grammar used in the proposed geometric growth modeling (see Figure 33a). It is inspired by the context-free OL-systems (denoted as an axial tree) illustrated in Figure 33b according to Lindenmayer and Prusinkiewicz [156]. In the proposed study, the production rule has been slightly modified to reduce the geometric complexity and to adapt to symmetrical tree growth. Table 10 enumerates and describes each input used in this study.

Table 9: L-systems structure and related turtle commands.

L-systems structure	**Turtle command**
F	Draw a segment of a length *l* and an angle *α*
X	Skip a segment of a length *l* and an angle *α*
+	Turn left
-	Turn right
[	Store the turtle's current position
]	Retrieve the turtle's current position

Table 10: Grammar of the L-systems used in the biomimetic design method.

Input	**Description**	**Specific L-systems in the study**
Axiom	Starting string for first recursion	F
Rule	Production rule that generates the L-systems	F=F[+F][-F]F[+F][-F]F[+F][F]F[+F][-F]
n	Number of recursions	2
l	Branch length	Adapted to the PSLs length
α	Branch angle	Adapted to the tilt of PSLs
Start Point	Specify the point where the L-systems generation starts	An extremity of the PSL on the design space boundary
Direction	Specify the plane and the vector to indicate the L-systems generation direction	Adapted to the direction of the PSLs

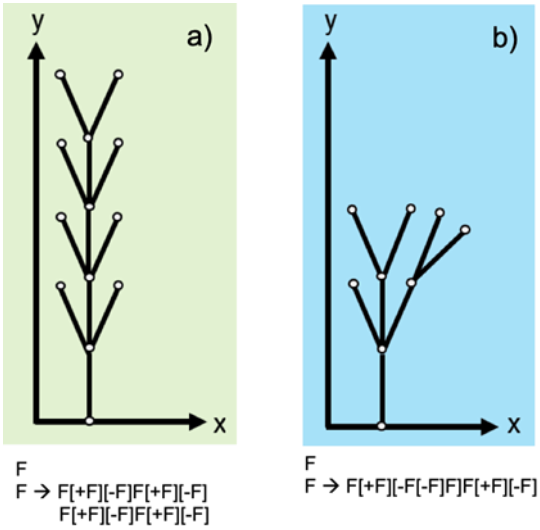

Figure 33: L-systems axioms and production rules used in this study (a) inspired by the context-free OL-systems defined by Lindenmayer and Prusinkiewicz (b) [156].

To construct the aforementioned L-systems along the PSLs within the design space, an algorithm has been proposed in Figure 34. It is important to mention that the method developed in this study is applicable for any static or dynamic load cases, boundary conditions, and design space dimension whether in 2D or 3D. The algorithm is able to take into account the integrality of these information in order to generate the L-systems inside the desired geometry. The first step consists in recovering the PSL data (points and vectors coordinates) with the design space. In a second step, the intersection points between the PSLs and the design space boundaries are determined. At each intersection point, the first generation or recursion of the L-systems is initiated. The geometric growth is governed by the production rules of the L-systems (see Table 10 and Figure 33a) according to several recursions. At each recursion, the algorithm fits the L-systems to be aligned with the PSLs direction. The L-systems and PSL lines are discretized into a precise number of points in a way to allow the algorithm to undergo neighboring points research. The number of points that discretize the different lines and L-systems is specified by the user: increasing the discretization of the L-systems and PSLs increases the fitting precision. The algorithm continues until the L-systems reach a distance ε from the design space boundaries. This distance is then evaluated as follows:

- if $\varepsilon < 0$, the L-systems branches are still inside the design space and still did not reach its boundary. The algorithm uses then the *Extend* function provided by a Rhinoceros Grasshopper to extend the floating branches to the boundary;
- if $\varepsilon = 0$, the L-systems reached the boundary. The algorithm continues to its next step;
- if $\varepsilon > 0$, the L-systems branches surpassed the boundary. Thus, the algorithm uses the *Trim* function provided by a Rhinoceros Grasshopper to trim the surplus branches.

Hence, the very final step of the algorithm consists in extending the floating branches linearly until reaching the nearest design space boundary or the nearest neighboring branch of another L-systems. This process necessitates the calculation of the branch angle and direction to ensure its extension linearly. This step also includes trimming the branches that surpass the design space boundary. The algorithm stops when all the L-systems are connected and delimited by the design space boundaries. An implementation of the algorithm has been made within Rhinoceros/Grasshopper environment via dedicated components developed in C# language.

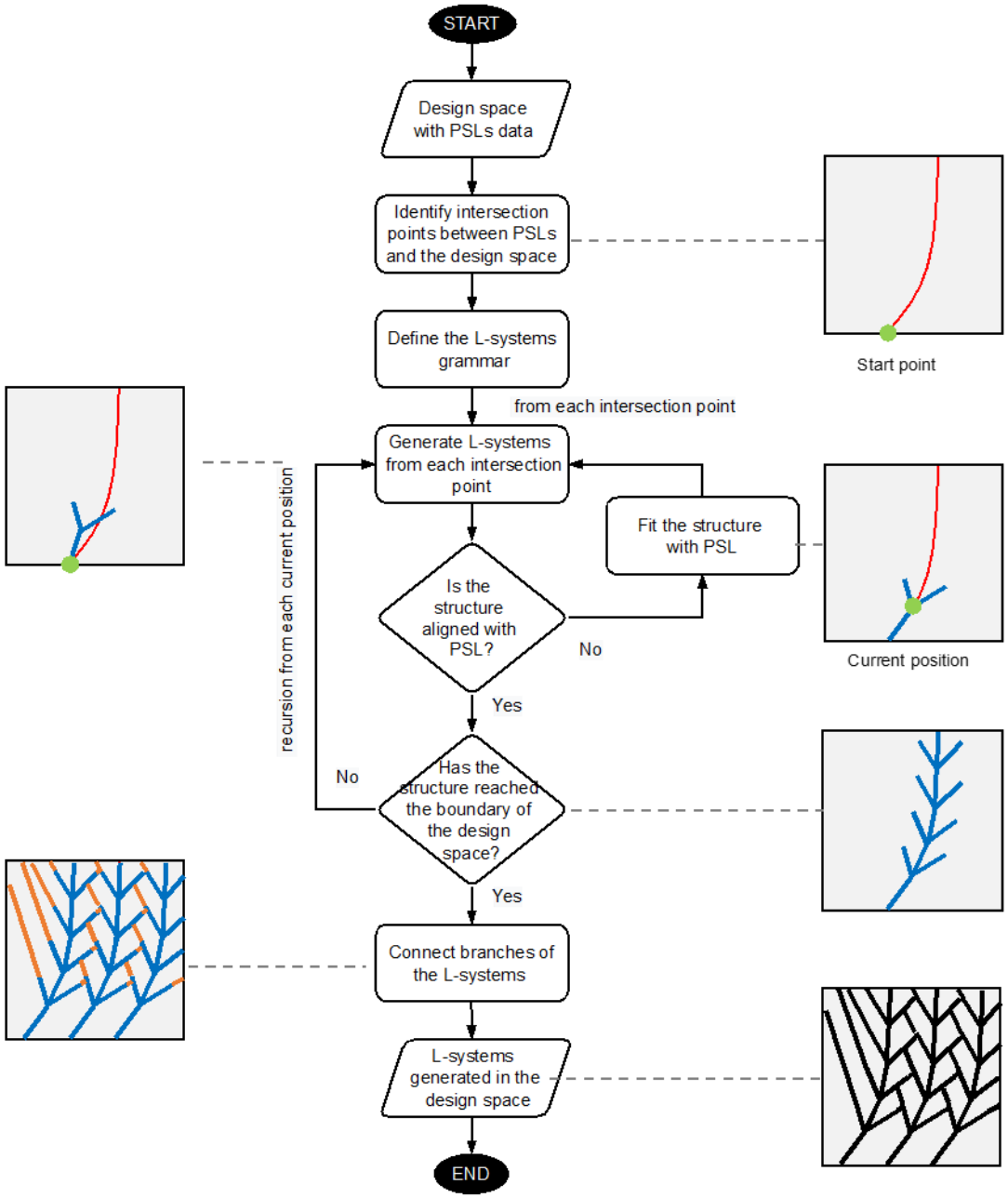

Figure 34: Flowchart describing the L-systems generation along PSLs' directions within a 2D design space.

4.3.4. Finite element analysis and design regions decomposition

Numerical simulations are then conducted on the six L-systems structures via the software COMSOL Multiphysics® 4.3a. Beam elements formulation is used for the calculations in this step of the proposed method. Similar to the 2D rough geometry, the L-systems structures are all clamped at their lower boundary and subjected to different loading types. For example, CL-1 and CL-2 are subjected to a compressive load of 60 N. Structures SH-1 and SH-2 are subjected to a shear load of 60 N, and structures CL-SL-1 and CL-SL-2 are subjected to a compressive load of 60 N and a shear load of 60 N (see Figure 35).

In order to reach the objective of light-weighting and stiffness increasing by emulating natural aspects, it was necessary to decompose the structures into two regions (see Figure 36). The first region represents the tree's trunk and the rectangular contour (in red) while the second region represents the tree branches (in blue). Beam elements with rectangular sections are used in these simulations. These sections present a thickness in the z-axis of 12.7 mm for both regions and are equal to the thickness used in the 2D rough design static and stationary simulation. Their thickness in the y axis is variable according to the region decomposition and presents three levels for each region. The thicknesses used for the first region vary between 1.5, 2, and 2.5 mm (denoted t_{FR1}, t_{FR2}, and t_{FR3} respectively) while those used for the second region vary between 1, 1.25, and 1.25 mm (denoted t_{SR1}, t_{SR2}, and t_{SR3} respectively).

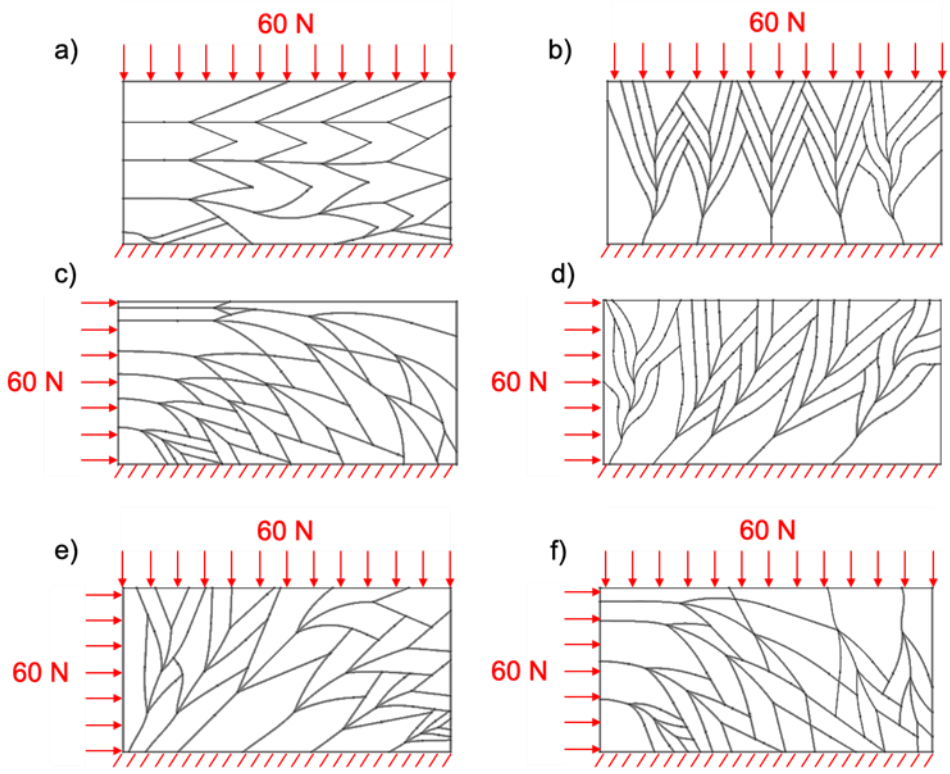

Figure 35: L-system models studied in this chapter: (a) CL-1, (b) CL-2, (c) SL-1, (d) SL-2, (e) CSL-1, and (f) CSL-2.

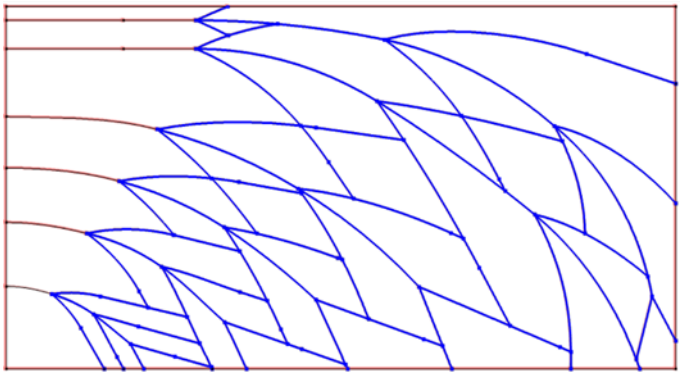

Figure 36: Design regions decomposition: region 1 (in red color) and region 2 (in blue color).

4.3.5. DOE-driven parametric optimization and determination of the optimal L-systems based structure

This section consists of a study of the influence of region 1 and region 2 cross-sections, on both the weight and the von Mises stress. This study is conducted for each of the six L-systems models via a Design of Experiments (DOE). One can identify the individual and interaction impacts of many elements that might influence the output findings of the measurements using Design of Experiments (DOE) methodologies. DOE can be also utilized to learn about a system, process, or product and determine the ideal operating conditions. It may be used for a variety of research goals, but it's especially useful early on in a screening study to assist in figuring out what the most significant parameters are. Thus, it assists in optimizing and better understanding how the most significant parameter that you can control affects replies or crucial quality features. The DOE here presents two factors: the y axis thickness of the first region and the y axis thickness of the second region. Each factor presents three levels as described in Table 11. The effect of these two factors is then analyzed in function of the von Mises stress and the structure weight using an L9 Taguchi Orthogonal Array Design [175].

Table 11 : DOE levels.

Level	Region 1 thickness [mm]	Region 2 thickness [mm]
1	1.5	1
2	2	1.25
3	2.5	1.5

4.4. Results

The results of the numerical simulations via COMSOL Multiphysics® 4.3a, which are conducted on the 2D rough design space and the L-systems structures, are presented in this section. It is important to

remind that the simulations conducted on the 2D rough design space use the solid mechanics formulation while those carried out on the L-systems structures use the beam elements formulation. Table 12 shows the maximal von Mises stress and the weight results for each load case (CL, SL, and CSL respectively), and Figure 37 illustrates the corresponding von Mises stress contours.

Table 12: Simulation results of 2D rough structure for each load case.

Load case	von Mises [MPa]	Weight [g]
CL	0.043	298.2
SL	0.173	298.2
CSL	0.13	298.2

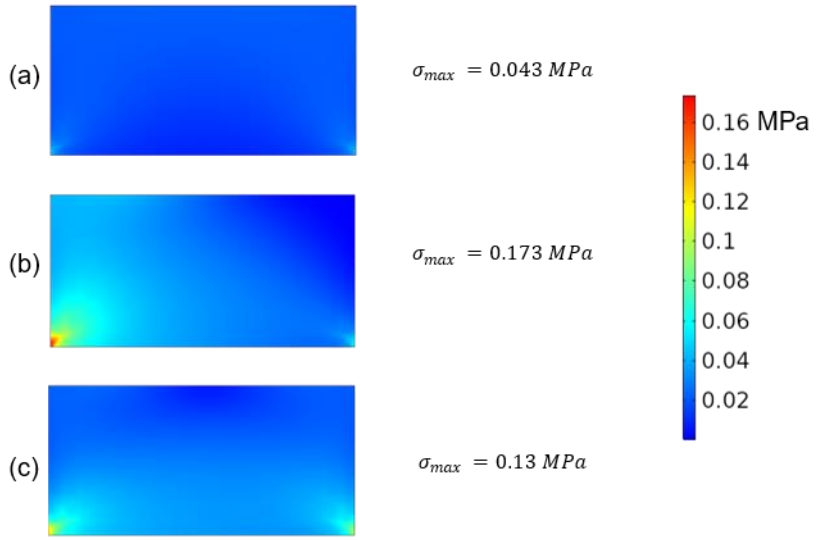

Figure 37: von Mises contours for the three load cases: (a) CL, (b) SL, and (c) CSL.

Figure 38 represents the implementation of the algorithm for the construction of L-systems along the PSLs directions within the Rhinoceros/Grasshopper environment. The L-systems components require all the parameters enumerated in Table 10 as entry inputs and have two outputs: The L-systems branches are represented by lines and the points of intersection of each line. The PSL component requires one text entry: it is the file that contains all the data exported by COMSOL Multiphysics® 4.3a. It has one output, which is the assembled lines. The third component permits gathering, all the output data of the first two components as well as the design space geometry in B-Rep type. It also uses two number sliders to allow the user to control the discretization of the L-systems and PSL segments. The output of this definition is then the L-systems structures constructed and fitted along the PSLs directions. These structures, as described in the previous section, were used later for numerical simulations and parametric optimization using Taguchi L9 DOE.

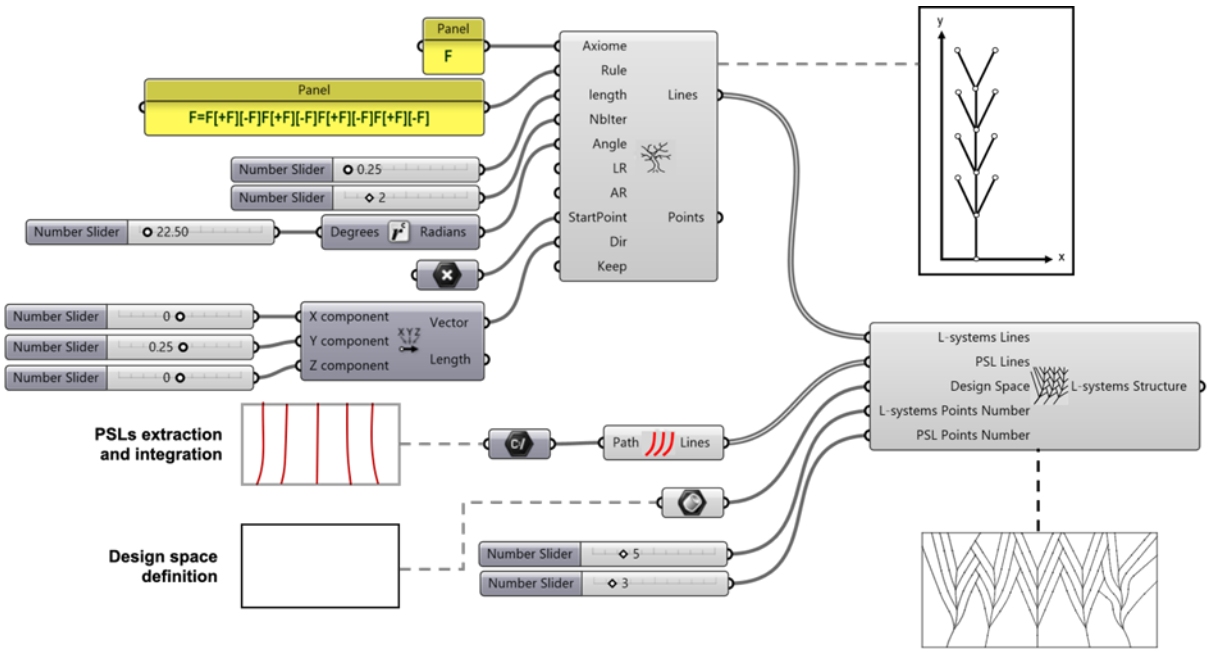

Figure 38: Grasshopper definition of the L-systems construction along the PSLs directions in the 2D design space.

Table 13 Table 14 represent the L9 Taguchi Orthogonal Array Design consisting of two factors and three levels. Table 13 gathers the von Mises and weight results for the L-systems following the first PSLs direction (CL-1, SL-1, and CSL-1) while Table 14 is dedicated to the second PSLs direction (CL-2, SL-2, and CSL-2). The numbers 1, 2, and 3 correspond to the level of each factor as explained in Table 11. Each experiment in the DOE contains the corresponding von Mises stress and the weight results.

Table 13: L9 DOE of von Mises and weight for the CL-1, SL-1, and CSL-1 configurations.

			CL-1 structure		**SL-1 structure**		**CSL-1 structure**	
Exp.	**Region 1 thickness level**	**Region 2 thickness level**	**von Mises [MPa]**	**Weight [g]**	**von Mises [MPa]**	**Weight [g]**	**von Mises [MPa]**	**Weight [g]**
1	1	1	91.49	39.30	17.04	48.15	119.87	43.79
2	1	2	73.37	45.02	12.13	55.54	118.37	50.35
3	1	3	61.41	50.74	9.11	62.93	117.48	56.91
4	2	1	67.30	44.77	14.72	54.34	69.36	49.63
5	2	2	55.01	50.49	10.66	61.73	68.18	56.20
6	2	3	46.02	56.21	8.08	69.12	67.43	62.76
7	3	1	51.29817	50.25	12.95	60.53	45.64	55.48
8	3	2	43.24	55.97	9.53	67.92	44.70	62.04
9	3	3	36.74	61.68	7.30	75.31	44.08	68.61

Table 14: L9 DOE of von Mises and weight for the CL-2, SL-2, and CSL-2 configurations.

	CL-2 structure	**SL-2 structure**	**CSL-2 structure**

Exp.	Region 1 thickness level	Region 2 thickness level	von Mises [MPa]	Weight [g]	von Mises [MPa]	Weight [g]	von Mises [MPa]	Weight [g]
1	1	1	5.61	48.88	82.66	48.07	32.22	47.37
2	1	2	5.00	57.26	69.25	56.12	31.47	54.75
3	1	3	4.96	65.65	58.51	64.18	30.99	62.14
4	2	1	5.03	54.00	55.30	53.35	19.04	53.31
5	2	2	3.65	62.38	48.86	61.40	18.41	60.70
6	2	3	2.79	70.76	42.89	69.46	18.00	68.08
7	3	1	4.77	59.11	38.95	58.63	14.98	59.26
8	3	2	3.52	67.49	35.57	66.68	12.29	66.64
9	3	3	2.73	75.88	32.29	74.74	11.93	74.02

Figure 39 shows the von Mises stress contour for Experiments 1, 3, and 9 in the DOE of Table 13Table 14 for each L-systems structure:

- Exp. 1 where the thicknesses are at their lowest levels. The thickness of the first region is t_{FR1} = 1.5 mm and that of the second is to t_{SR1} = 1 mm (see Figure 39 CL-1a, CL-2a, SL-1a, SL-2a, CSL-1a, CSL-2a).
- Exp. 3 where both regions have the same thickness (level 1 for the first region and level 3 for the second), $t_{FR1} = t_{SR3}$ = 1.5 mm (see Figure 39 CL-1b, CL-2b, SL-1b, SL-2b, CSL-1b, CSL-2b).
- Exp. 9 where the thicknesses are at their highest levels. The thickness of the first region is tFR3 = 2.5 mm and that of the second is to t_{SR3} = 1.5 mm (see Figure 39 CL-1c, CL-2c, SL-1c, SL-2c, CSL-1c, CSL-2c).

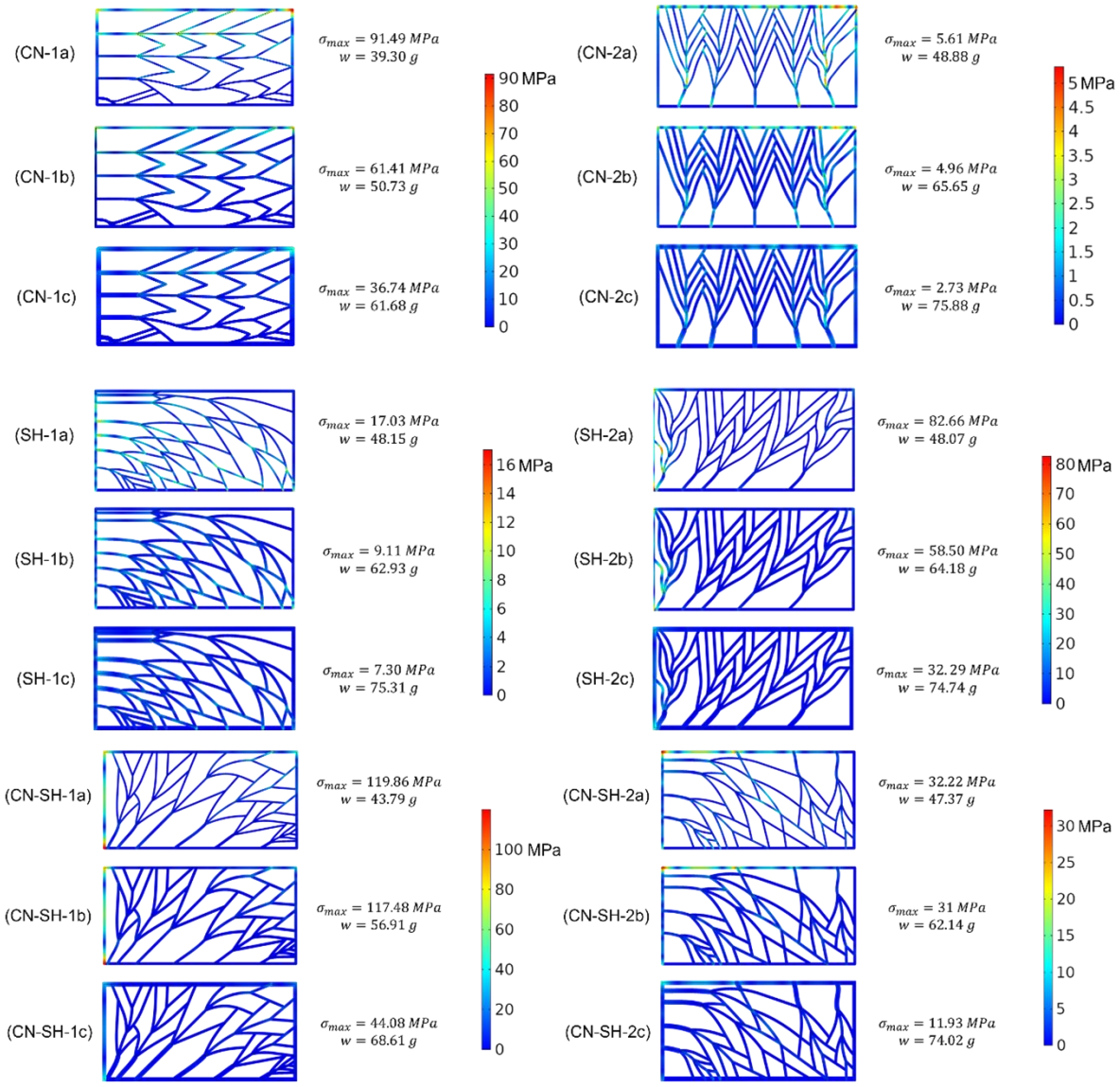

Figure 39: von Mises contours of Experiments 1, 3, and 9 for each load case and PSLs direction.

The main effect plot for the six structures is shown in Figure 40Figure 45. The influence of each factor on the response function is analyzed by the main effect plot respectively for the maximum value of the von Mises stress (Figure 40a to Figure 45a) and the structure weight (Figure 40 to Figure 45b). For the main effect plot, the slope justifies the effect of each parameter. Parameters having the highest inclination have a greater effect while parameters having a horizontal plot have minimal effect on the response function.

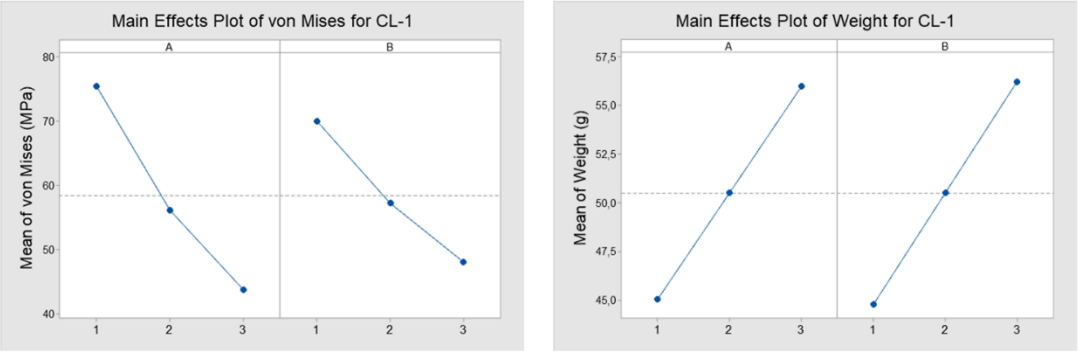

a) b)

Figure 40: Study of the effect of the thickness of the first and second regions for CL-1 structure. A and B refer respectively to the thickness of the first and second regions.

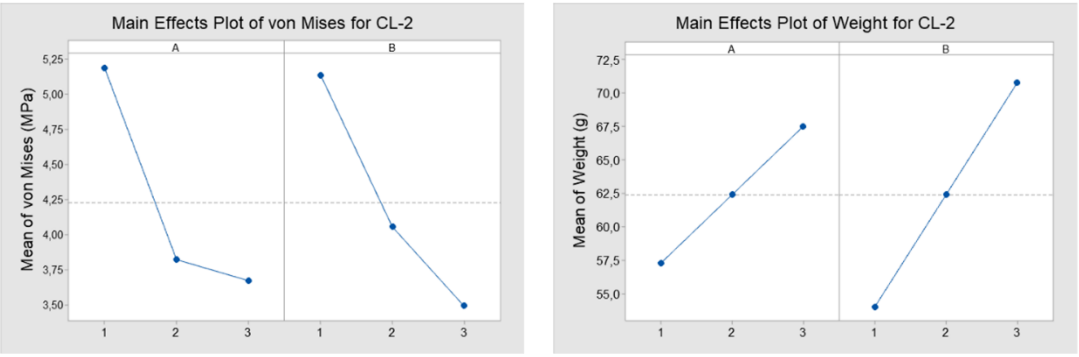

a) b)

Figure 41: Study of the effect of the thickness of the first and second regions for CL-2 structure. A and B refer respectively to the thickness of the first and second regions.

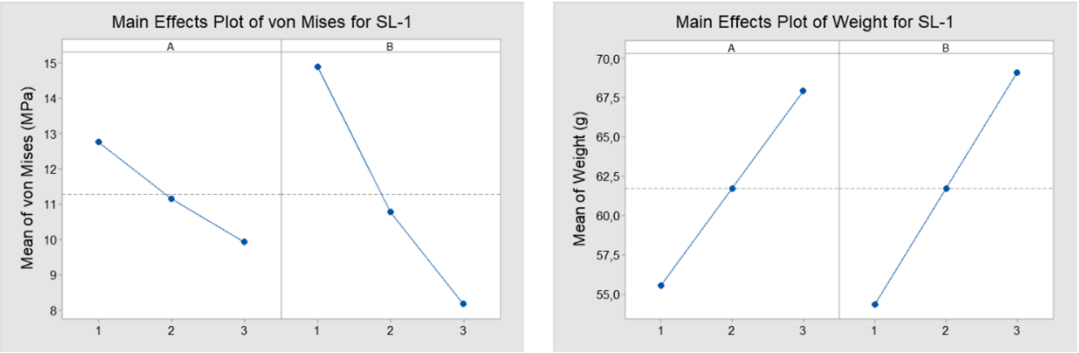

a) b)

Figure 42: Study of the effect of the thickness of the first and second regions for SL-1 structure. A and B refer respectively to the thickness of the first and second regions.

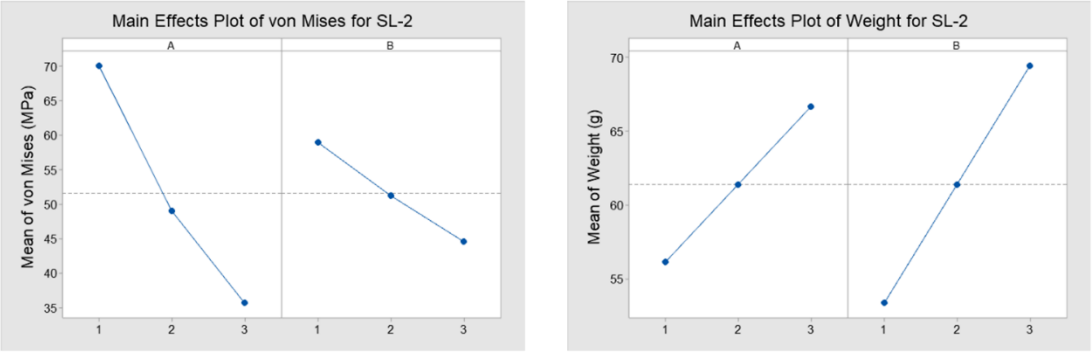

a) b)

Figure 43: Study of the effect of the thickness of the first and second regions for SL-2 structure. A and B refer respectively to the thickness of the first and second regions.

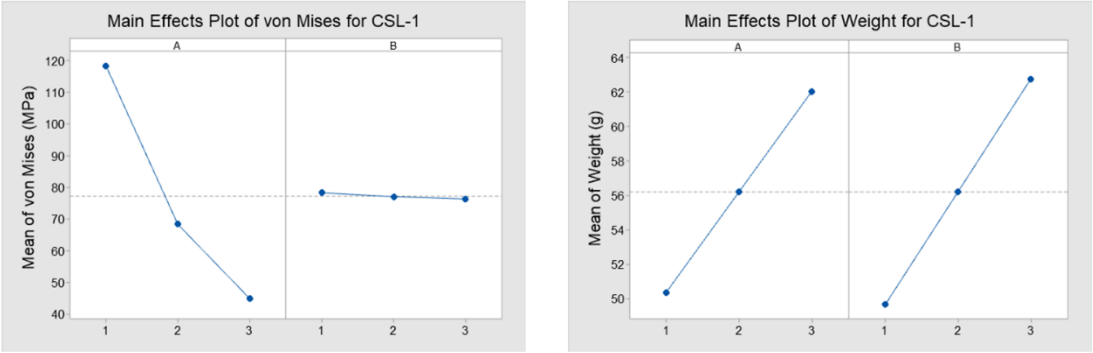

a) b)

Figure 44: Study of the effect of the thickness of the first and second regions for CSL-1 structure. A and B refer respectively to the thickness of the first and second regions.

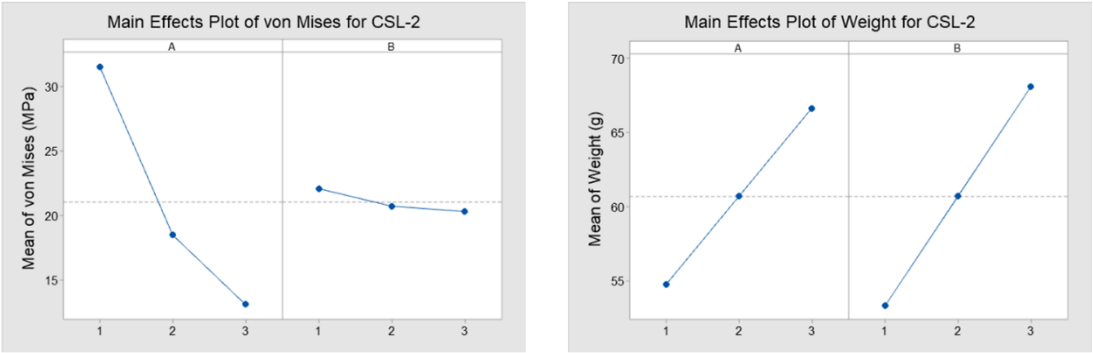

a) b)

Figure 45: Study of the effect of the thickness of the first and second regions for CSL-2 structure. A and B refer respectively to the thickness of the first and second regions.

4.5. Discussion

Table 12 represents the numerical simulation results of the 2D rough geometry for the three load cases. It is noticed that the von Mises stress is in the range between 0.043 and 0.173 MPa, which are values

lower than the yield strength of the VeroWhite material (49.9 MPa). The weight of the structure is equal to 298.2 g. As beforementioned, this study aims to find a better compromise between weight and strength. By integrating the biomimetic method of L-systems along the PSLs of the structure, it can be possible to reduce the initial weight in a way that the von Mises stress stays lower than the yield strength of the VeroWhite material used (49.9 MPa). To validate the hypothesis, numerical simulations were conducted on the six L-systems structures. The results of von Mises stress and weight were collected in the L9 DOE (Table 13 and Table 14).

Firstly, by analyzing the von Mises values in Table 13, it was noticed that some values are higher than the yield strength of the VeroWhite material. This is the case of the values in experiments 1 to 7 for CL-1 configuration (Table 13), experiments 1 to 6 for CSL-1 configuration (Table 13), and experiments 1 to 4 for SL-2 configuration (Table 14). The following combinations are hereafter excluded and cannot be considered optimal configurations:

- For CL-1 configuration, a thickness of 1.5 mm for the first region and thicknesses of 1, 1.25, and 1.5 mm for the second region cannot be used. Moreover, a thickness of 2 mm for the first region and a thickness of 1.5 mm for the second region cannot be employed together.
- For CSL-1 configuration, thicknesses of 1.5 and 2 mm for the first region cannot be used with any of the thicknesses of the second region (1, 1.25, and 1.5 mm).
- For SL-2 configuration, a thickness of 1.5 mm for the first region cannot be used with any of the thicknesses of the second region.

Furthermore, it was noticed that all configurations, including the ones that are excluded from the study, present a weight value lower than that of the 2D rough structure (298.2 g). The weight reduction percentage is shown in Table 15 below. The weight reduction with respect to the weight of the 2D rough structure is in a range between 74.55% and 86.82%. Logically when the thicknesses of the first and second regions are at level 1 (1.5 and 1 mm respectively), the weight reduction is the highest. Inversely, when the thicknesses of the first and second regions are at level 3 (2.5 and 1.5 mm respectively), the weight reduction is the lowest.

Table 15: Weight reduction percentage of the L-systems-based structures with respect to the weight of the 2D rough structure (298.2 g).

CL-1 configuration	SL-1 configuration	CSL-1 configuration	CL-2 configuration	SL-2 configuration	CSL-2 configuration
86.82	83.85	85.32	83.61	83.88	84.11
84.90	81.37	83.12	80.80	81.18	81.64
82.98	78.90	80.92	77.98	78.48	79.16
84.99	81.78	83.36	81.89	82.11	82.12
83.07	79.30	81.15	79.08	79.41	79.64
81.15	76.82	78.95	76.27	76.71	77.17
83.15	79.70	81.40	80.18	80.34	80.13
81.23	77.22	79.20	77.37	77.64	77.65

79.32	74.75	76.99	74.55	74.94	75.18

Figure 39 represents the von Mises stress results for each load case and PSLs direction configuration. It represents particularly the following cases:

- The case where both regions are at their lowest level 1 (1.5 mm and 1 mm for first and second region respectively). This case is denoted Case 1 (Figure 39a).
- The case where both regions have the same thickness (level 1 for the first region and level 3 for the second region). $t_{FR1} = t_{SR3} = 1.5$ mm. This case is denoted Case 2 (Figure 39b).
- The case where both regions are at their highest level 3 (2.5 mm and 1.5 mm for the first and second regions respectively). This case is denoted Case 3 (Figure 39c).

According to Figure 39, and as expected, for the three load cases, the structures that have a tree growth along the PSLs and the load direction, provide a lower von Mises value than those that have a growth orthogonal to the load direction. Until this stage of the study, one can predict that the CL-2 configuration is more suitable for the compressive load case, the SL-1 configuration is more adequate for the shear load case, and the CSL-2 configuration is better than the CSL-1 configuration for the compressive/shear load case.

In order to determine the optimal configuration for each load case, a sensibility study was conducted in Figure 40Figure 45. For von Mises stress, the effect slope is descending. Figure 40a and Figure 41a illustrate, for CL-1 and CL-2 configurations, the effect of the thickness for the first and second regions on the von Mises stress. The effect of the thickness of both regions is high but it was noticed that the thickness of the first region is more important than that of the second region. Figure 42a shows the opposite behavior than that mentioned before: for the SL-1 configuration, the effect of the thickness of the second region is higher than that of the first region. For SL-2, CSL-1, and CSL-2 configurations, Figure 43a, Figure 44a, andFigure 45a show that the effect of the thickness of the first region is much more important than that of the second region. As for the weight, Figure 40b toFigure 45b show that the effect of the thicknesses of the first and second regions is merely the same with more importance on the effect of the second region's thickness.

For the compressive load case, both CL-1 and CL-2 have shown the effectiveness of the method of integrating L-systems along PSLs directions in a structure in order to reduce its weight while keeping a reasonable stiffness and strength. However, it can be noticed that the CL-1 structures present higher von Mises values than CL-2. For a load of 60 N, the CL-1 configuration presented high von Mises values while for the CL-2 configuration, the von Mises stress stays lower than the yield strength of the VeroWhite material. Even if the CL-1 structure presents lower weight values than that of the CL-2 structure for each experience in the DOE, the CL-2 structure fulfills the objective of this study in a better way. The latter statement can be justified by the growth direction of the L-systems in the CL-2

configuration. Indeed, the direction of the branches is colinear to the compressive load direction thus the material distribution is closer to the zone where the load is applied as shown in Fig. 6b. While for the CL-1 structure, the L-systems branches' growth direction is orthogonal to the load direction which explains the higher von Mises values (Figure 35a). That means that the structure CL-2 is better adapted to the compressive load case.

For the shear load case, for both SL-1 and SL-2 structures, the effectiveness of the method of integrating L-systems along PSLs directions is again validated. SL-1 and SL-2 structures present approximatively the same weight values, but the SL-1 structure has remarkably lower von Mises stress values. This difference can be justified by the L-systems growth along the shear load direction (Figure 35a). SL-1 is then the structure that is better adapted to the shear loads. Hence, the effectiveness of this method is also proved for the combined compressive/shear load cases. The same interpretation done for the CL configurations can be used for the CSL configurations: CSL-2 is better adapted for the combined compressive/shear load.

To summarize the analysis of the study of the effect of the first and second region thicknesses on the von Mises stress and the weight for the six structures, the following observations can be stated:

- A thickness of 2 mm (level 1) for the first region and a thickness of 1 mm (level 1) for the second region gives a maximal von Mises stress value and a minimal weight (Exp. 1 in Table 13Table 14).
- A thickness of 3 mm (level 3) for the first region and a thickness of 2 mm (level 3) for the second region gives a minimal von Mises stress value and a maximal weight (Exp. 9 in Table 13Table 14).

Finally, it is concluded that integrating L-systems generated along the PSLs directions in a structure reduces its weight and maintains a reasonable stiffness. The latter statement validates the hypothesis raised at the beginning of the discussion section. For the three load cases, the CL-2, SL-1, and CSL-2 configurations are taken into account. Considering that, for all combinations, these configurations have shown low von Mises stress values, one can choose the minimal thicknesses levels as the parameters used for the optimal structures: t_{FR1} = 1.5 mm and t_{SR1} = 1 mm for CL-2 and SL-1 configurations. While for CSL-2 configuration, a minimal thickness for the first region equal to t_{FR1} = 1.5 mm combined with any of three thicknesses of the second region can be taken into account. A CSL-2 structure presenting a first region thickness of 1.5 mm and a second region thickness of 1.25 mm will be considered. The DOE optimization technique has then proved its effectiveness in determining structures having a lightweight and high stiffness. Further studies using different optimization algorithms will be conducted in order to obtain optimal structures with several variations of sections and thicknesses like the Moving Least Square (MLS) and the Kriging methods and sequential quadratic programming (SQP) techniques [173,174]. These three optimal structures are then additively manufactured by material jetting process

and more particularly with the PolyJet technique using VeroWhite material on a Stratasys Objet260 Connex3 machine (see Figure 46).

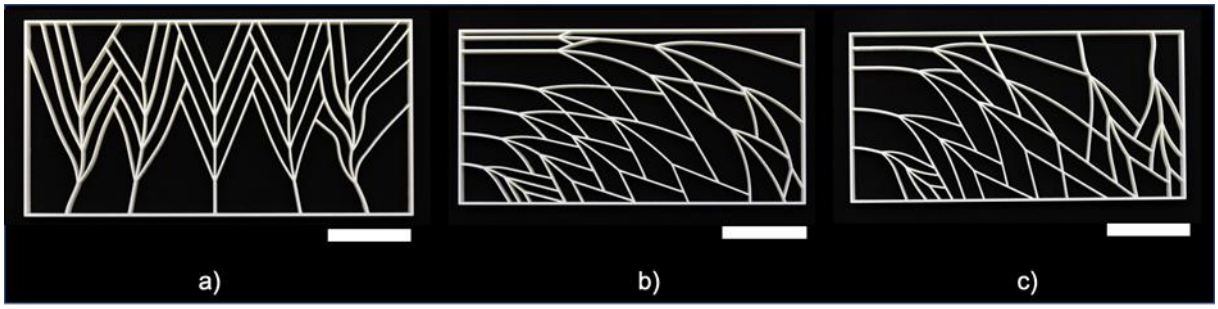

Figure 46: Structures (a) CL-1, (b) SL-2, and (c) CSL-1 printed with PolyJet technique on a Stratasys Objet260 Connex3 machine with VeroWhite material. All scale bars: 50 mm.

4.6. Conclusion

In this chapter, a novel biomimetic design and modeling method based on L-systems distributed along the PSLs' directions has been proposed. Numerical simulations and parametric optimization schemes based on an L9 DOE sensibility study were conducted to prove the effectiveness of this method in adapting mechanical structures to various loading cases as well as ensuring a good stiffness-to-weight ratio. The structures studied were all fixed at their lower boundary. Although the proposed method could be applied to any load cases (flexural, torsional, and impact), only three loading cases were considered: compression (CL), shear (SL), and combined compression/shear (CSL). Each load case presented two structures derived from the two significant PSLs' directions. Indeed, the DOE sensibility study helped us identify the optimal structure for each load case:

- For the compressive load case (CL-2), the weight reduction was estimated between 74 and 84% with respect to the initial rough geometry, and the maximal von Mises stress was equal to 5.61 MPa, a value much lower than the yield strength of VeroWhite material (49.9 MPa).
- For the shear load case (SL-1), the weight reduction was in the same range as the one of the compressive load case, and the maximal von Mises stress was equal to 17.04 MPa.
- For the combined compressive/shear load case (CSL-2), the weight reduction was between 75 and 84%, and the maximal von Mises stress was equal to 32.22 MPa.

The latter results of the conducted numerical simulations have demonstrated that this method helped reinforce the structure, thus obtaining high specific strength while reducing its weight. This study also highlighted the need of producing lightweight and stiff structures by AM since it was developed in a way to respect AM constraints and build orientations. In future horizons, this generative design method will be matured in terms of designing and optimizing 3D complex models and in conducting a combined

parametric and topology optimization scheme. In addition, future work will focus on different loading conditions, especially impact study cases.

Chapter 5: L-systems structures optimization using low-cost meta-modeling algorithm based on meta-heuristic knowledge

"He who loves practice without theory is like the sailor who boards ship without a rudder and compass and never knows where he may cast."

Leonardo Da Vinci

"The true sign of intelligence is not knowledge but imagination."

Albert Einstein

5.1. Abstract

In the previous chapter, a novel biomimetic method based on the L-systems growth along the PSLs was proposed. The parametric optimization using L9 Taguchi Orthogonal Array DOE was conducted on the resultant L-systems structures with different cross-section distributions. The results have shown that this biomimetic method has helped obtaining lightweight structures with a high specific strength. However, the scheme followed in studies depending on DOE is time-costly, and the optimal parameters' values are not precise and obtained through a prediction of their range. The approach presented in this work is related to sampling methods and model management in the optimization process of surrogate-based methods. This approach helps reaching the global optimum with a small number of numerical simulations using a sampling algorithm based on the Particle Swarm Optimization (PSO). A knowledge databas with intelligent sampling techniques has been incorporated into the management of the optimization model in order to enhance the (sampling) in each optimization iteration and increase the efficiency and accuracy of the metamodel (Kriging). By using this technique, the sampling size may be decreased while also improving the metamodel's accuracy. In other words, this method will be applied on L-systems structures in order to improve the stiffness-to-weight ratio, which a mechanical requirements of AM.

5.2. Introduction

In a previous study (cf. Chapter 4), biomimicking natural and biological structures in their growth and material adaptation, was of interest. Indeed, a biomimetic design and modeling method based on L-systems distributed along the PSLs' directions was proposed. To demonstrate the efficiency of this method in adapting mechanical structures to various loading cases and guaranteeing a good stiffness-to-weight ratio, numerical simulations and parametric optimization strategies based on a L9 DOE sensitivity study were carried out. Results of the latter method have shown that the studied parameters have an influence on the weight and stress variations. It helped reducing the weight of the initial solid structure from 73% to 84% while maintaining a stress value lower than the yield strength of the material (49.9 MPa). However, this method does not give precise optimal results. It relies on a range of cross-sections values that the engineer estimated to be optimal. An improvement of the results can be achieved through parametric optimization algorithms developed by several researchers.

Wu et al. [176] have conducted an evolutionary algorithm approach on an aperiodic meta-structure for the continuous and broadband wave attenuation with a low vibration transmissibility. Their approach has permitted a maximal attenuation increase of 90% compared with the conventional repetitive local resonance, without any weight increase. Rajeev et al. [177] have conducted a parametric optimization using a DOE to optimize corner radii in hexagonal honeycombs under in-plane compression. They have

found that the value of the optimum corner radius increases with the increase of the beams' thicknesses, thus influencing the maximal von Mises stress. Based on Rajeev et al. [177] study, one can say that parametric optimization is primordial when it comes to finding optimum design parameters for bar structures. In their study, Alekseytsev et al. [178] have outlined the procedure for developing parametric optimized algorithm for steel trusses. Given the strength, stability, and stiffness constraints defined for each truss component, parametric optimization has been carried out. The objective function has been defined depending on several specifications especially manufacturing and material costs. Kibkalo et al. [179] have defined and discussed solutions to a parametric optimization problem for thin-walled beam and bar structures. By adjusting the structural parameters while maintaining the necessary load-carrying capacity of structural members and the lowest possible production cost, the best solution has been found. An approach for parametric optimization of steel flat rod systems was suggested by Serpik et al. [180]. The optimization problem was addressed as a structural weight minimization problem taking into account strength, displacement, and overall stability constraints. As design factor, struts' cross-sections and the joint coordinates were taken into account. This approach has found the optimal parameters allowing a high level of safety for their structures' designs [181]. Mohanty et al. [182] have proposed a parametric optimization using a hybrid Taguchi MARCOS-nature inspired heuristic technique for FDM-printed parts. Their study considered the relationship between five significant processing constraints i.e. raster angle, part orientation, air gap, layer thickness, and raster width. This study has also focused on the effect of these constraints on the dimensional accuracy of the fabricated part. They have conducted twenty-seven experiments following a Taguchi's architecture coupled with their recent MARCOS method, which is based on ten different optimizations algorithms: the Genetic, Simulated Annealing, Particle Swarm, Grey-Wolf, Moth Flame, Whale, Jaya, Sunflower, Lichtenberg, and Forensic Based Investigation Optimization Algorithms. The comparative inspection of these bio-inspired algorithms in FDM printed parts was performed and the results have shown that part orientation is the most significant element.

However, most of the studies cited previously require high numbers of numerical trials and error corrections, and the use of computational analysis is limited by the high CPU time. Therefore, to reduce the CPU's running time for such analysis and simulations, metamodel techniques like Design and Analysis of Computer Experiments (DACE) in combination with Response Surface Models (RSM) are frequently employed in engineering design optimization. The latter proposed approach aims to generate a condensed approximation of the numerical simulation and ease the optimization of the design. The approximation model is referred to as a metamodel or surrogate approximation model of the numerical model.

In different optimization problems, several approximation methods have been developed especially the Response Surface Method [183-186] with second order polynomial approximation. To reach the global optimum, other researchers have been concentrating on the management of this RSM, such as by using

an auto adaptive research space approach. Examples of applications where this approach has been proven effective include clinching optimization issues [187] and polymer extrusion [173,188]. The generation of the response surfaces for system approximation has also used other approximation-based techniques such as Kriging [189-192], Radial Basis Functions (RBF) [193-195], Multivariable Adaptive Regression Splines (MARS) [196,197] , Neural Networks [198-200], and Support Vector Regression [201,202].

In the literature, the most used models are Kriging and Moving Least Square (MLS) Approximation utilizing second-order polynomials. These models are fast and effective to compute the RSM and to simulate low-order issues. However, this approach falls short when dealing with highly non-linear issues [203]. In comparison with the GA-based evolutionary methods and similar techniques, approximation methods often require fewer computer simulations than gradient-based algorithms, and they do not require derivative outputs. This has a significant impact on computing efficiency. On the other hand, as referenced by DACE, the resilience and effectiveness of approximation-based approaches rely on how approximation is accomplished and how sampling methods are employed. The management of approximation models in the optimization process is the subject of additional research including screening [186,204] and extended Kerhunen-Loeve Expansion (KLE) [205,206], which aim to minimize the dimensionality of the design space. The reduction of the design space, which may progressively increase the optimum solution's accuracy and convergence, is another important area of metamodeling study [207,208]. Another area of research focuses on the optimization algorithms that should be employed to find the best solution method [186,204]. In the design and analysis of numerical experiments, the objective of the metamodel optimization is to decrease the number of samples (computation cost) while maintaining acceptable approximation model accuracy. Kriging models show that the design space has a direct impact on the modeling efficiency. The sampling size and distribution in the design space are two crucial criteria.

DOE, has therefore emerged as the key variable in determining the precision and effectiveness of the metamodeling process. The optimization process's model management and sampling techniques have a significant impact on the meta-correctness model's and effectiveness [209-212].

The approach that is provided in this study addresses the latter statement and that for surrogate method optimization. The algorithm optimum can be reached with fewer samples by conducting FEA and throughout the optimization iterations, the approximation model can converge to the global optimum.

Hence, the conventional DACE approach is replaced by PSO as a sampling tool to build the metamodel. As a result, the Kriging-based metamodel will be able to scan the search space using the unique and combined knowledge of each sample. These techniques can solve local minima issues thanks to their stochastic character.

In an earlier work [173,184], an auto-adaptive sampling scheme that can gradually reduce the search space around the optimum has been adapted and integrated as DACE using Conventional Composite DOE. In contrast to space reduction approaches, every optimization iteration in this process takes into account the whole design space. This enables each sample to find more potential optimums. One may argue that sample points should be chosen to fill the whole design space because the form of the response function is not well known beforehand. In order to cover the whole design space with a known sampled number, a Central Composite Design (CCD) is employed as the first sampling method. In order to eliminate needless finite element computations and improve the samples in each optimization iteration, a knowledge database based on the history of the movement of each particle has also been included into the model management process.

This method is applied on the L-systems structures previously introduced in chapter 4 of the present thesis. These structures present a tree growth along the PSLs directions. In contrast to the previous study, the two PSL directions were combined: the first direction serves as a guideline for the L-systems' growth and the second serves for branch extensions and limitations. Thus, four design variables are considered: the design contour thickness, the trunk thickness, branches' thickness, and the second direction PSLs' thickness. The proposed optimization scheme will then prove its effectiveness in weight reduction and in maintaining a good stiffness for biomimetic designs and structures: two of the most important mechanical properties required by AM.

5.3. Materials and Methods

5.3.1. Structure definition

Besides obtaining lightweight structures presenting optimal stiffness, the research objective consists in finding the optimal beams' cross-sections (or the struts' thicknesses). In the previous chapter, the structures were built upon the L-systems generated and distributed along PSLs' directions, imitating material growth and distribution inside biological structures. Three load cases were studied: compression (CL), shear (SL), and combined compression/shear (CSL) loads, all equal to 60 N. All the structures were clamped at their lower boundary. For each load case, two PSLs directions were taken into account separately: the L-systems are generated along only one of the two directions. That results in six total studied structures. In contrast to what was presented in the previous study, the structure studied in this work is described as follows:

- The contour (or boundary) consists of a 2D rough geometry (100 × 200 mm). It has a thickness of 12.7 mm along the *z*-axis (Figure 47).
- The material used in the numerical simulations is the VeroPureWhite resin. This resin is used by the material jetting process (PolyJet®) on the Stratasys® 3D printing machine. It has a

Young's modulus of approximately 2500 MPa, a Poisson ratio of 0.38, a density of 1174 kg/m^3, and a yield strength of 54 MPa [41].

- Both PSLs' directions are used in one structure: the L-systems are generated along the first PSLs' direction and the branches are extended (or trimmed) according to the second PSLs' directions. The algorithm was described in Chapter 4 (Figure 48).
- The design space is divided into four zones; therefore, four optimization variables are taken into account: the thicknesses of the L-systems trunk, the L-systems branches, the second PSLs' direction, and the boundary (Figure 49). These variables are denoted TR, BR, PD, and BD respectively.

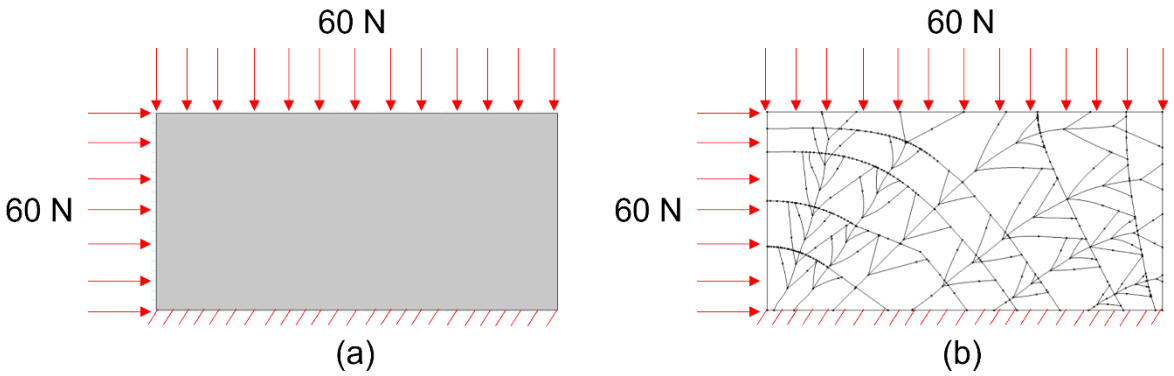

Figure 47: Representation of the load case and boundary condition for the rough design space (a) and the L-systems along PSLs structure (b).

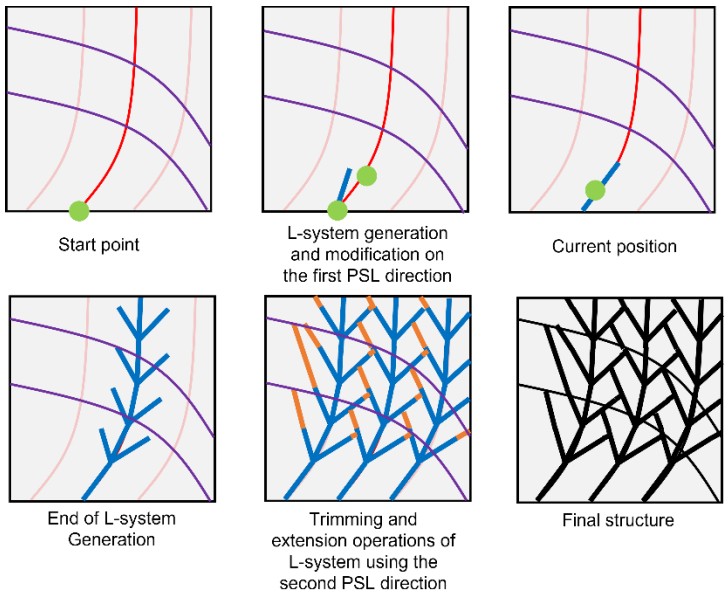

Figure 48: L-systems' generation steps along PSLs.

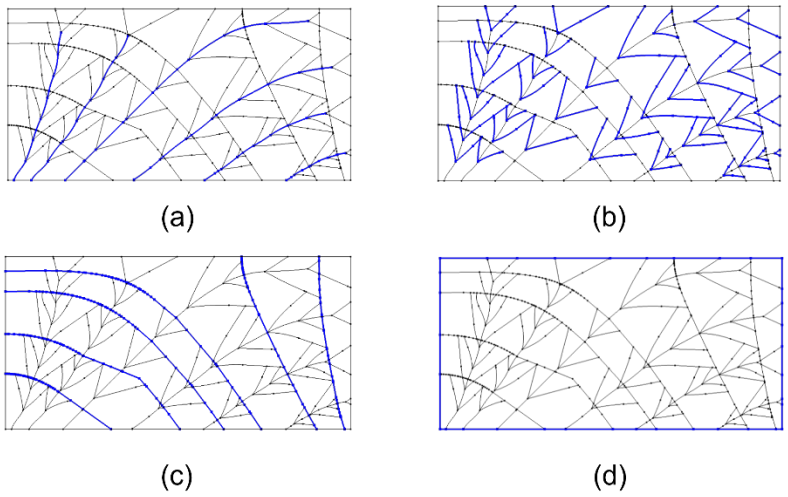

Figure 49: Decomposition of optimization variables into groups: L-systems' trunk (a), L-systems' branches (b), second PSLs' direction (c), and boundary (d).

5.3.2. Optimization problem definition

In order to find the optimal structure presenting the minimal weight and having a von Mises stress lower than the yield strength of the VeroPureWhite material ($\sigma_y = 54\ MPa$), the optimization problem is defined as follows:

$$\begin{cases} \min f(x) = \sum_{i=1}^{n} M_i(x) \\ g(x) = \frac{\max(\sigma(x) - \sigma_y)}{\sigma_y} \leq 0 \\ LB \leq x \leq UB \end{cases} \qquad (4)$$

- x is the vector of variables that consist of the cross-section of each group defined previously (L-systems trunks and branches, second PSLs' direction, and the boundary).
- M_i are the weights calculated in function of the variables x for each group.
- $f(x)$ is the objective function (total weight).
- $g(x)$ is the optimization constraint. A negative value of this function means that the calculated von Mises stress stays lower than the yield strength of the material.
- $\sigma(x)$ and σ_y are the calculated von Mises stress and the yield strength respectively.
- LB and UB stand for lower bound and upper bound respectively.

5.3.3. Optimization algorithm

As mentioned previously, the aim of this study is to find optimal thicknesses of each optimization variable that allow obtaining a good compromise between lightweight and high stiffness. This optimization is conducted using a meta-modeling algorithm based on a meta-heuristic and knowledge database approach.

The determination of the objective and constraint functions becomes implicitly tied to the optimization parameters, when FEA is used, necessitating a costly numerical simulation. The metamodeling

technique with Kriging interpolation is applied and linked with an intelligent sampling and model management strategy in order to achieve the optimal parameters at cheap cost but excellent accuracy. In this study, the Kriging interpolation is used to explicitly express the metamodel in accordance with the optimization variables [171, 200, 213-217].

The approximate function $\tilde{J}(x)$ (objective or constraint function) can be expressed as follows:

$$\tilde{J}(x) = P^T(x)a + Z(x) \qquad (5)$$

Where $a = [a_1, \dots, a_m]^T$ is the vector of the unknown parameters, m is the number of samples, and $Z(x)$ is the random hypothetical realization of a stochastic process with a mean of zero and a spatial correlation function represented by:

$$cov\left[Z(x_i), Z\left(x_j\right)\right] = \sigma^2 R(x_i, x_j) \qquad (6)$$

Where σ^2 is the process variance and R is the correlation matrix made up of the correlation function that has been assessed for every conceivable combination of design samples and analysis of computer experiments.

In the vector P with $P(x) = [P_1(x), \dots, P_m(x)]^T$, the value of the m-basis functions $p(x)$ is evaluated at each sample.

The implicit output responses vector of the function are represented by:

$$F(x) = [f_1(x), \dots, f_n(x)]^T \qquad (7)$$

Then the coefficient vector a is estimated as follows:

$$a = (P^T R^{-1} P)^{-1} P^T R^{-1} F \qquad (8)$$

$Z(x)$ figuring in the Eq. (5) is used to model the deviation form of the regression to interpolate the response data from the function:

$$Z(x) = r^T(x)\beta \qquad (9)$$

Where $r^T(x)$ is the correlation vector between x and the sampled data points given by:

$$r^T(x) = [R(x_1, x_1), \dots, R(x_1, x_n)] \qquad (10)$$

The parameters β are defined as follows:

$$\beta = R^{-1}(F - Pa) \qquad (11)$$

The optimization process's model management and sampling techniques have a significant impact on the accuracy and effectiveness of metamodels. In this application, the Kriging Swarm Optimization

(KSO) formulation is used in order to decrease the sample size while simultaneously improving the metamodel's accuracy.

5.3.4. KSO formulation

DACE, is now considered to be essential to the metamodeling process. The PSO algorithm [218-222] is employed as a smart sampling tool to construct the metamodel. The PSO algorithm is then used instead of the conventional DACE approach. By using the unique and collective knowledge of each particle, the metamodel based on Kriging will be able to move over the search space (or sample). Additionally, these techniques work to narrow the search space surrounding the global optimum by overcoming the drawbacks of local minima due to their stochastic character. The optimization method has been combined with knowledge databases that are based on the history of each particle's trajectory. And that in order to share the unique information of each particle and eliminate pointless FEA computations. Moreover, every optimization iteration might enrich the sample thanks to the knowledge database. The method used in this study is represented by the flowchart in Figure 50.

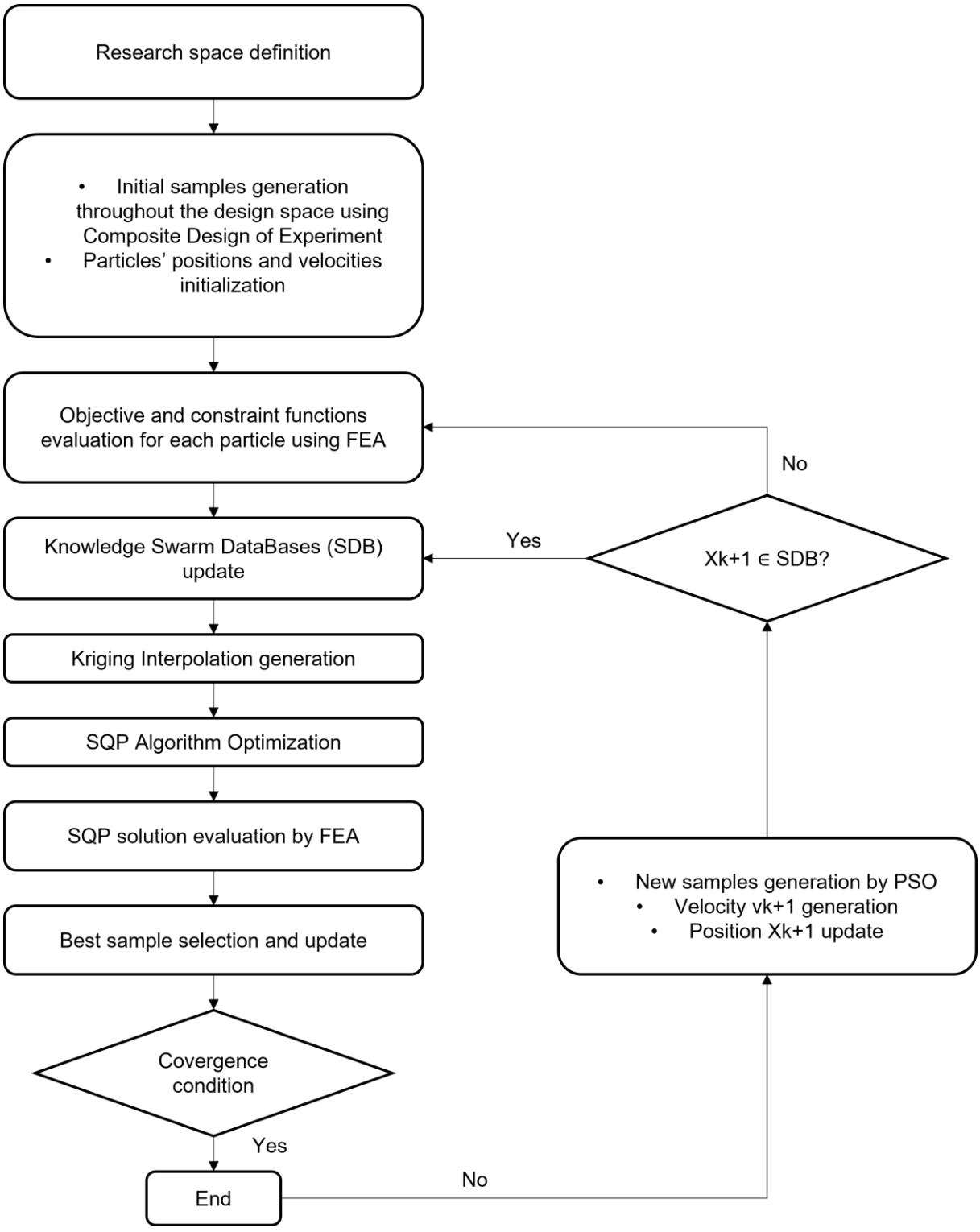

Figure 50: KSO algorithm flowchart recreated from Lebaal (2019) [223].

This method is then divided into ten steps. Three of these steps (steps 5,6, and 7 are described in details in [224]) :

Steps 1 and 2: The search space is defined, and the population array of particles and their velocities is initialized. A composite experimental design is used to disperse the initial sampling over the search space:

$$\boldsymbol{X^{ij\ (DO)}} \begin{cases} \boldsymbol{i = 1, 2, \dots, n} \\ \boldsymbol{j = 1, 2, \dots, D} \end{cases}$$

Where $\boldsymbol{n}$ is the swarm size and $\boldsymbol{D}$ is the dimension size.

Step 3: For each sample ($\boldsymbol{i}$), the problem is evaluated using FEA. And at iteration $\boldsymbol{k}$, the implicit evaluation of the required fitting functions for optimization $\boldsymbol{F_k^i}$ is performed.

Step 4: The knowledge Swarm DataBases (SDB) are created and updated. They contain information for each particle (fitting $\boldsymbol{F_k^i}$, position fitting $\boldsymbol{x_k^{ij\ (PSO)}}$, and velocity $\boldsymbol{v_k^{ij\ (PSO)}}$ for all optimization iterations). The collection (memory of the prior fitting and locations) is then enhanced using the SDB in order to build an accurate metamodel using Kriging interpolation. At the first iteration $\boldsymbol{k = 1}$:

The particle position defined by the composite DOE is the position stored in the databases $\boldsymbol{X_k^{ij\ (SDB)}}$.

$$\begin{cases} \boldsymbol{X_k^{ij\ (SDB)} = X^{ij\ (DOE)}} \\ \boldsymbol{v_k^{ij\ (SDB)} = 0} \\ \boldsymbol{F_k^{i\ (SDB)} = F_k^i} \end{cases} \qquad (12)$$

Where $\boldsymbol{v_k^{ij}}$ is the $\boldsymbol{jth}$ dimension velocity of particle $\boldsymbol{i}$ at iteration $\boldsymbol{k}$. Else:

The updated particle position, velocity, and stiffness stored in the databases $X_k^{ij\ (SDB)}$, represent a new set that contains all of the elements that are in the last of the two sets. For example, the previous $(k-1)$ stored parameters ($X_{k-1}^{I_{k-1}j\ (SDB)}$, $v_{k-1}^{I_{k-1}j\ (SDB)}$, and $F_{k-1}^{I_{k-1}j\ (SDB)}$), and respectively the i particle's position $x_k^{ij\ (PSO)}$, velocity $v_k^{ij\ (PSO)}$, and fitting obtained by PSO algorithm at iteration k.

$$\begin{cases} \boldsymbol{X_k^{I_k j\ (SDB)} = X_{k-1}^{I_{k-1} j\ (SDB)} \cup x_k^{ij\ (PSO)}} \\ \boldsymbol{v_k^{I_k j\ (SDB)} = v_{k-1}^{I_{k-1} j\ (SDB)} \cup v_k^{ij\ (PSO)}} \\ \boldsymbol{F_k^{I_k\ (SDB)} = F_{k-1}^{I_{k-1}\ (SDB)} \cup F_k^i} \end{cases} \qquad (13)$$

Where I_k=1, 2, …, n_k are the new sampling size at the iteration k, $x_k^{ij\ (PSO)}$, and $v_k^{ij\ (PSO)}$ are respectively the i particle's position and velocity obtained by PSO algorithm at iteration k.

Step 5: In this step, Kriging is used in the metamodel's construction. All samples kept in the swarm databases $X_k^{I_k j\ (SDB)}$ are added to the sampling process used to build this model. This can greatly increase the metamodel's correctness.

Step 6: An automated process is employed to solve the optimization problem via SQP algorithms starting from each sample. The best approximation among those achieved by the various optimizations is then taken into account in the optimization operation to prevent reaching a local optimum.

Step 7: The optimum is implicitly evaluated at iteration k using FEA.

Step 8: The best samples found in the search process are selected, updated, and listed. The value of the fitting at this point F_k^i determines the quality of each particle's location. Additionally, the swarm includes the optimal value implicitly assessed from the SQP and Kriging optimization outputs. Then the following process continues:

- The swarm size increases by one $i = i + 1$.
- Each particle retains its best previous location (designated by $P_k^{best\ i}$).
- Particle's fitting evaluation is compared to $F_k^{best\ i}$. If the current value F_k^i is better than $F_{k-1}^{best\ i}$, particle's the set is equal to the current value of the objective function $F_k^{best\ i} = F_k^i$, and $P_k^{best\ i}$ is equal to the current design value position X_k^{ij} in the design space.
- Else $P_k^{best\ i} = P_{k-1}^{best\ i}$.
- The best position of the neighborhood, or the best position reached by the particle of the rated swarm G_k^{best} is thus equal to the position of all swarms with the incorporation of Kriging-SQP solution of steps 5, 6, and 7.

Step 9: New samples are created using the PSO algorithm. Each particle (sampling point) advances at iteration k. These are calculated as follows:

$$v_{k+1}^{ij} = wv_k^{ij} + c_1 r_{1k}^{ij}\left(P_k^{best\ ij} - x_k^{ij\ (PSO)}\right) + c_2 r_{2k}^{ij}\left(G_k^{best\ j} - x_k^{ij\ (PSO)}\right) \quad (14)$$

$$x_{k+1}^{ij\ (PSO)} = x_k^{ij\ (PSO)} + \chi v_{k+1}^{ij}, i = 1, 2, \ldots, n\ ; j = 1, 2, \ldots, D \quad (15)$$

Where χ is a constriction factor used to control and constrict velocities, w is an inertia weight factor, c_1 is a cognition weight factor, c_2 is a social weight factor, r_{1k}^{ij} and r_{2k}^{ij} are two random numbers varying between 0 and 1. The vector $P_k^{best\ ij}$ is the best jth dimension of the own best position of particle i, and $G_k^{best\ j}$ is the jth dimension of the best sample in the swarm.

The following weighting inertia function is used:

$$w = w_{max} - \frac{w_{max} - w_{min}}{k_{max}} k \quad (16)$$

Where w_{max} and $w_{min}$are the initial and the final weight respectively. k is the current iteration number and $k_{max}$is the maximal iteration number.

Step 10: Using the knowledge database: the values of the objective and constraint functions of the current particles are replaced by the values of the matching particle stored in the database if the position of the new sample is sufficiently near to a particle stored in the database. The positions are then restored but the particle's velocities does not change in order for the particle to follow its trajectory.

$$\text{If} \quad \left\| x_{k+1}^{i\ (PSO)} - X_k^{I_k j\ (SDB)} \right\| < \varepsilon \qquad \forall\, i = 1, \dots, n \ \& \ \forall I_k = 1, \dots, n_k$$

$$\begin{cases} x_{k+1}^{i\ (PSO)} = X_k^{I_k j\ (SDB)} \\ v_{k+1}^{ij} = v_k^{ij} \\ F_{k+1}^{i} = F_k^{I_k\ (SDB)} \end{cases} \tag{17}$$

Then go back to step 4.

Otherwise, the objective and constraint functions are implicitly evaluated for each new particle's position using FEA (Step 3).

5.4. Results

In this section, the results of the numerical simulations via COMSOL Multiphysics® 4.3a conducted on the rough design space are presented (Figure 51). In addition, the evaluation of the constraint and objective functions, the optimization variables values, at each iteration of the optimization process, are presented. This section also shows the finite element analysis (FEA) carried out on the L-systems' structures that result from the optimization algorithm.

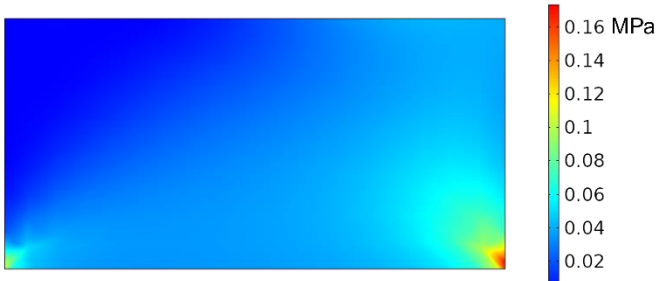

$\sigma_{max} = 0.13\ MPa$

$weight = 298.2\ g$

Figure 51: von Mises contour, and weight value of the rough design space.

Table 16 represents the number of samples' evaluations at each optimization iteration as well the thicknesses (variables), the objective function $f(x)$ (weight), and the constraint function $g(x)$ (von Mises stress) values.

Table 16: The results of the KSO carried out on the L-systems structure. The parameters TR, BR, PD, and BD correspond to the thicknesses of the L-systems trunk, the L-systems branches, the second PSLs' direction, and the boundary respectively.

Iterations	Evaluations	TR [mm]	BR [mm]	PD [mm]	BD [mm]	f(x) [kg]	g(x)
0	0	1.10	1.10	1.10	1.10	0.0539	-0.602
1	25	1.10	0.20	1.10	1.10	0.0326	-0.594
2	47	0.71	0.20	0.92	1.22	0.0276	-0.341
3	74	0.31	0.23	0.56	0.97	0.0195	-0.16
4	101	0.44	0.22	0.36	0.94	0.0180	0.0446
5	124	0.37	0.26	0.21	1.07	0.0173	-0.0428
6	149	0.38	0.22	0.22	1.07	0.0165	0,00

Figure 52 represents the constraint function $g(x)$ (von Mises stress) and objective function $f(x)$ (weight) evaluation and variation at each of the six optimization iterations. These functions were defined in Equation (4) in section 2. It is important to indicate that when $g(x)$ is equal to zero, it means that the calculated von Mises stress $\sigma(x)$ is equal to the yield strength of the VeroPureWhite material ($\sigma_y = 54\ MPa$). The calculated von Mises stress is lower than the yield strength if the value of $g(x)$ is negative and higher than the yield strength if the value is positive.

$$\begin{cases} \sigma(x) = \sigma_y & g(x) = 0 \\ \sigma(x) < \sigma_y & g(x) < 0 \\ \sigma(x) > \sigma_y & g(x) > 0 \end{cases}$$

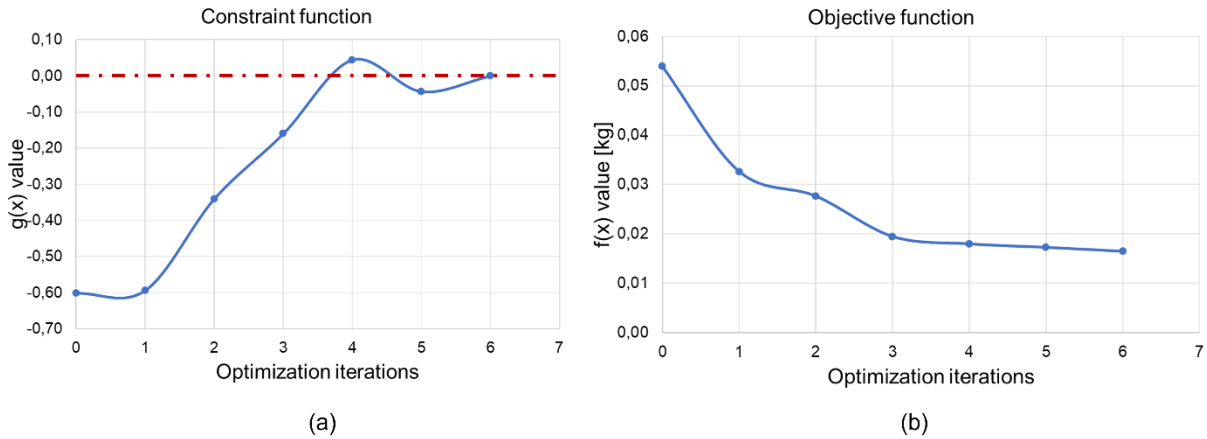

Figure 52: Constraint function g(x) (a) and objective function f(x) (b) evaluation at each iteration of the KSO.

Figure 53 represents the variables (thicknesses at each optimization iteration respectively. TR is the thickness of the L-systems trunks (Figure 53a), BR is that of their branches (Figure 53b), PD is the thickness of the second PSLs' direction (Figure 53c), and BD is the thickness of the outer boundary of the structure (Figure 53d).

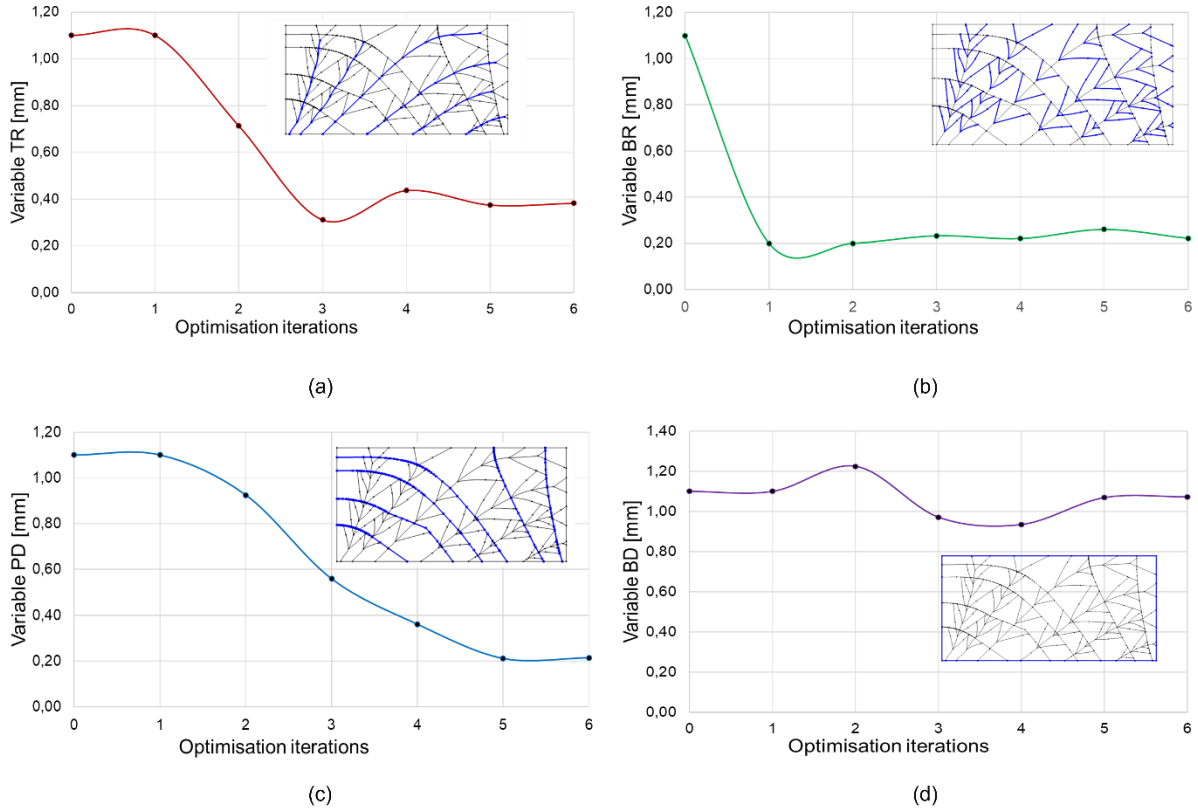

Figure 53: Optimization variables (thicknesses) variation at each optimization iteration.

Figure 54 shows the results of the FEA resulting from each optimization iteration. The von Mises stress contour and the weight value are represented at each point of the variation of the objective function curve $f(x)$. The contours presented in this figure incorporate the variations of the different sections' thicknesses (the parameters TR, BR, PD, and BD) in the L-systems structure.

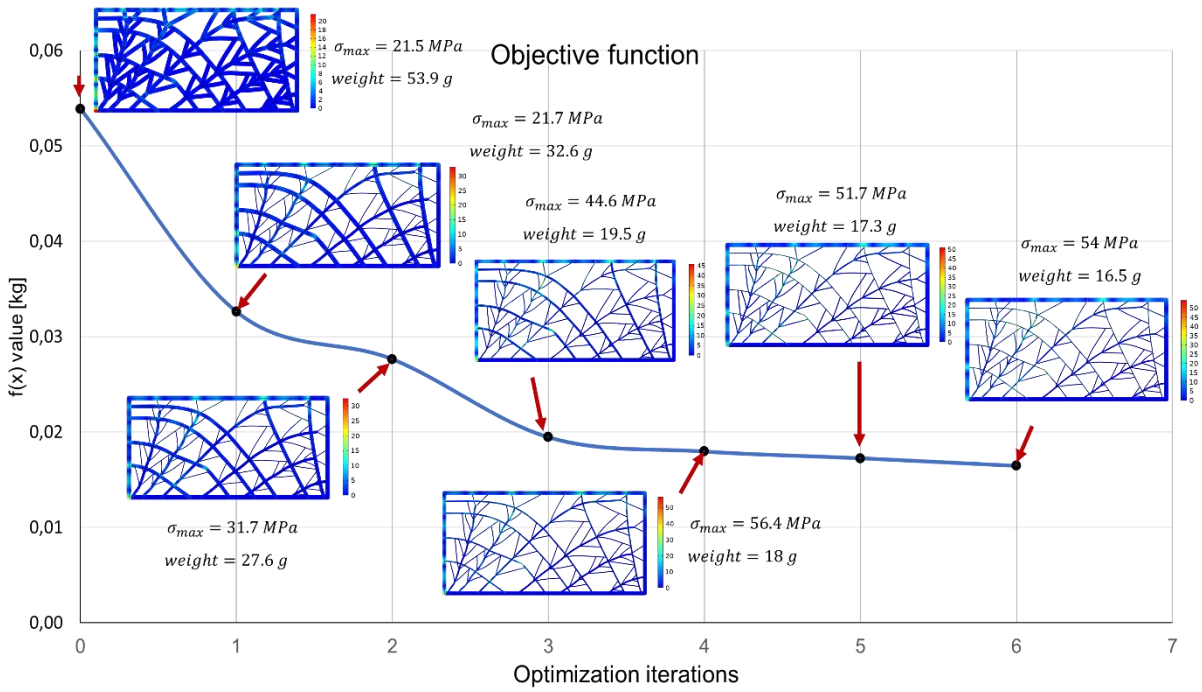

Figure 54: Objective function f(x) variation and evaluation at each iteration of the optimization process.

5.5. Discussion

Figure 51 shows the numerical simulation results of the 2D rough geometry for the load case studied in this work (compression/shear). The von Mises stress is equal to 0.13 MPa and the weight is equal to 298.2 g. By transforming the rough geometry into a cellular structure using L-systems generated along the first PSLs' direction and extended to those of the second direction, the following hypothesis can be highlighted: "In order to find the optimal cross-sections of the beams forming the structure, the metamodel optimization system based on a smart sampling method and knowledge databases with Kriging interpolation permits finding the optimal cross-sections of the beams forming the L-systems structure. In other words, this method allows for a weight reduction and a von Mises stress value lower than the yield Strength of the VeroPureWhite material (54 MPa)."

The results of this method, which is also referred to KSO, are shown in Table 16 and Figure 52Figure 53Figure 54. Table 16 represents the number of samples' evaluation at each iteration. It is the number of times that the Knowledge Swarm DataBases (SDB) are updated (step 4 in section 5.3.4) until reaching an optimum. For a better analysis of this table, the results were developed in Figure 52 Figure 54. Thus, at each iteration:

- The values of the optimization (thickness of each group defined by Figure 49) are shown. The initial valu;e ($i = 0$) for all thicknesses is equal to 1.1 mm. Their variation curves are presented in Figure 52. It is noticed in Figure 52a that the thickness of the L-systems trunks only stabilizes at the forth iteration ($i = 4$) (TR ≈ 0.4 mm). Whereas, as seen in Figure 52b, the thickness of their branches stabilizes at the second iteration ($i = 2$) (BR ≈ 0.2 mm). The thickness of the second PSLs' direction keeps decreasing drastically until reaching a stable value (PD ≈ 0.2 mm) (Figure 52c). And the thickness of the structures' boundary fluctuates in a range between 0.9 and 1.2 mm (0.9 mm < BD < 1.2 mm) (Figure 52d). The results can be interpret as follow: "Starting from the fifth iteration ($i = 5$), the optimization becomes stable, and an optimum is reached. However, the corresponding weight should be analyzed, and the resepect of the yield strength of the material must be checked."
- Figure 53 shows the evaluation of the constraint and objective functions introduced in Eq. 4 in section 5.3.2. Six iterations were needed to reach the exact value of the elasticity limit of 54 MPa (where $g(x) = 0$). In Figure 53, it can be noticed that the function $g(x)$ at iterations ($i = 0, 1, 2, 3, 5, and\ 6$) possesses a negative value. That means that the structures remain within the elasticity limit. Which is not the case for the function at the forth iteration ($i = 4$) where $g(x)$ is positive: the structure that results from this iteration can then be neglected. In Figure 53b, the weight function $f(x)$ (equal to the sum of the weight of each group shown in Figure 49) strongly decreases from iteration 0 to 3 then it slowly stabilizes. The structures resulting from these four iterations are not considered to be strong optimal candidates. The challenge is, then, to find the structure that presents the best stiffness-to-weight compromise (or ratio).
- Figure 54 is a representation of the numerical simulations of the structures resulting from the FEA of the optimization process. Throughout the optimization iterations, the weight drops from 53.9 g to 16.5 g, but the von Mises stress increases from 21.5 MPa to 56.4 MPa. As mentioned previously, the structure at the iteration ($i = 4$) cannot be taken into account due to the negative value of $g(x)$. It is noticed that the function $f(x)$ becomes more stable and constant starting from the sixth iteration ($i = 5$). However, the optimal structure is the one obtained at the last iteration ($i = 6$). It has a von Mises stress value equal to the elasticity limit (54 MPa) and a weight equal to 16.5 g. This structure is denoted LS1.

  Table 17 below shows the weight reduction percentage, allowed by the latter structures resulting from the KSO algorithm, in comparison to the rough geometry's weight (298.2 g) and one of the optimal CSL-2 structures of the previous study (Chapter 4) (54.75 g). All these structures present the same boundary conditions, and load case and value but different material distribution. Figure 55 shows the representation of the optimal beams' thicknesses of the CSL-2 and LS1 structures. It also shows the maximal von Mises stress and weight values in comparison to those of the rough design space.

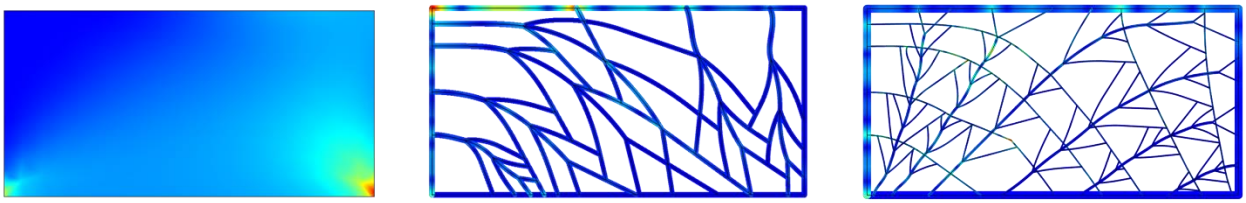

Figure 55: Representation of beams' thicknesses of the CSL-2 (b) and LS1 (c) structures and their maximal von Mises stress and weight values in comparison to those of the rough design space (a).

It is shown in that the use of the KSO method and the strategy of L-systems generation adopted in this study, permits the reduction of the weight of the rough design geometry by approximately 94.47% and of that of the CSL-2 structure by approximately 69.86% (Table 17). The LS1 structure presents then a good compromise between a lightweight and a sufficient stiffness.

Table 17: Weight reduction percentage: L-systems structure (LS1) weight of the current study in comparison to the rough design geometry and the CSL-2 structure in the previous chapter.

	Rough design geometry	**CSL-2**
LS1	94.47	69.86

5.6. Conclusion

This work suggests a metamodel optimization system that uses knowledge databases with Kriging interpolation and a smart sampling technique. With the use of a knowledge database and the combination of two optimization methods, the KSO technique aims to reduce the number of function evaluations required to build the metamodel. In fact, combining two optimization algorithms is fundamental to KSO. The first is a metaheuristic algorithm where the best samples' information is used to determine the weight of all samples as a solution. The metamodel is then built using the sample data, and the gradient method (SQP) resolves it. The best solution is then used in PSO algorithm as a generation of new samples for a new KSO iteration. The metamodel in this study is the results of the FEA of the structures using the L-systems method. Six iterations were required to reach the optimization goal: the optimal structure (LS1) has a von Mises stress exactly equal to the value of the yield strength of the

VeroPureWhite material. It has shown a weight reduction of 94.47% and 69.86% in comparison to the rough geometry and a previously studied structure respectively. The efficiency of this method has been proven in terms of providing structures presenting a good stiffness-to-weight ratio. The KSO method provides precise values for optimization variables without the need to run several numerical simulations, in contrast to the optimization scheme utilizing only Taguchi DOE. In future work, this method will be applied to 3D biomimetic structures respecting not only the mechanical requirements of AM but also the fabrication constraints. Moreover, more load cases will be studied, and structures will be tested experimentally in order to provide a better validation of the results.

Chapter 6: Conclusions and Perspectives

"It is easier to resist at the beginning than at the end."

Leonardo Da Vinci

"Let us not forget that human knowledge and skills alone cannot lead humanity to a happy and dignified life."

Albert Einstein

This thesis is one of the first research work that uses bio-inspiration in mechanical engineering applications in the ICB-CO2M lab. It couples all the disciplines in the laboratory: design, modeling, simulation, and optimization. Bio-inspiration, as mentioned in previous chapters, is increasingly used for several applications. In this research work, a lightweight cellular structures with important stiffness are generated and optimized.This chapter summarizes the proposed contributions and talks about future work that will be conducted to improve the techniques used in this study.

6.1. Conclusions

This PhD titled "Generative Design and Parametric/Topology Optimization of Bio-inspired Cellular Structures for AM" addresses a multitude of domains. The challenge in this PhD was to progressively address the cross-domains intersecting AM, optimization, design, and bio-inspiration.

Indeed, AM, also known as 3D printing, is a rapidly growing technology that allows for the creation of complex and intricate structures. As the technology continues to advance, researchers and engineers are looking for ways to optimize the design of these structures to make them even more efficient and effective. One approach that has gained attention in recent years is the use of bio-inspired design principles, which take inspiration from the structures found in nature.

One key aspect of bio-inspired design is the use of cellular structures, which are characterized by their repeating patterns of small interconnected cells. These structures can be found in many natural materials, such as bone, wood, and coral, and are known for their strength and light weight. By replicating these structures in AM, engineers can create materials that are both lightweight and strong, which is essential for many applications such as aerospace and biomedical engineering.

One way to design bio-inspired cellular structures for AM is through the use of generative design. Generative design is a computational design method that uses algorithms to generate design options based on specified constraints and parameters. By inputting specific requirements such as weight and strength, the algorithm can generate a variety of design options that meet these requirements. This allows engineers to quickly and easily explore a wide range of design options and find the best solution for their specific application.

Another important aspect of bio-inspired cellular structure design is the use of parametric and topology optimization. Parametric optimization involves varying the parameters of a design, such as cell size and shape, to optimize its performance. Topology optimization, on the other hand, involves varying the overall shape and structure of the design to find the optimal configuration. Together, these methods allow engineers to fine-tune the design of their cellular structures to meet specific requirements, such as stiffness or flexibility.

In conclusion, biomimetic cellular structures are an exciting area of research and development in additive manufacturing. By using generative design and parametric/topology optimization, engineers can quickly and easily create structures that are both lightweight and strong, and can be optimized for specific properties. These bio-inspired structures have the potential to revolutionize a wide range of industries, from aerospace to biomedical engineering, and will likely play an important role in the future of AM.

By coupling the beformentioned domains, this PhD thesis allowed for the development for novel biomimetic methods and tools that meet the objective of creating strong lightweight lattice structures. Hence, these tools can be used in the industrial domains where lightweight, flexibility, and stiffness properties are required such the creation of strong weing structures for aircraft and spacefract in the aerospace domain, lightweight energy-efficient vehicles in the automotive domain, and artificial limbs and joints that mimic the mechanical properties of natural bones in the biomedical field. The research in the industrial fields continues to evolve and it is expected that the use of biomimetic design will continue to expand in the future [26,27,77,78,88].

In the light of what was presented previously and taking into account what was stated in chapter 2 in terms of state of the art introduction and in terms of research questions (RQ1, RQ2, and RQ3), chapters 3, 4, and 5 were able to answer the cross-domains issues as follows:

RQ1: Which strategy should be used to achieve a lattice structure with a good stiffness-to-weight ratio? Which is more suitable: a uniform or a variable-density lattice distribution?

In the first chapter a design and optimization approach for variable-density lattice structures has been put forward. **To design a lightweight structure suitable for AM, a strategy combining parametric and TO is adopted.** More particularly, the complete and effective digital chain that creates AM-friendly lattice structures in a topologically optimal design space is the originality of the approach. Numerous DOE configurations have demonstrated that adding reinforcement to the structure in the form of lattice distribution density where necessary may assist in achieving a high specific strength. The method for creating strong structures that are appropriate for AM is now seamless, effective, and adaptable to any design solution. A case study has been provided and developed with the use of computational tools and algorithms to show the proposal's additional value. The study was divided into two cases, and particular attention was paid to the comparison between the two cases, in order to validate the effectiveness of the suggested strategy in achieving the goals of weight reduction and strength increase. **A DOE and sensitivity study are carried out in both cases. While the second case involved a study of a variable-density lattice distribution, the first case had a uniform lattice distribution. The second case gave a better weight and a better strength, achieving the desired aim of having a higher strength-to-weight ratio despite the closeness of the outcomes of the two cases. The entire processes are**

demonstrated in a reasonable computer time, providing a solution to one of the problems with design optimization: computational time and expense.

This chapter addressed the production of lattice structures that are biomimetic. Lattice structures are often inspired by the structural properties of natural materials such as bones, shells, and wood. These natural materials have evolved over millions of years to be lightweight yet strong, and efficient in carrying loads. Engineers and scientists often use the principles of bio-inspiration to replicate these properties in man-made materials [23-25].

Despite the bio-inspired aspect that the lattice structures present, the biomimetic strategy is not clear. This study counts on a trial and error procedure. Hence, an automated biomimetic method permitting the elaboration of lightweight structures in a generative manner is of interest. This method is developed via a novel tool in the next chapter.

RQ2: How can one improve the stiffness of bio-inspired mechanical parts and structures while assisting the designer in defining a preliminary design space using biological algorithms and aspects?

In the second research work**, a novel biomimetic design and modeling approach and tool based on L-systems distributed along the PSL directions was suggested**.

L-systems, are a type of formal grammar used to model and generate fractal-like shapes and patterns in various fields, including computer graphics, biology, and architecture. L-systems can be applied in the field of mechanical engineering to generate complex and optimized structures for various applications [156]. In mechanical engineering, L-systems can be used to generate lightweight and efficient structures, such as trusses and frames, that have a good strength-to-weight ratio. L-systems can also be used to generate compliant mechanisms, which are structures that can change their shape or stiffness in response to external forces. The use of L-systems in mechanical engineering allows for the generation of complex and optimized structures that are not easily obtained through traditional design methods. However, it is important to note that the use of L-systems in mechanical engineering is still in the early stages of development and further research is needed to fully exploit its potential in mechanical engineering applications.

There is a direct link between the use of L-systems and generative design. It lies in the fact that both techniques can be used to generate complex and optimized structures (section 2.3.3). Both methods use computer algorithms to explore a wide range of possible solutions to a design problem, and then select the best solution based on specific design criteria.

To be able to meet the requirements of generative design, a generation strategy should be defined. Generative design consists in the generation of material within a limited design space. In the tool and method developed in this chapter, PSLs serve as guidelines for L-systems generation within a given design space. This material growth is considered biomimetic since it mimics the pores distribution

within trabecular bone structures. can be affected by the direction and magnitude of the forces acting on the bone. In general, the pores in trabecular bone tend to be oriented parallel to the direction of the applied stress. This is because the porous structure of trabecular bone allows for the redistribution of stress, and the channels and spaces within the bone can help to dissipate and distribute the stress more evenly.

To demonstrate the efficiency of the L-systems growth along PSLs in adapting mechanical structures to various loading cases and ensuring a reasonable stiffness-to-weight ratio, numerical simulations and parametric optimization strategies based on a L9 DOE sensitivity analysis were carried out. Only three loading cases—compression, shear, and combined compression/shear—were taken into consideration. Each load case had two structures that were generated from the directions of the two main PSLs. The best structure for each load condition thanks to the DOE sensitivity study was determined. **And the latter outcomes of the carried out numerical simulations have shown that this strategy helped in strengthening the structure, obtaining high specific strength while reducing its weight.**

However, there are some issues related to the use of DOE in the third and fourth chapters. In fact, DOE is a statistical method used to systematically vary the factors of a process or system in order to understand their effect on the output. While DOE is a powerful tool for understanding the relationship between inputs and outputs, it is not a precise method, as it does not guarantee that the results will be exact or that the results will be repeatable. One of the reasons why DOE is not precise is that it relies on probability and statistics, which inherently have a level of uncertainty. Additionally, DOE typically involves taking a sample of data, rather than testing every possible combination of inputs, which can introduce uncertainty into the results.Another reason why DOE is not precise is that it assumes that the relationship between inputs and outputs is linear and additive, which is not always the case. In reality, the relationship between inputs and outputs can be non-linear and interaction effects can occur. Despite its limitations, DOE is still a widely used and powerful tool in the field of engineering and science. It allows to identify the factors that have the most significant effect on the output, and can be used to optimize a process or system. It is also important to validate the results obtained by DOE through further experimentation [175].

To solve the issues related to DOE, the last research work is developed in order to bring more precision to the biomimetic method of the fourth chapter.

RQ3: Which optimization technique is more suitable to obtain a better parametrized cellular biomimetic structure?

In the third chapter, **a metamodel optimization system is proposed. The KSO strategy tries to reduce the amount of function evaluations necessary to generate the metamodel by using intelligent sampling and a knowledge base while combining two optimization methods**. In fact, KSO is based on the basic combination of two optimization techniques. The first uses a metaheuristic algorithm to

calculate the weight of all samples as a solution based on the information from the best samples. The gradient approach (SQP) is then used to resolve the metamodel once it has been constructed using the sample data. The best solution is then used by the PSO algorithm to generate new samples for a subsequent KSO cycle. The cross-sections of the L-systems generated along the PSLs' directions serve as the study's metamodel. The ideal lightweight structure is attained starting from the fiveth iteration, although it required six iterations to reach the optimization objective. Thus, it was decided that the structure obtained at the last iteration is optimal. This approach's effectiveness has been demonstrated in terms of producing structures with a favorable stiffness-to-weight ratio. **The KSO method provides precise values for optimization variables without the need to run several numerical simulations, in contrast to the optimization scheme utilizing only Taguchi DOE.**

In this PhD thesis, the numerical simulations are simplified by using a beam formulation. It is important to note that this process simplifies the analysis, but it can lead to loss of accuracy and realism of the results. Therefore, it is recommended to use this method only in cases where the structure is symmetric or has a simple shape, and the accuracy of the results is not critical. However, a solid mechanics formulation would have been of interest: it would have allowed to add a more realistic aspect to show the proper weight reduction with respect to the solid geometry. But in most cases, lattice structures are directly linked to beam elements.

In addition a comparative analysis using different cross-sections types (circular, I-shape, hollow,…), different lattices arrangements and distributions (honeycomb, rectangular, auxetic,…), or different L-systems rules and patterns would have provided a wider visualization of the effectiveness of the methods and tools developed in the studies in terms of weight reduction and strength increase.

It's worth noting that the optimal structures, particularly in the first two studies, were printed using the PolyJet technique with the aim of conducting experimental studies in the future. This allows for the validation of numerical simulation results. Additionally, other forms of validation could be carried out such as:

- A mesh convergence study: three different mesh types (coarse, normal, and fine) were applied to the beam structure. This validation mean was tried and the results of von Mises stress showed a maximum variation of 6%, which demonstrates that the influence of the mesh and geometry imperfections on the von Mises stress and singularity is insignificant.

- Reproduction of an existing geometry. A geometry from literature could have been used in the studies presented in this thesis, applying the same methods in order to demonstrate their effectiveness in comparison to previous works.

6.2. Perspectives

The research that was conducted offers a wide range of viewpoints in the short, mid, and long terms. In fact, the following can be developed for this work:

- Augmenting the study in terms of designing, modeling and optimization 3D models. In fact, the studies in this thesis focused on 2.5D structures, or 2D structures extruded evenly and uniformally along the *z*-axis. It is more realistic to work on 3D structures presenting several variations in thicknesses. Indeed, the algorithm described in Chapter 4 is under further development: L-systems will be generated along the three PSLs' directions. The interlocking of the L-systems branches will then create 3D cellular structures.
- Integrating the AM build constraints and orientations in the procedure of biomimetic structures generation. A library of all AM constraints should be taken into account in the algorithms in order to respect the requirements of each AM technique. The two most important constraints' types that should be taken into account are [16,42,108] :
    - Build size limitations: The size of the final product is limited by the build envelope of the equipment. Larger objects may need to be printed in sections and then assembled.
    - Design constraints: Design constraints such as overhangs, self-supporting structures, and internal geometries must be taken into consideration when designing parts for AM.
- Adopting a strategy that uses multiple materials in one structure: the focus should not only be directed at the thicknesses of the cross-sections in order to increase stiffness and reduce weight. Utilizing different materials in the structure can help achieving this goal. Indeed, multimaterial structures refer to structures that are made up of more than one type of material. The importance of multimaterial structures is that they can provide a combination of properties that cannot be achieved with a single material [225,226] :
    - Optimization of properties: Multimaterial structures can be designed to optimize specific properties such as strength, stiffness, weight, and thermal conductivity. This can lead to structures that are lighter, stronger, and more efficient than those made from a single material.
    - Tailored properties: Multimaterial structures can be tailored to have specific properties in specific areas. For example, a structure could have a high strength material in areas where strength is needed and a low density material in areas where weight is a concern.
    - Enhanced performance: Multimaterial structures can provide enhanced performance in specific applications. For example, a structure that combines a metal with a polymer can provide improved impact resistance and damping properties.
    - Reduced manufacturing costs: Multimaterial structures can reduce manufacturing costs by using lower-cost materials in areas where they will not affect performance, and reserving higher-cost materials for areas where they are needed most.

- Biomimetics: Multimaterial structures can mimic the structures found in nature, where different materials are used in different parts of the organism to provide specific properties.
- Adaptability: Multimaterial structures can be adapted to different environments and conditions. They can be designed to respond and adapt to changes in temperature, pressure, load, and other factors.
- Durability: Multimaterial structures can be more durable and resistant to wear and tear compared to single material structures.

- Covering all the possible loading cases and scenaris encountered in the mechanical field could be of interest. In this thesis, only three loading types were taken into account. The studies can be extended and consider the torsional, bending, and flexural loadings. Dynamic and impact studies can also be considered as an added value (ballistic impact on a 3D L-systems structures to study the penetration of the bullet in order to create protective systems and parts, for example).
- The study of metamaterials using these tools would be revolutionary. Metamaterials are artificially engineered materials that possess properties not found in naturally occurring materials. They are designed to have specific electromagnetic or other physical properties, such as negative refraction or superlensing. In fact, metamaterials and biomimetic design are closely related as biomimetics can be used to inspire the design and development of metamaterials for several reasons [227-229]:
    - Negative refraction: Biomimetics can be used to design metamaterials with negative refraction, which is a property that allows light to bend in the opposite direction of a normal material. This property can be found in certain natural structures such as the eyes of certain animals and can be mimicked in metamaterials to improve the performance of optical devices.
    - Superlensing: Biomimetics can be used to design metamaterials with superlensing, which is a property that allows an object to be viewed in greater detail than is possible with a conventional lens. This property can be found in certain natural structures such as the eyes of certain animals and can be mimicked in metamaterials to improve the performance of imaging devices.
    - Artificial muscles: Biomimetics can be used to design metamaterials that can mimic the properties of natural muscles such as the ability to change shape, stretch, and contract. These materials can be used in a wide range of applications such as robotics, medicine, and aerospace.
    - Self-healing: Biomimetics can be used to design metamaterials that can mimic the self-healing properties of certain natural materials such as spider silk. These materials can

be used in applications where self-healing is important, such as in aerospace and transportation.

- Biomimetic metamaterials can be used to create structures that are optimized for specific applications and environments, by mimicking the structures, properties, and functions found in nature.
- Biomimetic metamaterials can be used to create structures that are lightweight, strong, and efficient, and that can withstand dynamic loads and impacts.
- Biomimetic metamaterials can be used to create structures that have multiple functionalities such as self-healing, adaptability, and energy dissipation.

Research Work Publications

Journal Papers

[1] M. Al Khalil, N. Lebaal, F. Demoly, and S. Roth, (2021). A design and optimization framework of variable-density lattice structures for additive manufacturing. Mechanics of Advanced Materials and Structures, 1-15. https://doi.org/10.1080/15376494.2021.1936704.

[2] M. Al Khalil, H. Belkebir, N. Lebaal, F. Demoly, S. Roth, (2022). A Biomimetic Design Method for 3D-Printed Lightweight Structures Using L-Systems and Parametric Optimization. *Applied Sciences*. 12(11):5530. https://doi.org/10.3390/app12115530.

[3] M. Al Khalil, H. Belkebir, N. Lebaal, F. Demoly, S. Roth, (2022). L-systems structures optimization using low-cost meta-modeling algorithm based on meta-heuristic knowledge (Under Review).

Conference Paper

[4] M. Al Khalil, N. Lebaal, F. Demoly, S. Roth, (3 au 5 avril 2019). Vers une approche intégrée de conception-simulation-optimisation de structures lattices. 16ème Colloque National S-mart, Les Karellis.

References

[1] J. Sun and B. Bhushan, "Hierarchical structure and mechanical properties of nacre: a review," RSC Advances, vol. 2, no. 20, pp. 7617–7632, Aug. 2012, doi: 10.1039/C2RA20218B.

[2] Y. Mengüç, S. Y. Yang, S. Kim, J. A. Rogers, and M. Sitti, "Gecko-inspired controllable adhesive structures applied to micromanipulation," Advanced Functional Materials, vol. 22, no. 6, pp. 1246–1254, Mar. 2012, doi: 10.1002/ADFM.201101783.

[3] J. Benyus, "Biomimicry: Innovation Inspired by Nature," 1997.

[4] Z. Huang, X. Shi, G. Wang, P. Leukkunen, M. Huttula, and W. Cao, "Antireflective design of Si-based photovoltaics via biomimicking structures on black butterfly scales," Solar Energy, vol. 204, pp. 738–747, Jul. 2020, doi: 10.1016/J.SOLENER.2020.05.031.

[5] Miyake, "Application Data (63) Continuation-in-part of application No. 16 / 404," vol. 255, 2019.

[6] N. B. Duc and N. T. Binh, "Investigate on structure for transparent anti-icing surfaces," AIP Advances, vol. 10, no. 8, p. 085101, Aug. 2020, doi: 10.1063/5.0019119.

[7] S. D. Cezan, H. T. Baytekin, and B. Baytekin, "Self-Regulating Plant Robots: Bioinspired Heliotropism and Nyctinasty," Soft Robotics, vol. 7, no. 4, pp. 444–450, Aug. 2020, doi: 10.1089/SORO.2019.0036/SUPPL_FILE/SUPP_MOVIE5.MP4.

[8] H. Hedayati, R. Suzuki, D. Leithinger, and D. Szafir, "PufferBot: Actuated Expandable Structures for Aerial Robots," IEEE International Conference on Intelligent Robots and Systems, pp. 1338–1343, Aug. 2020, doi: 10.1109/IROS45743.2020.9341088.

[9] B. B. Patel et al., "Tunable structural color of bottlebrush block copolymers through direct-write 3D printing from solution," Science Advances, vol. 6, no. 24, pp. 7202–7212, Jun. 2020, doi: 10.1126/SCIADV.AAZ7202/SUPPL_FILE/AAZ7202_SUPPLEMENTAL_HARDWARE_SOFTWARE.ZIP.

[10] L. Pham, G. Lu, and P. Tran, "Influences of Printing Pattern on Mechanical Performance of Three-Dimensional-Printed Fiber-Reinforced Concrete," https://home.liebertpub.com/3dp, vol. 9, no. 1, pp. 46–63, Feb. 2022, doi: 10.1089/3DP.2020.0172.

[11] N. Huebsch and D. J. Mooney, "Inspiration and application in the evolution of biomaterials," Nature, vol. 462, no. 7272, pp. 426–432, Nov. 2009, doi: 10.1038/NATURE08601.

[12] U. G. K. Wegst, H. Bai, E. Saiz, A. P. Tomsia, and R. O. Ritchie, "Bioinspired structural materials," Nature Materials 2014 14:1, vol. 14, no. 1, pp. 23–36, Oct. 2014, doi: 10.1038/nmat4089.

[13] R. Müller et al., "Biodiversifying bioinspiration," Bioinspiration and Biomimetics, vol. 13, no. 5, Jul. 2018, doi: 10.1088/1748-3190/AAC96A.

[14] D. Baumeister, Biomimicry resource handbook : a seed bank of best practices. Missoula Montana: Biomimicry 3.8, 2014.

[15] J. Pandremenos, E. Vasiliadis, and G. Chryssolouris, "Design Architectures in Biology," Procedia CIRP, vol. 3, no. 1, pp. 448–452, Jan. 2012, doi: 10.1016/J.PROCIR.2012.07.077.

[16] M. K. Thompson et al., "Design for Additive Manufacturing: Trends, opportunities, considerations, and constraints," C I R P Annals, vol. 65, no. 2, p. 24, 2016, doi: 10.1016/J.CIRP.2016.05.004.

[17] A. Díaz Lantada, A. de Blas Romero, Á. Sánchez Isasi, and D. Garrido Bellido, "Design and Performance Assessment of Innovative Eco-Efficient Support Structures for Additive Manufacturing by Photopolymerization," Journal of Industrial Ecology, vol. 21, no. S1, pp. S179–S190, Nov. 2017, doi: 10.1111/JIEC.12660.

[18] J. Liu et al., "Current and future trends in topology optimization for additive manufacturing," Structural and Multidisciplinary Optimization 2018 57:6, vol. 57, no. 6, pp. 2457–2483, May 2018, doi: 10.1007/S00158-018-1994-3.

[19] C. Emmelmann, P. Sander, J. Kranz, and E. Wycisk, "Laser Additive Manufacturing and Bionics: Redefining Lightweight Design," Physics Procedia, vol. 12, no. PART 1, pp. 364–368, Jan. 2011, doi: 10.1016/J.PHPRO.2011.03.046.

[20] T. Zegard and G. H. Paulino, "Bridging topology optimization and additive manufacturing," Structural and Multidisciplinary Optimization, vol. 53, no. 1, pp. 175–192, Jan. 2016, doi: 10.1007/S00158-015-1274-4/FIGURES/22.

[21] D. W. Rosen, "Computer-Aided Design for Additive Manufacturing of Cellular Structures," Computer-Aided Design and Applications, vol. 4, no. 5, pp. 585–594, 2007, doi: 10.1080/16864360.2007.10738493.

[22] J. Z. C. Chang, P. I. Tsai, M. Y. P. Kuo, J. S. Sun, S. Y. Chen, and H. H. Shen, "Augmentation of DMLS Biomimetic Dental Implants with Weight-Bearing Strut to Balance of Biologic and Mechanical Demands: From Bench to Animal," Materials 2019, Vol. 12, Page 164, vol. 12, no. 1, p. 164, Jan. 2019, doi: 10.3390/MA12010164.

[23] J. Souza, A. Großmann, and C. Mittelstedt, "Micromechanical analysis of the effective properties of lattice structures in additive manufacturing," Additive Manufacturing, vol. 23, pp. 53–69, Oct. 2018, doi: 10.1016/J.ADDMA.2018.07.007.

[24] X. Cao, S. Duan, J. Liang, W. Wen, and D. Fang, "Mechanical properties of an improved 3D-printed rhombic dodecahedron stainless steel lattice structure of variable cross section," International Journal of Mechanical Sciences, vol. 145, pp. 53–63, Sep. 2018, doi: 10.1016/J.IJMECSCI.2018.07.006.

[25] M. G. Rashed, M. Ashraf, R. A. W. Mines, and P. J. Hazell, "Metallic Microlattice Materials: A Current State of The Art on Manufacturing, Mechanical Properties and Applications," 2016, doi: 10.1016/j.matdes.2016.01.146.

[26] M. Dumas, P. Terriault, and V. Brailovski, "Modelling and characterization of a porosity graded lattice structure for additively manufactured biomaterials," Materials & Design, vol. C, no. 121, pp. 383–392, May 2017, doi: 10.1016/J.MATDES.2017.02.021.

[27] E. del Olmo et al., "Lattice Structures For Aerospace Applications," ESASP, vol. 691, p. 6, 2012, Accessed: Jan. 31, 2022. [Online]. Available: https://ui.adsabs.harvard.edu/abs/2012ESASP.691E...6D/abstract

[28] X. P. Tan, Y. J. Tan, C. S. L. Chow, S. B. Tor, and W. Y. Yeong, "Metallic powder-bed based 3D printing of cellular scaffolds for orthopaedic implants: A state-of-the-art review on manufacturing, topological design, mechanical properties and biocompatibility," Mater Sci Eng C Mater Biol Appl, vol. 76, pp. 1328–1343, Jul. 2017, doi: 10.1016/J.MSEC.2017.02.094.

[29] A. du Plessis et al., "Beautiful and Functional: A Review of Biomimetic Design in Additive Manufacturing," Additive Manufacturing, vol. 27, pp. 408–427, May 2019, doi: 10.1016/J.ADDMA.2019.03.033.

[30] G. Pohl and W. Nachtigall, “Biomimetics for Architecture & Design,” Biomimetics for Architecture & Design, 2015, doi: 10.1007/978-3-319-19120-1.

[31] K. Fu, D. Moreno, M. Yang, and K. L. Wood, “Bio-inspired design: An overview investigating open questions from the broader field of design-by-analogy,” Journal of Mechanical Design, Transactions of the ASME, vol. 136, no. 11, Nov. 2014, doi: 10.1115/1.4028289.

[32] T. Kamps, C. Münzberg, L. Stacheder, C. Seidel, G. Reinhart, and U. Lindemann, “TRIZ-based biomimetic part-design for Laser Additive Manufacturing,” 2015.

[33] T. Kamps, M. Gralow, G. Schlick, and G. Reinhart, “Systematic Biomimetic Part Design for Additive Manufacturing,” Procedia CIRP, vol. 65, pp. 259–266, Jan. 2017, doi: 10.1016/J.PROCIR.2017.04.054.

[34] I. Gibson, D. Rosen, B. Stucker, and M. Khorasani, “Design for Additive Manufacturing,” Additive Manufacturing Technologies, pp. 555–607, 2021, doi: 10.1007/978-3-030-56127-7_19.

[36] G. A. O. Adam and D. Zimmer, “On design for additive manufacturing: Evaluating geometrical limitations,” Rapid Prototyping Journal, vol. 21, no. 6, pp. 662–670, Oct. 2015, doi: 10.1108/RPJ-06-2013-0060/FULL/XML.

[37] G. Sossou, F. Demoly, S. Gomes, and G. Montavon, “An Assembly-Oriented Design Framework for Additive Manufacturing,” Designs (Basel), vol. 6, no. 1, p. 20, Feb. 2022, doi: 10.3390/DESIGNS6010020.

[38] C. Chu, G. Graf, and D. W. Rosen, “Design for additive manufacturing of cellular structures,” Computer-Aided Design and Applications, vol. 5, no. 5, pp. 686–696, 2008, doi: 10.3722/CADAPS.2008.686-696.

[39] L. Zhang et al., “Topology-optimized lattice structures with simultaneously high stiffness and light weight fabricated by selective laser melting: Design, manufacturing and characterization,” Journal of Manufacturing Processes, vol. 56, pp. 1166–1177, Aug. 2020, doi: 10.1016/J.JMAPRO.2020.06.005.

[40] T. Zegard and G. H. Paulino, “Bridging topology optimization and additive manufacturing,” Structural and Multidisciplinary Optimization, vol. 53, no. 1, pp. 175–192, Jan. 2016, doi: 10.1007/S00158-015-1274-4.

[41] J. Zhu, H. Zhou, C. Wang, L. Zhou, S. Yuan, and W. Zhang, “A review of topology optimization for additive manufacturing: Status and challenges,” Chinese Journal of Aeronautics, vol. 34, no. 1, pp. 91–110, Jan. 2021, doi: 10.1016/J.CJA.2020.09.020.

[42] D. Brackett, I. Ashcroft, and R. Hague, “Topology Optimization for Additive Manufacturing”.

[43] P. E. Merloti and J. Of, “Optimization Algorithms Inspired by Biological Ants and Swarm Behavior”.

[44] G. R. (George R.) Lindfield and John. Penny, Introduction to nature-inspired optimization.

[45] S. Welsh, “The Man Who Lived in the Future,” 54 Feature EIR October 25, 2013Exhibition of “Leonardo da Vinci’s Codex on ‘the Flight of Birds’ ” National Air and Space Museum, Washington, D.C, 2013.

[46] E. A. Jamsari, “Ibn Firnas and His Contribution to the Aviation Technology of the World,” Advances in Natural and Applied Sciences, Jan. 2013, Accessed: Feb. 08, 2022. [Online]. Available: https://www.academia.edu/3408287/Ibn_Firnas_and_His_Contribution_to_the_Aviation_Technology_of_the_World

[47] J. F. V. Vincent, O. A. Bogatyreva, N. R. Bogatyrev, A. Bowyer, and A. K. Pahl, “Biomimetics: its practice and theory,” Journal of The Royal Society Interface, vol. 3, no. 9, pp. 471–482, Aug. 2006, doi: 10.1098/RSIF.2006.0127.

[48] J. Hwang, Y. Jeong, J. M. Park, K. H. Lee, J. W. Hong, and J. Choi, “Biomimetics: forecasting the future of science, engineering, and medicine,” International Journal of Nanomedicine, vol. 10, no. 1, pp. 5701–5713, Sep. 2015, doi: 10.2147/IJN.S83642.

[49] M. Eggermont, “Biomimetics As Problem-solving, Creativity And Innovation Tool,” Proceedings of the Canadian Engineering Education Association (CEEA), Aug. 2011, doi: 10.24908/PCEEA.V0I0.3767.

[50] R. L. Ripley and B. Bhushan, “Bioarchitecture: bioinspired art and architecturea perspective,” Philosophical Transactions of the Royal Society A: Mathematical, Physical and Engineering Sciences, vol. 374, no. 2073, Aug. 2016, doi: 10.1098/RSTA.2016.0192.

[51] J. Laarman design | Dezeen. https://www.dezeen.com/tag/joris-laarman/ (accessed Feb. 08, 2022).

[52] ISO/TC266, "Biomimetics - Terminology, concepts and methodology, ISO 18458:2015," ed: Beuth Verlag, 2015b.

[53] Eliot Graeff. innovation bio-inspirée: modélisation d’un processus interdisciplinaire de conceptionbiomimétique outillé et intégration d’un nouvel acteur, le Biomiméticien. Biotechnologie. HESAM Université, 2020. Français.

[54] Pierre-Emmanuel Fayemi. Innovation par la conception bio-inspirée : proposition d’un modèle structurant les méthodes biomimétiques et formalisation d’un outil de transfert de connaissances. Génie mécanique [physics.class-ph]. Ecole nationale supérieure d’arts et métiers - ENSAM, 2016.

[55] M. H. Dickinson, “Bionics: Biological insight into mechanical design”.

[56] C. L. Merril, “Biomimicry Of The Dioxygen Active Site In The Copper Proteins Hemocyanin And Cytochrome Oxidase: Part I: Copper(I) Complexes Which React Reversibly With Dioxygen And Serve To Mimic The Active Site Function Of Hemocyanin. Part II: Mu-imidazolato Binuclear Metalloporphyrin Complexes Of Iron And Copper As Models For The Active Site Structure In Cytochrome Oxidase,” 1982, Accessed: Feb. 11, 2022. [Online]. Available: https://scholarship.rice.edu/handle/1911/15707

[57] R. H. C. Bonser and J. F. V. Vincent, “Technology trajectories, innovation, and the growth of biomimetics:,” http://dx.doi.org/10.1243/09544062JMES522, vol. 221, no. 10, pp. 1177–1180, Sep. 2007, doi: 10.1243/09544062JMES522.

[58] W. Nachtigall, “Vorbild Natur : Bionik-Design für funktionelles Gestalten,” Springer-Verlag Berlin Heidelbe, 1997.

[59] S. Jacobs, “Biomimetics: A simple foundation will lead to new insight about process,” International Journal of Design and Nature and Ecodynamics, vol. 9, no. 2, pp. 83–94, 2014, doi: 10.2495/DNE-V9-N2-83-94.

[60] M. Helms, S. S. Vattam, and A. K. Goel, “Biologically inspired design: process and products,” Design Studies, vol. 30, no. 5, pp. 606–622, Sep. 2009, doi: 10.1016/J.DESTUD.2009.04.003.

[61] H. Hashemi Farzaneh and U. Lindemann, “A Practical Guide to Bio-inspired Design,” A Practical Guide to Bio-inspired Design, 2019, doi: 10.1007/978-3-662-57684-7.

[62] F. E. Fish and J. T. Beneski, “Evolution and Bio-Inspired Design: Natural Limitations,” Biologically Inspired Design, pp. 287–312, 2014, doi: 10.1007/978-1-4471-5248-4_12.

[63] S. Vogel, “Comparative biomechanics: Life’s physical world,” Comparative Biomechanics: Life’s Physical World, Sep. 2011, doi: 10.1119/1.4868958.

[64] P. Silver, “Biology in this century | Harvard Magazine.” https://www.harvardmagazine.com/2011/09/biology-in-this-century (accessed Feb. 12, 2022).

[65] J. Benyus, “A Biomimicry Primer - Biomimicry 3.8.” https://biomimicry.net/the-buzz/resources/a-biomimicry-primer/ (accessed Feb. 16, 2022).

[66] C. G. Williams, “Origins of form : the shape of natural and man-made things,” p. 143, 2013.

[67] Y. L. Yap and W. Y. Yeong, “Additive manufacture of fashion and jewellery products: a mini review,” http://dx.doi.org/10.1080/17452759.2014.938993, vol. 9, no. 3, pp. 195–201, 2014, doi: 10.1080/17452759.2014.938993.

[68] J. Wolff, “The classic: on the inner architecture of bones and its importance for bone growth. 1870.,” Clin Orthop Relat Res, vol. 468, no. 4, pp. 1056–1065, Apr. 2010, doi: 10.1007/S11999-010-1239-2.

[69] L. J. Gibson, M. F. Ashby, B. A. Harley, “Cellular Materials in Nature and Medicine - Google Books.” https://books.google.fr/books?hl=en&lr=&id=AKxiS4AKpyEC&oi=fnd&pg=PR9&ots=JmVQ0vB9pU&sig=lmQ_m0t0oM7-kAFUOKTWN0TSw0M&redir_esc=y#v=onepage&q&f=false (accessed Jun. 17, 2022).

[70] M. Maglic, “Biomimicry: Using Nature as a Model for Design,” Masters Theses 1911 - February 2014, Jan. 2012, Accessed: Jun. 20, 2022. [Online]. Available: https://scholarworks.umass.edu/theses/871

[71] D. Bhate, C. A. Penick, L. A. Ferry, and C. Lee, “Classification and Selection of Cellular Materials in Mechanical Design: Engineering and Biomimetic Approaches,” Designs 2019, Vol. 3, Page 19, vol. 3, no. 1, p. 19, Mar. 2019, doi: 10.3390/DESIGNS3010019.

[72] “A Framework for the Design of Biomimetic Cellular Materials for Additive Manufacturing.” https://repositories.lib.utexas.edu/handle/2152/90013 (accessed Jun. 20, 2022).

[73] “nTopology | Engineering, Design & Simulation Software.” https://ntopology.com/ntopology-software/ (accessed Jul. 10, 2022).

[74] O. Al-Ketan and R. K. Abu Al-Rub, “MSLattice: A free software for generating uniform and graded lattices based on triply periodic minimal surfaces,” Material Design and Processing Communications, vol. 3, no. 6, p. e205, Dec. 2021, doi: 10.1002/MDP2.205.

[75] N. Soro, E. G. Brodie, A. Abdal-hay, A. Q. Alali, D. Kent, and M. S. Dargusch, “Additive manufacturing of biomimetic Titanium-Tantalum lattices for biomedical implant applications,” Materials & Design, vol. 218, p. 110688, Jun. 2022, doi: 10.1016/J.MATDES.2022.110688.

[76] A. du Plessis, I. Yadroitsava, I. Yadroitsev, S. G. le Roux, and D. C. Blaine, “Numerical comparison of lattice unit cell designs for medical implants by additive manufacturing,” https://doi.org/10.1080/17452759.2018.1491713, vol. 13, no. 4, pp. 266–281, Oct. 2018, doi: 10.1080/17452759.2018.1491713.

[77] V. K. Meena, P. Kumar, T. Panchal, P. Kalra, and R. K. Sinha, “Investigation of Titanium Lattice Structures for Biomedical Implants,” Advanced Materials for Biomechanical Applications, pp. 159–168, May 2022, doi: 10.1201/9781003286806-8.

[78] I. Kondakov, A. Chernov, N. Guseva, and M. Levchenkov, “Protective elements for lattice composite fuselage structures against low-velocity impacts,” Aerospace Systems 2022 5:1, vol. 5, no. 1, pp. 1–9, Jan. 2022, doi: 10.1007/S42401-022-00130-4.

[79] S. Moreno et al., “Experimental and Numerical Investigation of a Lattice Structure for Energy Absorption: Application to the Design of an Automotive Crash Absorber,” Polymers 2022, Vol. 14, Page 1116, vol. 14, no. 6, p. 1116, Mar. 2022, doi: 10.3390/POLYM14061116.

[80] M. B. Frank et al., “A Protocol for Bioinspired Design: A Ground Sampler Based on Sea Urchin Jaws,” JoVE (Journal of Visualized Experiments), vol. 2016, no. 110, p. e53554, Apr. 2016, doi: 10.3791/53554.

[81] G. Sossou, F. Demoly, G. Montavon, and S. Gomes. An additive manufacturing-oriented design approach to mechanical assemblies. Journal of Computational Design and Engineering. vol. 5. no. 1. pp. 3-18. 2018.

[82] J. C. André. From additive manufacturing to 3D/4D printing 1: From concepts to achievements. Wiley-ISTE. 2017.

[83] G. Sossou, F. Demoly, H. Belkebir, H. J. Qi, S. Gomes;, and G. Montavon. Design for 4D printing: Modeling and computation of smart materials distributions. Materials & Design. vol. 181. 108074. 2019.

[84] G. Sossou, F. Demoly, H. Belkebir, H. J. Qi, S. Gomes, and G. Montavon. Design for 4D printing: A voxel-based modeling and simulation of smart materials. Materials & Design. vol. 175. 107798. 2019.

[85] W. Tao and M. C. Leu. "Design of lattice structure for additive manufacturing." 2016 International Symposium on Flexible Automation (ISFA). Cleveland. OH. 2016. pp. 325-332. doi: 10.1109/ISFA.2016.7790182.

[86] G. Dong, Y. Tang, and Y. Zhao (2017). A Survey of Modeling of Lattice Structures Fabricated by Additive Manufacturing. Journal of Mechanical Design. 139. 10.1115/1.4037305.

[87] C. Pan, Y. Han, J. Lu. 2020. "Design and Optimization of Lattice Structures: A Review" Appl. Sci. 10. no. 18: 6374.

[88] J. Xiong, R. Mines, R. Ghosh, A. Vaziri, L. Ma, A. Ohrndorf, H. Christ, J, H, and L. Wu (2015). Advanced Micro-Lattice Materials. Adv. Eng. Mater.. 17: 1253-1264. https://doi.org/10.1002/adem.201400471

[89] B. Vayre. F. Vignat. F. Villeneuve. Designing for Additive Manufacturing. Procedia CIRP. Volume 3. 2012. Pages 632-637. ISSN 2212-8271.

[90] I. Flores, N. Kretzschmar. A. H. Azman, S. Chekurov. D. Bue Pedersen, A. Chaudhuri. Implications of lattice structures on economics and productivity of metal powder bed fusion. Additive Manufacturing. Volume 31. 2020. 100947. ISSN 2214-8604.

[91] J. Lim, C. You, I. Dayyani. Multi-objective topology optimization and structural analysis of periodic spaceframe structures. Materials & Design. Volume 190. 2020. 108552. ISSN 0264-1275. https://doi.org/10.1016/j.matdes.2020.108552.

[92] G. H. Loh, E. Pei, D. Harrison, M. D. Monzón. An overview of functionally graded additive manufacturing. Additive Manufacturing. Volume 23. 2018. Pages 34-44. ISSN 2214-8604. https://doi.org/10.1016/j.addma.2018.06.023.

[93] L. Cheng, P. Zhang, E. Biyikli, J. Bai, J. Robbins, and A. To (2017). "Efficient design optimization of variable-density cellular structures for additive manufacturing: theory and experimental validation". Rapid Prototyping Journal. Vol. 23 No. 4. pp. 660-677. https://doi.org/10.1108/RPJ-04-2016-0069

[94] Y. Tang, A. Kurtz, YF. Zhao (2015) Bidirectional Evolutionary Structural Optimization (BESO) Based Design Method for Lattice Structure to be Fabricated by Additive Manufacturing. Computer-Aided Design 69:91–101.

[95] J. Nguyen. S. I. Park. and D. Rosen. "Heuristic Optimization Method for Cellular Structure Design of Light Weight Components." International Journal of Precision Engineering and Manufacturing. vol. 14. pp. 1071-1078. Jun 2013.

[96] Y. Chen. "3d texture mapping for rapid manufacturing." Computer-Aided Design & Applications. vol. 4. pp. 761-771. 2007.

[97] H. V. Wang and D. Rosen. "Computer-aided design methods for the additive fabrication of truss structure." Master. School of Mechanical Engineering. Georgia Institute of Technology. 2001.

[98] H. Wang and D. W. Rosen. "Parametric modeling method for truss structures." in 22nd Computers and Information in Engineering Conference. Montreal. Que.. 2002. pp. 759-767.

[99] H. V. Wang. "A unit cell approach for lightweight structure and compliant mechanism." Doctor. Georgia Institute Of Technology. Georgia. Atlanta. 2005.

[100] S. R. Teufelhart. G. "Optimization of Strut Diameters in Lattice Structures." presented at the Proceedings of the 23 rd Solid Freeform Fabrication (SFF) Symposium. 2012.

[101] G. Reinhart and S. Teufelhart. "Load-Adapted Design of Generative Manufactured Lattice Structures." Physics Procedia. vol. 12. Part A. pp. 385-392. // 2011.

[102] G. Reinhart and S. Teufelhart. "Optimization of mechanical loaded lattice structures by orientating their struts along the flux of force." in 8th CIRP International Conference on Intelligent Computation in Manufacturing Engineering. ICME 2012. Ischia. 2013. pp. 175-180.

[103] T. Matsumoto, T. Yamada, S. Shichi, and T. Takahashi (2012). A study on topology optimization using the level-set function and BEM. WIT Transactions on Modelling and Simulation. 10.2495/BE120111.

[104] Ge Qi. Bin Ji, and Li Ma (2019) Mechanical response of pyramidal lattice truss core sandwich structures by additive manufacturing. Mechanics of Advanced Materials and Structures. 26:15. 1298-1306. DOI: 10.1080/15376494.2018.1432805

[105] N. Lebaal, Y. Zhang, F. Demoly, S. Roth, S. Gomes, A. Bernard. Optimised lattice structure configuration for additive manufacturing. CIRP Annals. Volume 68. Issue 1. 2019. Pages 117-120. ISSN 0007-8506. https://doi.org/10.1016/j.cirp.2019.04.054.

[106] N. Lebaal, A. Settar, S. Roth, S. Gomes, Conjugate heat transfer analysis within in lattice-filled heat exchanger for additive manufacturing, Mechanics of Advanced Materials and Structures, 1-9, https://doi.org/10.1080/15376494.2020.1819489.

[107] GH. Song, SK. Jing, FL. Zhao, et al. Design of Lattice Structures Using Local Relative Density Mapping Method. Chin. J. Mech. Eng. 31, 89 (2018). https://doi.org/10.1186/s10033-018-0289-3

[108] Y. Wang, S. Li, Y. Yu, Y. Xin, X. Zhang, Q. Zhang, S. Wang, Lattice structure design optimization coupling anisotropy and constraints of additive manufacturing, Materials & Design, Volume 196, 2020, 109089, ISSN 0264-1275, https://doi.org/10.1016/j.matdes.2020.109089.

[109] B. Hanks, J. Berthel, M. Frecker, T. W. Simpson. Mechanical properties of additively manufactured metal lattice structures: Data review and design interface. Additive Manufacturing. Volume 35. 2020. 101301. ISSN 2214-8604. https://doi.org/10.1016/j.addma.2020.101301.

[110] M. R. Ward Rashidi, G. Frank, R. Seifert, W. Chapkin, J. Baur, and P. Walgren (2019). Biomimicry of the armadillo carapace for the design of bending cylinders for aerospace applications. In AIAA Scitech 2019 Forum (p. 1632). https://doi.org/10.2514/6.2019-1632.

[111] I. D. Wijegunawardana, I. D., and W. R. de Mel, W. R. (2021). Biomimetic Designs for Automobile Engineering: A Review. International Journal of Automotive and Mechanical Engineering, 18(3), 9029-9041. https://doi.org/10.15282/ijame.18.3.2021.15.0692

[112] F. Xu, J. Wang, and L. Hua (2021). Multi-objective biomimetic optimization design of stiffeners for automotive door based on vein unit of dragonfly wing. Proceedings of the Institution of Mechanical Engineers, Part C: Journal of Mechanical Engineering Science, 09544062211053471. https://doi.org/10.1177/09544062211053471

[113] I. Yadroitsev, P. Krakhmalev, I. Yadroitsava, and A. Du Plessis (2018). Qualification of Ti6Al4V ELI alloy produced by laser powder bed fusion for biomedical applications. Jom, 70(3), 372-377. https://doi.org/10.1007/s11837-017-2655-5.

[114] J.C. André, A. Le Méhauté, O. De Witte, Dispositif pour réaliser un modèle de pièce industrielle. Brevet français n° 84 11 241 du 16.07.1984, 1984.

[115] I. Gibson, D. W. Rosen, and B. Stucker (2020). Additive manufacturing technologies: rapid prototyping to direct digital manufacturing.

[116] Y. Yang, X. Song, X. Li, Z. Chen, C. Zhou, Q. Zhou, and Y. Chen (2018). Recent progress in biomimetic additive manufacturing technology: from materials to functional structures. Advanced Materials, 30(36), 1706539. https://doi.org/10.1002/adma.201706539

[117] H. Prüss, T. Vietor, Design for fiber-reinforced additive manufacturing, J. Mech. Des., 2015, 137(11), 111409.

[118] B. Barroqueiro, A. Andrade-Campos, J. Dias-de-Oliveira, RAF. Valente, Bridging between topology optimization and additive manufacturing via Lapacian Smoothing, J. Mech. Des., 2021, 143(9), 091703.

[119] Y. Wang, S. E. Naleway, B. Wang, Biological and bioinspired materials: Structure leading to functional and mechanical performance, Bioactive Materials, Volume 5, Issue 4, 2020, Pages 745-757, ISSN 2452-199X,https://doi.org/10.1016/j.bioactmat.2020.06.003.

[120] V. Nimbagal, N.R. Banapurmath, A.M. Sajjan, et al. Studies on Hybrid Bio-Nanocomposites for Structural Applications. J. of Materi Eng and Perform 30, 6461–6480 (2021). https://doi.org/10.1007/s11665-021-05843-9

[121] J. Martin, B. Fiore, and R. Erb. Designing bioinspired composite reinforcement architectures via 3D magnetic printing. Nat Commun 6, 8641 (2015). https://doi.org/10.1038/ncomms9641

[122] R. W. Ibrahim, Conformal geometry of the turtle shell, Journal of King Saud University - Science, Volume 32, Issue 3, 2020, Pages 2202-2206, ISSN 1018-3647, https://doi.org/10.1016/j.jksus.2020.02.024.

[123] D. Wang, D. Chen, and Z. Chen, (2020) Recent Progress in 3D Printing of Bioinspired Structures. Front. Mater. 7:286. doi: 10.3389/fmats.2020.0028

[124] M. Maghsoudi-Ganjeh, L. Lin, X. Wang & X. Zeng, (2019) Bioinspired design of hybrid composite materials, International Journal of Smart and Nano Materials, 10:1, 90-105, DOI: 10.1080/19475411.2018.1541145

[125] P. Zhang, J. Toman, Y. Yu, E. Biyikli, M. Kirca, M. Chmielus, and A. C. To, (2015). Efficient design-optimization of variable-density hexagonal cellular structure by additive manufacturing: theory and validation. Journal of Manufacturing Science and Engineering, 137(2). https://doi.org/10.1108/RPJ-04-2016-0069

[126] Y. Tang and Y. F. Zhao, (2015). Lattice-skin structures design with orientation optimization. In 2015 International Solid Freeform Fabrication Symposium. University of Texas at Austin.

[127] P. F. Egan, I. Bauer, K. Shea, S.J. Ferguson, Mechanics of three-dimensional printed lattices for biomedical devices. J. Mech. Des., 2019, 141(3), 031703.

[128] SI. Park, DW. Rosen, Homogenization of mechanical properties for material extrusion periodic lattice structures considering joint stiffening effect, J. Mech. Des., 2018, 140(11), 111414.

[129] C. Sharpe, CC. Seepersad, Lattice structure optimization with orientation-dependent material properties, J. Mech. Des., 2021, 143(9), 091708.

[130] Y. Han, WF. Lu, A novel design method for nonuniform lattice structures based on topology optimization, J. Mech. Des., 2018, 140(9), 091403.

[131] CS. Verma, B. Rankouhi, K. Suresh, A combinatorial approach for constructing lattice structures, J. Mech. Des., 2020, 142(4), 041404.

[132] Y. Tang, Y. F. Zhao, (2016). A survey of the design methods for additive manufacturing to improve functional performance. Rapid Prototyping Journal. https://doi.org/10.1108/RPJ-01-2015-0011

[133] A. Challapalli, (2015). Loading mode dependent effective properties of octet-truss lattice structures using 3D-printing. University of North Texas.

[134] A. Rainer, S. M. Giannitelli, D. Accoto, S. De Porcellinis, E. Guglielmelli, and M. Trombetta, (2012). Load-adaptive scaffold architecturing: a bioinspired approach to the design of porous additively manufactured scaffolds with optimized mechanical properties. Annals of biomedical engineering, 40(4), 966-975. https://doi.org/10.1007/s10439-011-0465-4

[135] O. Stava, J. Vanek, B. Benes, N. Carr, and R. Měch, (2012). Stress relief: improving structural strength of 3D printable objects. ACM Transactions on Graphics (TOG), 31(4), 1-11. https://doi.org/10.1145/2185520.2185544

[136] M. Alzahrani, S. K. Choi, and D. W. Rosen, (2015). Design of truss-like cellular structures using relative density mapping method. Materials & Design, 85, 349-360. https://doi.org/10.1186/s10033-018-0289-3

[137] J. Stampfl, H. E. Pettermann, and R. Liska, (2011). Bioinspired cellular structures: Additive manufacturing and mechanical properties. In Biomimetics--Materials, Structures and Processes (pp. 105-123). Springer, Berlin, Heidelberg. https://doi.org/10.1007/978-3-642-11934-7_6

[138] Y. Li, Z. Feng, L. Hao, L. Huang, C. Xin, Y. Wang, and T. Peijs, (2020). A review on functionally graded materials and structures via additive manufacturing: from multi-scale design to versatile functional properties. Advanced Materials Technologies, 5(6), 1900981. https://doi.org/10.1002/admt.201900981

[139] J. A. Robles-Linares, E. Ramírez-Cedillo, H. R. Siller, C. A. Rodríguez, and J. I. Martínez-López, (2019). Parametric modeling of biomimetic cortical bone microstructure for additive manufacturing. Materials, 12(6), 913. https://doi.org/10.3390/ma12060913

[140] C. Santiuste, M. Rodríguez-Millán, E. Giner, and H. Miguélez, (2014). The influence of anisotropy in numerical modeling of orthogonal cutting of cortical bone. Composite Structures, 116, 423-431. https://doi.org/10.1016/j.compstruct.2014.05.031.

[141] S. M. Ali Banijamali, R. Oftadeh, A. Nazarian, R. Goebel, A. Vaziri, and H. Nayeb-Hashemi, (2015). Effects of different loading patterns on the trabecular bone morphology of the proximal femur using adaptive bone remodeling. Journal of biomechanical engineering, 137(1), 011011. https://doi.org/10.1115/1.4029059

[142] S. Limmahakhun, A. Oloyede, K. Sitthiseripratip, Y. Xiao, and C. Yan, (2017). 3D-printed cellular structures for bone biomimetic implants. Additive Manufacturing, 15, 93-101. https://doi.org/10.1016/j.addma.2017.03.010

[143] R. Aversa, F. I. Petrescu, R. V. Petrescu, and A. Apicella, (2016). Biomimetic finite element analysis bone modeling for customized hybrid biological prostheses development. American Journal of Applied Sciences, 13(11), 1060-1067. https://doi.org/10.3844/ajassp.2016.1060.1067

[144] C. Simoneau, P. Terriault, B. Jetté, M. Dumas, and V. Brailovski, (2017). Development of a porous metallic femoral stem: Design, manufacturing, simulation and mechanical testing. Materials & Design, 114, 546-556. https://doi.org/10.1016/j.matdes.2016.10.064.

[145] S. Daynes, S. Feih, W. F. Lu, and J. Wei, (2017). Optimisation of functionally graded lattice structures using isostatic lines. Materials & Design, 127, 215-223. https://doi.org/10.1016/j.matdes.2017.04.082.

[146] C. Audibert, J. Chaves-Jacob, J. M. Linares, and Q. A. Lopez, (2018). Bio-inspired method based on bone architecture to optimize the structure of mechanical workspieces. Materials & Design, 160, 708-717. https://doi.org/10.1016/j.matdes.2018.10.013.

[147] K. M. M. Tam, C. T. Mueller, J. R. Coleman, N. W. Fine, (2016). Stress line additive manufacturing (SLAM) for 2.5-D shells. Journal of the International Association for Shell and Spatial Structures, 57(4), 249-259. https://doi.org/10.20898/j.iass.2016.190.856

[148] S. Teufelhart, (2014). Investigation of the capability of flux of force oriented lattice structures for lightweight design. In Advanced Materials Research (Vol. 907, pp. 75-87). Trans Tech Publications Ltd. https://doi.org/10.4028/www.scientific.net/AMR.907.75

[149] O. A. Pereira and J. M. de Almeida, J. M. (1994). Automatic drawing of stress trajectories in plane systems. Computers & structures, 53(2), 473-476.

[150] K. M. M. Tam and C. T. Mueller, (2017). Additive manufacturing along principal stress lines. 3D Printing and Additive Manufacturing, 4(2), 63-81. https://doi.org/10.1089/3dp.2017.0001

[151] W. Prager, (1974). A note on discretized Michell structures. Computer Methods in Applied Mechanics and Engineering, 3(3), 349-355. https://doi.org/10.1016/0045-7825(74)90019-X.

[152] T. H. Kwok, Y. Li, and Y. Chen, (2016). A structural topology design method based on principal stress line. Computer-Aided Design, 80, 19-31. https://doi.org/10.1016/j.cad.2016.07.005.

[153] Y. Li, and Y. Chen, (2010, September). Beam structure optimization for additive manufacturing based on principal stress lines. In 2010 International Solid Freeform Fabrication Symposium. University of Texas at Austin. http://dx.doi.org/10.26153/tsw/15231

[154] T. Kirk, E. Galvan, R. Malak, R. Arroyave, Computational design of gradient paths in additively manufactured functionnnaly graded materials. J. Mech. Des., 2018, 140(11), 111410.

[155] E. Ulu, E. Korkmaz, K. Yay, O. B. Ozdoganlar, L. B. Kara, Enhancing the structural performance of additively manufactured objects thrugh build orientation optimization, J. Mech. Des., 2015, 137(11), 111410.

[156] P. Prusinkiewicz and A. Lindenmayer, (2012). The algorithmic beauty of plants. Springer Science & Business Media.

[157] M. Cieslak and P. Prusinkiewicz, (2019). Gillespie-lindenmayer systems for stochastic simulation of morphogenesis. in silico Plants, 1(1), diz009. https://doi.org/10.1093/insilicoplants/diz009

[158] B. Lane and P. Prusinkiewicz, (2002, May). Generating spatial distributions for multilevel models of plant communities. In Graphics interface (Vol. 2002, pp. 69-87). https://doi.org/10.20380/GI2002.09

[159] P. Prusinkiewicz, (1986, May). Graphical applications of L-systems. In Proceedings of graphics interface (Vol. 86, No. 86, pp. 247-253).

[160] A. Suyantohadi, A. Alfiyan, M. Hariadi, and M. H. Purnomo, (2010). Plant growth modeling using l-system approach and its visualization. Makara Journal of Technology, 14(2), 7. doi:10.7454/699.

[161] H. Xu, X. Y. Wang, C. N. Liu, J. N. Chen, and C. Zhang, (2021). A 3D root system morphological and mechanical model based on L-Systems and its application to estimate the shear strength of root-soil composites. Soil and Tillage Research, 212, 105074. https://doi.org/10.1016/j.still.2021.105074.

[162] D. Leitner, S. Klepsch, G. Bodner, and A. Schnepf, (2010). A dynamic root system growth model based on L-Systems. Plant and soil, 332(1), 177-192. https://doi.org/10.1007/s11104-010-0284-7

[163] B. R. Bielefeldt, E. Akleman, G. W. Reich, P. S. Beran, D. J. Hartl, (2019). L-system-generated mechanism topology optimization using graph-based interpretation. Journal of Mechanisms and Robotics, 11(2). https://doi.org/10.1115/1.4042512

[164] N. Inou and H. Kimoto, (2000). A Cellular Automaton Self-organizing a Mechanical Structure : Transformation of topological structure by use of L systems. The Proceedings of The Computational Mechanics Conference. 2000.13. 177-178. 10.1299/jsmecmd.2000.13.177.

[165] Z. Huang, Y. Hwang, V. Aute, and R. Radermacher, (2016). Review of fractal heat exchangers.

[166] S. Hallad, A. Patil, N. Banapurmath, A. M. Hunashyal, A. Shettar, and N. Ayachit, (2017). Experimental and Numerical Validation on the Utilization of Polymer Based Nano-Composites for Structural Applications Using FEA Software Tool. Materials Focus. 6. 685-690. 10.1166/mat.2017.1466.

[167] S. A. Hallad, N. R. Banapurmath, A. Y. Patil, A. M. Hunashyal, A. S. Shettar, Studies on the effect of multi-walled carbon nanotube–reinforced polymer-based nano-composites using finite element analysis software tool. Proceedings of the Institution of Mechanical Engineers, Part N: Journal of Nanomaterials, Nanoengineering and Nanosystems. 2016;230(4):200-212. doi:10.1177/1740349915599182

[168] T. H. M. Mysore, A. Y. Patil, G. U. Raju, N. R. Banapurmath, P. M. Bhovi, A. Afzal, S. Alamri, C. A. Saleel, Investigation of Mechanical and Physical Properties of Big Sheep Horn as an Alternative Biomaterial for Structural Applications. Materials 2021, 14, 4039. https://doi.org/10.3390/ma14144039

[169] N. Letov, P. T. Velivela, S. Sun, Y. F. Zhao, Challenges and opportunities in geometric modeling of complex bio-inspired three-dimensional objects designed for additive manufacturing, J. Mech. Des., 2021, 143(12), 121705.

[170] T. Stankovic, K. Shea, Investigation of a Voronoi diagram representation for the computational design of additively manufactured discrete lattice structures, J. Mech. Des., 2020, 142(11), 111704.

[171] Stratasys VeroWhite data-sheet https://www.stratasys.com/siteassets/materials/materialscatalog/polyjetmaterials/verovivid/mds_pj_vero_1020a.pdf?v=48d11e

[172] I. I. Kokcharov and A. E. Burov, (2001). Analysis of stress state with the force lines method. choice, 10, 2.

[173] N. Lebaal, S. Puissant, F. M. Schmidt, and D. Schläfli, (2012). An optimization method with experimental validation for the design of extrusion wire coating dies for a range of different materials and operating conditions. Polymer Engineering & Science, 52(12), 2675-2687. https://doi.org/10.1002/pen.23203

[174] M. S. Chebbah and N. Lebaal, (2020). Tube hydroforming optimization using a surrogate modeling approach and genetic algorithm. Mechanics of Advanced Materials and Structures, 27(6), 515-524. https://doi.org/10.1080/15376494.2018.1482578

[175] K. V. Sabarish and P. Pratheeba, (2020). An experimental analysis on structural beam with Taguchi orthogonal array. Materials Today: Proceedings, 22, 874-878. DOI: 10.35940/ijitee.L1109.10812S19

[176] K. Wu, H. Hu, L. Wang, and Y. Gao, "Parametric optimization of an aperiodic metastructure based on genetic algorithm," International Journal of Mechanical Sciences, vol. 214, 2022, doi: 10.1016/j.ijmecsci.2021.106878.

[177] A. Rajeev et al., "Parametric optimization of corner radius in hexagonal honeycombs under in-plane compression," Journal of Manufacturing Processes, vol. 79, pp. 35–46, Jul. 2022, doi: 10.1016/J.JMAPRO.2022.04.041.

[178] A. v. Alekseytsev, "Evolutionary optimization of steel trusses with the nodal joints of rods," Magazine of Civil Engineering, vol. 40, no. 5, pp. 28–37, 2013, doi: 10.5862/MCE.40.3.

[179] A. Kibkalo, M. Lebedeva, and M. Volkov, "Methods of Parametric Optimization of Thin-Walled Structures and Parameters which Influence on it," MATEC Web of Conferences, vol. 53, Apr. 2016, doi: 10.1051/MATECCONF/20165301051.

[180] I. N. Serpik, A. v. Alekseytsev, P. Y. Balabin, and N. S. Kurchenko, "Flat rod systems: optimization with overall stability control," Magazine of Civil Engineering, vol. 76, no. 8, pp. 181–192, 2017, doi: 10.18720/MCE.76.16.

[181] I. N. Serpik and A. v. Alekseytsev, "Optimization of frame structures with possibility of emergency actions," Magazine of Civil Engineering, vol. 44, no. 9, Dec. 2013, doi: 10.5862/MCE.44.3.

[182] A. Mohanty et al., "Parametric optimization of parameters affecting dimension precision of FDM printed part using hybrid Taguchi-MARCOS-nature inspired heuristic optimization technique," Materials Today: Proceedings, vol. 50, pp. 893–903, Jan. 2022, doi: 10.1016/J.MATPR.2021.06.216.

[183] N. Lebaal, S. Puissant, and F. M. Schmidt, "Rheological parameters identification using in situ experimental data of a flat die extrusion," Journal of Materials Processing Technology, vol. 164–165, pp. 1524–1529, May 2005, doi: 10.1016/J.JMATPROTEC.2005.02.218.

[184] H. Naceur, Y. Q. Guo, and S. Ben-Elechi, "Response surface methodology for design of sheet forming parameters to control springback effects," Computers & Structures, vol. 84, no. 26–27, pp. 1651–1663, Oct. 2006, doi: 10.1016/J.COMPSTRUC.2006.04.005.

[185] H. Wang, L. Tang, and G. Y. Li, "Adaptive MLS-HDMR metamodeling techniques for high dimensional problems," Expert Systems with Applications, vol. 38, no. 11, pp. 14117–14126, Oct. 2011, doi: 10.1016/J.ESWA.2011.04.220.

[186] S. Chakraborty and A. Sen, "Adaptive response surface based efficient Finite Element Model Updating," Finite Elements in Analysis and Design, vol. 80, pp. 33–40, Mar. 2014, doi: 10.1016/J.FINEL.2013.11.002.

[187] N. Lebaal, M. Oudjene, and S. Roth, "The optimal design of sheet metal forming processes: Application to the clinching of thin sheets," International Journal of Computer Applications in Technology, vol. 43, no. 2, pp. 110–116, 2012, doi: 10.1504/IJCAT.2012.046041.

[188] M. Oudjene, L. Ben-Ayed, A. Delamézière, and J. L. Batoz, "Shape optimization of clinching tools using the response surface methodology with Moving Least-Square approximation," Journal of Materials Processing Technology, vol. 209, no. 1, pp. 289–296, Jan. 2009, doi: 10.1016/J.JMATPROTEC.2008.02.030.

[189] M. Azaouzi, N. Lebaal, G. Rauchs, and S. Belouettar, "Optimal design of multi-step stamping tools based on response surface method," Simulation Modelling Practice and Theory, vol. 24, pp. 1–14, May 2012, doi: 10.1016/J.SIMPAT.2012.01.006.

[190] E. Roux and P. O. Bouchard, "Kriging metamodel global optimization of clinching joining processes accounting for ductile damage," Journal of Materials Processing Technology, vol. 213, no. 7, pp. 1038–1047, Jul. 2013, doi: 10.1016/J.JMATPROTEC.2013.01.018.

[191] S. J. Yakowitz and F. Szidarovszky, "A comparison of kriging with nonparametric regression methods," Journal of Multivariate Analysis, vol. 16, no. 1, pp. 21–53, Feb. 1985, doi: 10.1016/0047-259X(85)90050-8.

[192] X. Liu, L. Gao, M. Xiao, and Y. Zhang, "Kriging-assisted design of functionally graded cellular structures with smoothly-varying lattice unit cells," Computer Methods in Applied Mechanics and Engineering, vol. 390, p. 114466, Feb. 2022, doi: 10.1016/J.CMA.2021.114466.

[193] G. Sun, G. Li, and Q. Li, "Variable fidelity design based surrogate and artificial bee colony algorithm for sheet metal forming process," Finite Elements in Analysis and Design, vol. 59, pp. 76–90, Oct. 2012, doi: 10.1016/J.FINEL.2012.04.012.

[194] S. Jakobsson, B. Andersson, and F. Edelvik, "Rational radial basis function interpolation with applications to antenna design," Journal of Computational and Applied Mathematics, vol. 233, no. 4, pp. 889–904, Dec. 2009, doi: 10.1016/J.CAM.2009.08.058.

[195] N. Tanguy, N. Iassamen, M. Telescu, and P. Cloastre, "Parameter optimization of orthonormal basis functions for efficient rational approximations," Applied Mathematical Modelling, vol. 39, no. 16, pp. 4963–4970, Aug. 2015, doi: 10.1016/J.APM.2015.04.017.

[196] Y. C. Chiang and A. Borgart, "A form-finding method for membrane shells with radial basis functions," Engineering Structures, vol. 251, p. 113514, Jan. 2022, doi: 10.1016/J.ENGSTRUCT.2021.113514.

[197] J. F.-T. annals of statistics and undefined 1991, "Multivariate adaptive regression splines," projecteuclid.org, Accessed: Jul. 06, 2022. [Online]. Available: https://projecteuclid.org/journals/annals-of-statistics/volume-19/issue-1/Multivariate-Adaptive-Regression-Splines/10.1214/aos/1176347963.short

[198] H. M. Gomes, A. M. Awruch, and P. A. M. Lopes, "Reliability based optimization of laminated composite structures using genetic algorithms and Artificial Neural Networks," Structural Safety, vol. 33, no. 3, pp. 186–195, May 2011, doi: 10.1016/J.STRUSAFE.2011.03.001.

[199] D. J. Fonseca, D. O. Navaresse, and G. P. Moynihan, "Simulation metamodeling through artificial neural networks," Engineering Applications of Artificial Intelligence, vol. 16, no. 3, pp. 177–183, Apr. 2003, doi: 10.1016/S0952-1976(03)00043-5.

[200] E. B. Moustafa, A. H. Hammad, and A. H. Elsheikh, "A new optimized artificial neural network model to predict thermal efficiency and water yield of tubular solar still," Case Studies in Thermal Engineering, vol. 30, p. 101750, Feb. 2022, doi: 10.1016/J.CSITE.2021.101750.

[201] Y. F. Li, S. H. Ng, M. Xie, and T. N. Goh, "A systematic comparison of metamodeling techniques for simulation optimization in Decision Support Systems," Applied Soft Computing, vol. 10, no. 4, pp. 1257–1273, Sep. 2010, doi: 10.1016/J.ASOC.2009.11.034.

[202] J. V. Soares do Amaral, J. A. B. Montevechi, R. de C. Miranda, and W. T. de S. Junior, "Metamodel-based simulation optimization: A systematic literature review," Simulation Modelling Practice and Theory, vol. 114, Jan. 2022, doi: 10.1016/J.SIMPAT.2021.102403.

[203] T. W. Simpson, A. J. Booker, D. Ghosh, A. A. Giunta, P. N. Koch, and R. J. Yang, "Approximation methods in multidisciplinary analysis and optimization: a panel discussion," Structural and Multidisciplinary Optimization 2004 27:5, vol. 27, no. 5, pp. 302–313, Jun. 2004, doi: 10.1007/S00158-004-0389-9.

[204] G. G. Wang and S. Shan, "Review Of Metamodeling Techniques For Product Design With Computation-intensive Processes", Proceedings of the Canadian Engineering Education Association (CEEA), Aug. 2005, doi: 10.24908/PCEEA.V0I0.3940.

[205] J. Zheng, H. Chen, and C. Jiang, "Robust topology optimization for structures under thermo-mechanical loadings considering hybrid uncertainties," Structural and Multidisciplinary Optimization, vol. 65, no. 1, pp. 1–16, Jan. 2022, doi: 10.1007/S00158-021-03121-9/TABLES/5.

[206] M. Diez, E. F. Campana, and F. Stern, "Design-space dimensionality reduction in shape optimization by Karhunen–Loève expansion," Computer Methods in Applied Mechanics and Engineering, vol. 283, pp. 1525–1544, Jan. 2015, doi: 10.1016/J.CMA.2014.10.042.

[207] M. Azaouzi, N. Lebaal, A. Makradi, and S. Belouettar, "Optimization based simulation of self-expanding Nitinol stent," Materials & Design, vol. 50, pp. 917–928, Sep. 2013, doi: 10.1016/J.MATDES.2013.03.012.

[208] G. G. Wang, "Adaptive Response Surface Method Using Inherited Latin Hypercube Design Points," Journal of Mechanical Design, vol. 125, no. 2, pp. 210–220, Jun. 2003, doi: 10.1115/1.1561044.

[209] Z. Beiramzadeh, M. Baqersad, and M. Aghababaei, "Application of the response surface methodology (RSM) in heavy metal removal from real power plant wastewater using electrocoagulation," https://doi.org/10.1080/19648189.2019.1640139, vol. 26, no. 1, pp. 1–20, 2019, doi: 10.1080/19648189.2019.1640139.

[210] H. Wang, G. Li, and E. Li, "A comparative study of boundary-based intelligent sampling approaches for nonlinear optimization," Applied Soft Computing, vol. 11, no. 2, pp. 2227–2238, Mar. 2011, doi: 10.1016/J.ASOC.2010.08.002.

[211] H. Wang, E. Li, and G. Y. Li, "The least square support vector regression coupled with parallel sampling scheme metamodeling technique and application in sheet forming optimization," Materials & Design, vol. 30, no. 5, pp. 1468–1479, May 2009, doi: 10.1016/J.MATDES.2008.08.014.

[212] W. Hu, L. Enying, and L. G. Yao, "Optimization of drawbead design in sheet metal forming based on intelligent sampling by using response surface methodology," Journal of Materials Processing Technology, vol. 206, no. 1–3, pp. 45–55, Sep. 2008, doi: 10.1016/J.JMATPROTEC.2007.12.002.vero

[213] G. Jia and A. A. Taflanidis, "Kriging metamodeling for approximation of high-dimensional wave and surge responses in real-time storm/hurricane risk assessment," Computer Methods in Applied Mechanics and Engineering, vol. 261–262, pp. 24–38, Jul. 2013, doi: 10.1016/J.CMA.2013.03.012.

[214] N. Lebaal, F. Schmidt, and S. Puissant, "Optimisation of extrusion flat die design and die wall temperature distribution, using Kriging and response surface method," International Journal of Materials and Product Technology, vol. 38, no. 2–3, pp. 307–322, 2010, doi: 10.1504/IJMPT.2010.032107.

[215] J. Zhang, M. Xiao, P. Li, and L. Gao, "Quantile-based topology optimization under uncertainty using Kriging metamodel," Computer Methods in Applied Mechanics and Engineering, vol. 393, p. 114690, Apr. 2022, doi: 10.1016/J.CMA.2022.114690.

[216] G. Yu, C. Chen, H. Hou, M. Chen, and R. Zhang, "Experimental evaluation of CV-Voronoi based adaptive sampling for Kriging meta-modeling of multiple responses through real-time hybrid

simulation," Earthquake Engineering & Structural Dynamics, vol. 51, no. 8, pp. 1943–1961, Jul. 2022, doi: 10.1002/EQE.3646.

[217] J. P. C. Kleijnen, "Kriging metamodeling in simulation: A review," European Journal of Operational Research, vol. 192, no. 3, pp. 707–716, Feb. 2009, doi: 10.1016/J.EJOR.2007.10.013.

[218] Y. Cui, X. Meng, and J. Qiao, "A multi-objective particle swarm optimization algorithm based on two-archive mechanism," Applied Soft Computing, vol. 119, p. 108532, Apr. 2022, doi: 10.1016/J.ASOC.2022.108532.

[219] T. M. Shami, A. A. El-Saleh, M. Alswaitti, Q. Al-Tashi, M. A. Summakieh, and S. Mirjalili, "Particle Swarm Optimization: A Comprehensive Survey," IEEE Access, vol. 10, pp. 10031–10061, 2022, doi: 10.1109/ACCESS.2022.3142859.

[220] Y. Shi and R. Eberhart, "Modified particle swarm optimizer," Proceedings of the IEEE Conference on Evolutionary Computation, ICEC, pp. 69–73, 1998, doi: 10.1109/ICEC.1998.699146.

[221] Y. Zhang, Z. An, and J. Zhou, "Optimization design of flash structure for forging die based on Kriging-PSO strategy," Lecture Notes in Computer Science (including subseries Lecture Notes in Artificial Intelligence and Lecture Notes in Bioinformatics), vol. 6145 LNCS, no. PART 1, pp. 373–381, 2010, doi: 10.1007/978-3-642-13495-1_46/COVER/.

[222] J. Kennedy and R. Eberhart, "Particle swarm optimization," Proceedings of ICNN'95 - International Conference on Neural Networks, vol. 4, pp. 1942–1948, doi: 10.1109/ICNN.1995.488968.

[223] N. Lebaal, "Robust low cost meta-modeling optimization algorithm based on meta-heuristic and knowledge databases approach: Application to polymer extrusion die design," Finite Elements in Analysis and Design, vol. 162, pp. 51–66, Sep. 2019, doi: 10.1016/J.FINEL.2019.05.004.

[224] N. Lebaal, M. Nouari, and A. Ginting, "A new optimization approach based on Kriging interpolation and sequential quadratic programming algorithm for end milling refractory titanium alloys," Applied Soft Computing, vol. 11, no. 8, pp. 5110–5119, Dec. 2011, doi: 10.1016/J.ASOC.2011.05.048.

[225] B. Bader, E. Türck, T. Vietor, A Current Overview Of The Used Potential In Automotive Industries, 2021, Multi Material Design, In: Dröder, K., Vietor, T. (eds), Technologies for economical and functional lightweight design, Zukunftstechnologien für den multifunktionalen Leichtbau, Springer Vieweg, Berlin, Heidelberg, https://doi.org/10.1007/978-3-662-58206-0_1

[226] S. Kleemann, T. Fröhlich, E. Türck, T. Vietor, A Methodological Approach Towards Multi-material Design of Automotive Components, Procedia CIRP, Volume 60, 2017, Pages 68-73, ISSN 2212-8271, https://doi.org/10.1016/j.procir.2017.01.010.

[227] N. Karathanasopoulos, Oraib Al-Ketan, Towards biomimetic, lattice-based, tendon and ligament metamaterial designs, Journal of the Mechanical Behavior of Biomedical Materials, Volume 134, 2022, 105412, ISSN 1751-6161, https://doi.org/10.1016/j.jmbbm.2022.105412.

[228] B. Yazici & Z. Sü, Biomimetic Metamaterial Design Simulation and Evaluation for Building Acoustics by Impedance Measurements, 2021, Journal of Testing and Evaluation. 50. 20200469. 10.1520/JTE20200469.

[229] X. Yuan, M. Chen, Y. Yao, X. Guo, Y. Huang, Z. Peng, B. Xu, B. Lv, R. Tao, S. Duan, H. Liao, K. Yao, Y. Li, H. Lei, X. Chen, G. Hong, D. Fang, Recent progress in the design and fabrication of multifunctional structures based on metamaterials, Current Opinion in Solid State and Materials Science, Volume 25, Issue 1, 2021, 100883, ISSN 1359-0286, https://doi.org/10.1016/j.cossms.2020.100883.